Dynamical Behaviour of Small Molecules Clathrated in Syndiotactic Polystyrene.

A Solid State Deuterium NMR Investigation

Der Fakultät für Naturwissenschaften
der Universität Duisburg – Essen
(Standort Duisburg)
zur Erlangung des akademischen Grades eines

Doktors der Naturwissenschaften

genehmigte Dissertation von

Elena Trezza

aus Salerno/Italien

Referent: Prof. Dr. W. S. Veeman
Korreferent: Prof. Dr. C. Mayer

Tag der mündlichen Prüfung: 14. May 2003

A mia madre.

Acknowledgements

I sincerely thank Prof. Dr. Wiebren Veeman that gave me the chance to perform my research work at the University of Duisburg and for directing me during this time. These years in Germany contributed to my scientific and personal growth.

I thank Prof. Dr. Christian Mayer very much for the interest he showed in my research and for being the co-promotor.

I thank Prof. Alfonso Grassi, the supervisor of my degree thesis at the University of Salerno, who helped me both supplying the materials investigated and giving me interesting suggestions. He encouraged me and gave a fundamental support to my work.

I acknowledge Mr. Manfred Zähres for the patience he always had with me and his helpfulness to overcome practical obstacles I came across during the experimental part of the work.

I am thankful also to Dr. Westphal who made the x-ray analysis of my samples.

I would like to thank all my colleagues, in particular Mr. Holger Schmidt whose practical and moral support was fundamental to me. I thank also my room mates Mr. Daniel Lattner and Mr. Christian Galle, whose jokes I will miss (incredible but true!), and because they did not let me feel alone. Mr. Martin Horstmann whose computer knowledge "saved me" several times and Mr. Hermann Kampermann for the interesting discussion we had.

Finally I would like to thank my family that, notwithstanding the distance, I felt very close to me and always present when I needed.

Naturalmente li omini boni desiderano sapere.

Leonardo da Vinci

Contents

Chapter 3 Experimental Section

Chapter 4 ^{2}H NMR Investigation

Chapter 5 Simulation of ^{2}H NMR Spectra and Discussion

Introduction

The application of solid state deuterium NMR spectroscopy mainly developed after the implementation by Bloom and co-workers of the quadrupolar echo pulse sequence.[1, 2] Deuteron is a suitable nucleus for the investigation of molecular mobility because of the following advantages:[3]

- Deuterium line shape is sensitive to molecular motions.
- The dynamic range over which the molecular motions can be followed is high.
- Deuterons showing different dynamics contribute with different signals to the spectrum and inter- and intra-molecular motional heterogeneities can be detected.
- By deuterium NMR it is possible to selectively investigate the mobility of isotopically enriched molecules or molecular groups.

^{2}H NMR investigation of solid systems in which deuterated molecules are hosted within the regular voids of crystalline inclusion compounds provides accurate information on structural and dynamic characteristics of the guest molecules.[4] This approach has been typically developed for molecules included in crystalline compounds, e.g. urea,[5] cyclophosphazene channels,[6] zeolites,[7] polycyano-polycadmates,[8] or the amorphous phase of polymeric materials.[9] Investigation of the mobility of molecules adsorbed in the crystalline phase of polymer materials is quite unusual and only few examples are reported to date in the literature.[10]

Syndiotactic polystyrene, in one of the possible semicrystalline forms, the δ form, presents a nonporous structure that enables the polymer to selectively absorb small organic molecules. This peculiar behavior assimilates the δ form of this polymer to thermoplastic molecular sieves in which the cavities located in the crystalline structure can be selectively occupied by appropriate molecules: novel applications of this polymer in the field of selective sensors are likely to be expected.

In this work syndiotactic polystyrene clathrates hosting benzene-d_6, toluene-d_8 1,2-dichloroethane-d_4, dichloromethane-d_2, 1,2-dibromoethane-d_4, and chloroform-d in the cavities of the δ crystalline form are prepared. The mobility of the deuterated molecules

clathrated in the cavities of the s-PS δ form is investigated by solid state ^{2}H NMR spectroscopy to get information about the size of the cavities and to identify specific host-guest interaction.

We give a short survey of the content of the various chapters. Chapter 1 gives a brief description of the polymer investigated (syndiotactic polystyrene). The principles of solid state deuterium NMR spectroscopy and the theoretical description of how ^{2}H NMR spectra can give information on molecular motions are outlined in Chapter 2. Chapter 3 gives a description of the sample preparation. The NMR results are presented in Chapter 4 and discussed in Chapter 5 where a dynamical model is proposed for all the molecules investigated.

Bibliography

1) Davis, J. H.; Jeffrey, K. R.; Bloom, M.; Valic, M. I.; Higgs, T.P. *Chem. Phys. Lett.* **1976**, *42*, 390.
2) Sternin, E.; Bloom, M.; MacKay, A. L.; *J. Magn. Res.* **1983**, *55*, 274.
3) Spiess, H. W. *Adv. Polym. Sci.* **1985**, 66, 23.
4) R. R. Vold, In *Nuclear Magnetic Resonance Probes of Molecular Dynamics*; R. Tycko , Ed.; Kluwer Academic Publisher: Dordrecht, The Netherlands, 1994.
5) J. Schmider, K. Müller, *J. Phys. Chem. A* **1998**, *102*, 1181.
6) E. Meirovitch, *J. Phys. Chem.* **1984**, *88*, 6411.
7) R. R. Eckman, A. J. Vega, *J. Phys. Chem*. **1986**, *90*, 4679.
8) S. Nishikiori, T. Kitazawa, C.-H. Kim, T. Iwamoto, *J. Phys. Chem. A* **2000**, *104*, 2591.
9) M. Mehring, In *NMR Basic Principles and Progress*; Diehl, P., Fluck, E., Kosfeld, R., Eds.; Springer-Verlag: West Berlin, 1976; Vol. 11, p. 30.
10) Some representative examples include: (a) Zwick, M. M. *J. Appl. Polym. Sci.* **1965**, *9*, 2393. (b) Kakida, H.; Makino, D.; Chatani, Y.; Takodoro, H. *Macromolecules* **1970**, *3*, 569. (c) Chatani, Y.; Kobatake, T.; Takodoro, H. *Macromolecules* **1983**, *16*, 199.

Chapter 1

Syndiotactic Polystyrene

We start with a short introduction to the characteristics of the polymer investigated, i.e. syndiotactic polystyrene. This thermoplastic material potentially has important applications and for this reason many efforts have been done to characterize this polymer. Nevertheless further work can still be done and in this our work finds its perspective.

1.1 Introduction

The discovery of the Ziegler-Natta catalyst enabled stereospecific polymerization of olefins. Highly syndiotactic polystyrene (s-PS), with a degree of stereospecificity higher than 96%, (Figure 1.1) was first synthesized in 1985 by IDEMITSU KOSAN Co. Ltd. (Tokyo, Japan), [1-3] and has been under joint product and process development by Idemitsu and Dow Plastics (Midland, MI) since 1988.

The features that made this material interesting for industrial application are the high melting point of 270° C, the crystallization rate on cooling from the melt and the high chemical stability as well as excellent processability in most thermoplastic fabrication technologies.[4] Syndiotactic polystyrene crystallizes to a level of 60 % at such a high rate that this polystyrene could be industrialized as a plastic with a high heat resistance. Because of its semi-crystalline nature, s-PS products exhibit good chemical and moisture resistance and a high degree of dimensional stability, significantly different from those of amorphous polystyrene.

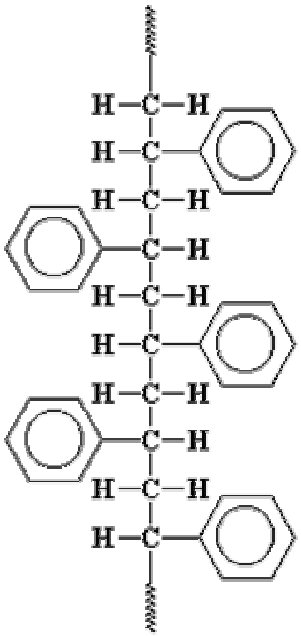

Figure 1.1: Molecular structure of syndiotactic polystyrene, showing side chains arranged in a symmetrical regularly alternating pattern on either side of the polymer backbone.

1.2 Polymorphism of s-PS

Syndiotactic polystyrene exhibits a very complex polymorphic behaviour as evidenced in several structural studies by X-ray diffraction (XRD),[5-9] Fourier Transform infrared spectroscopy (FTIR),[10, 11] and solid state Cross Polarization Magic Angle Spinning (CP MAS) NMR spectroscopy.[12, 13] Four semi-crystalline forms of s-PS are known, namely α, β, γ and δ, according to the nomenclature proposed by Guerra *et al.* (Ref. 6). The first two, α and β, show a *trans* planar conformation of the chains (Figures 1.2a and b), while the other two, γ and δ, present a s(2/1)2 helical conformation and an identity period close to 7.7 Å (Figures 1.2c and d).

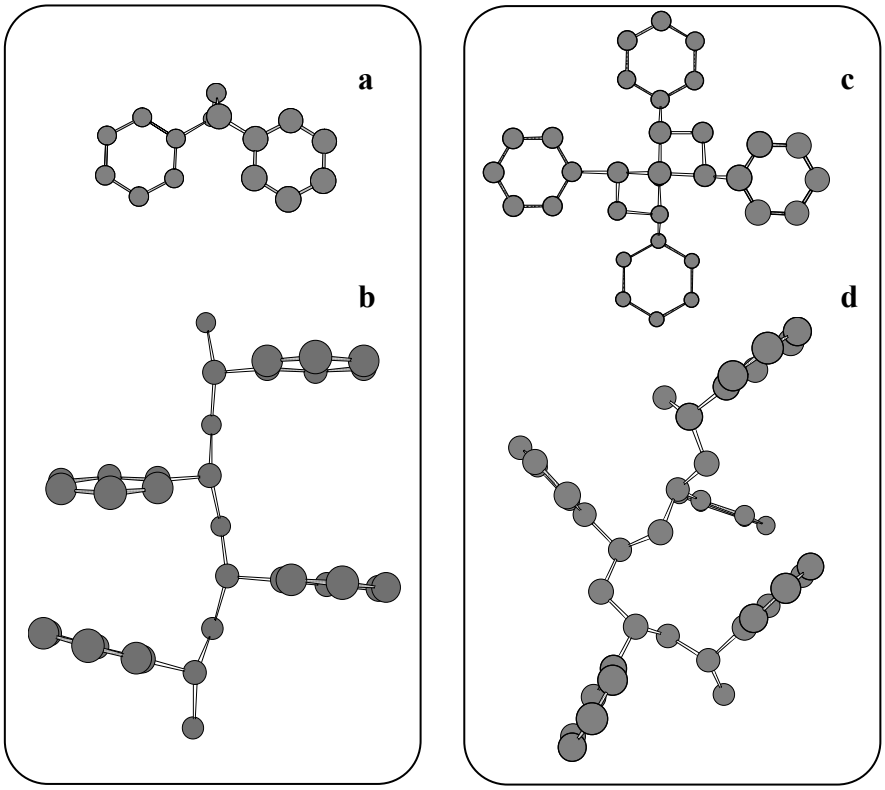

Figure 1.2: Chains of syndiotactic polystyrene **a**) in the α and the β forms viewed along the chain axis and **b**) in the α and the β forms viewed along an axis perpendicular to the chain axis; **c**) in the γ and the δ forms viewed along the chain axis **d**) in the γ and the δ forms viewed along axis perpendicular to the chain axis.

On the basis of different degrees of structural order it is possible to further distinguish different modifications of both α and β forms. Two limit-disordered modifications are known, i.e. α′ and β′, as well as two limit-ordered modifications, i.e. α″ and β″. The disorder in α′ refers to the orientation of triplets of chains statistically distributed between two values, while in the case of β′ the disorder correspond to the stacking of ordered macromolecular bilayers.[8]

Only the structure of one of the other semi-crystalline forms, the δ form, has been completely elucidated, but there are evidences of a very important feature distinguishing the two forms: the δ, unlike the γ, presents a nanoporous structure. This structure enables small organic molecules to be hosted in the crystalline phase of s-PS to give the corresponding δ clathrates. The compounds that can clathrate are aromatic molecules, like benzene or toluene, small halogenated molecules, e.g. 1,2-dichloroethane, chloropropane or chloroform, or small oxygenated molecules such as tetrahydrofurane.

The X-ray diffraction patterns of the four s-PS crystalline forms as well as a clathrate form are showed in Figure 1.3.[4]

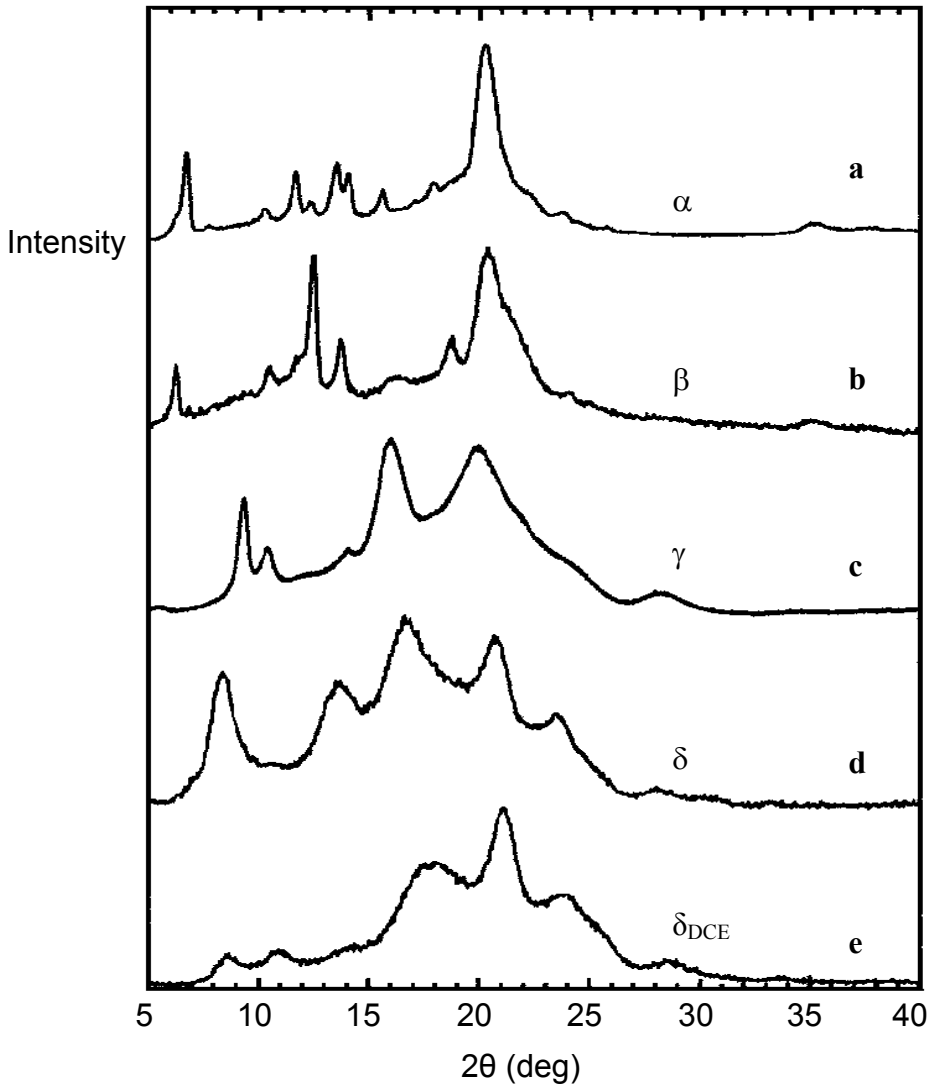

Figure 1.3: Typical X-ray diffraction patterns of the s-PS semicrystalline forms: **a**) α, **b**) β, **c**) γ, **d**) δ and **e**) δ clathrated form including 1,2-dichloroethane (DCE).

It is necessary to specify that the diffraction pattern displayed in Figure 1.3e refers to s-PS δ form clathrate with 1,2-dichloromethane because the intensities and the precise location of the reflections depend on the kind and amount of the molecules included.

It is possible to interconvert the various physical forms of s-PS according to the conditions displayed in the schema of Figure 1.4. This representation is quite complex, nevertheless it is important to notice that crystallization from the melt yields both thermodynamically favorable, high melting α[14-16] and β[8] forms, while the thermally unstable δ and γ forms are obtained from solution crystallization. Moreover δ clathrates can be obtained from s-PS

in the α or γ crystalline forms as well as from the amorphous by sorption of suitable organic compounds.

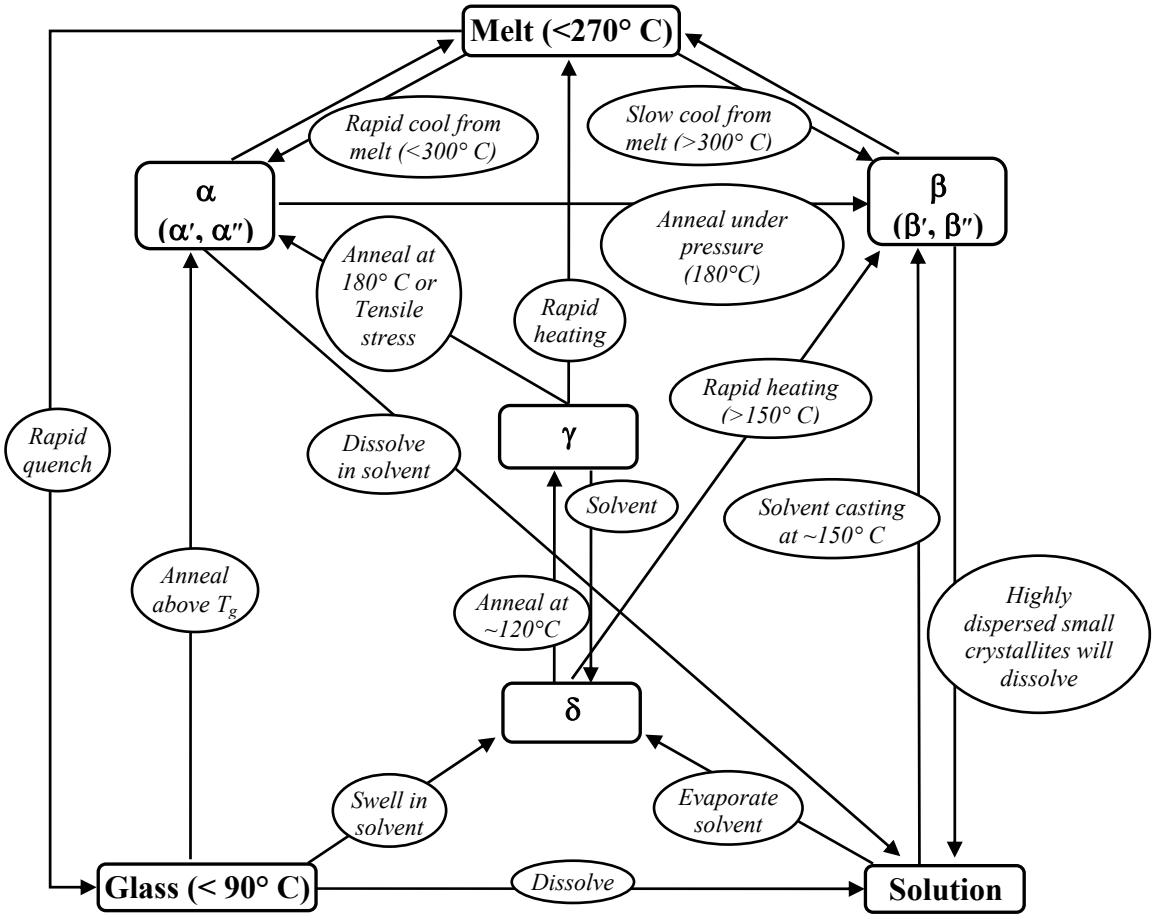

Figure 1.4: Complex schema representing the conditions relative to the interconversion between the different physical forms of s-PS.

The δ-clathrated form can be transformed into the "empty" δ form by a proper treatment with acetone, by which the included molecules can be removed, leaving voids in the crystalline phase. Then the empty δ form can be treated with proper solvents to obtain new clathrates. Several of these clathrates have been characterized by X-ray diffraction[17, 18] and the packing model proposed presents one guest molecule pro nanopore trapped between two polymeric chains belonging to different unit cells of the crystalline network. A model of packing of s-PS proposed for the clathrate with toluene and for the δ form are reported in Figures 1.5 and 1.6.[19]

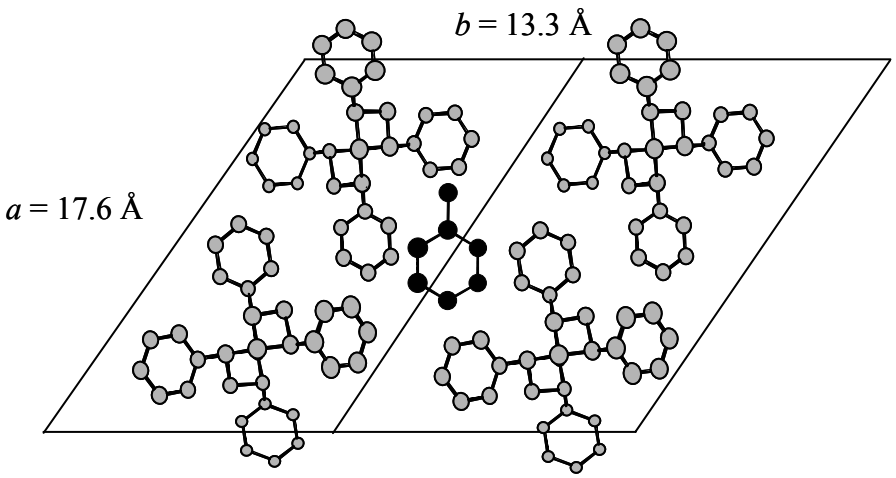

Figure 1.5: Model of packing and unit cell for the crystal structure of the δ clathrate form of s-PS with toluene proposed in Ref. 19.

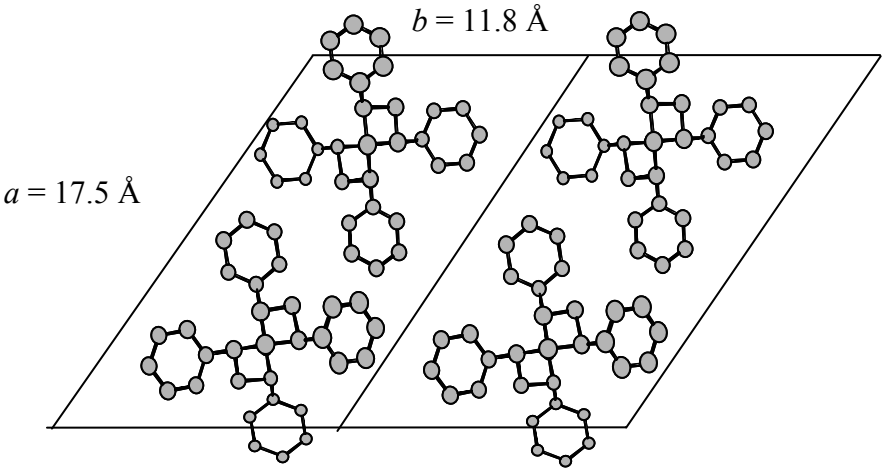

Figure 1.6: Model of packing and unit cell for the crystal structure of the "empty" δ form of s-PS proposed in Ref. 19.

By comparing Figure 1.5 with Figure 1.6 it is evident that the dimensions of the cell vary after the inclusion of the molecules proving the occurrence of host-guest interaction. The parameters characterizing the monoclinic unit cell of the empty δ form are a = 17.4 Å, b = 11.85 Å, c = 7.70 Å and γ = 117°. The presence of guest molecules in the cavities affects only two of these parameters causing an increase of the length of b and of the amplitude of the angle γ to an extent that varies with the kind of the molecule included.

1.3 Features of the δ Form

The characteristic property of δ s-PS is that it is the first polymeric semi-crystalline material that has higher sorption ability in the crystalline phase than in the amorphous phase. This is a consequence of the lower density of the crystalline phase (0.977) with respect to that of the amorphous phase (1.05).

Isotactic poly(4-methyl-1-pentene) also absorbs gases like CO_2 or CH_4,[20] but the molecules do not form a clathrate structure, they dissolve into the crystalline phase but in a lower concentration compared to the amorphous phase. The ratio of absorbed species in the two phases ranges from one third to one fourth.

The absorption of small organic molecules by the thermoplastic material in the δ form from different environments is selective and takes place also at low activities.[21- 24] The results of sorption studies demonstrate the potential applicability of this polymeric form in the process of water or air purification as well as in chemical separation.

The chemical separation can proceed with different mechanisms according to the nature of the molecular mixture as explained in the following example.

In the case of the separation of the acetone-chloroform azeotropic solution, the retention of the halogenated compound is promoted by an increase of enthalpy. This is provided by electrostatic interactions that occur between the phenyl rings of the polymer and the halogen atoms.[25, 26] For the separation of a hexane-cyclohexane solution the driving force for the preferential retention of the cyclic isomer is represented by the entropy factor. In fact, while the absorption of these two compounds is accomplished by a similar enthalpy effect, for the linear isomer the interaction with the cavity would reduce the conformational freedom of the molecule. In contrast no substantial drop of entropy is expected to accomplish the formation of clathrate with the cyclohexane.

Furthermore, FTIR investigations of the clathrate forms demonstrated that in some cases specific interactions between the guest molecules and the cavities produce an unusual distribution of the conformer populations. E.g. the *gauche* and *trans* conformations of 1,2-dichloroethane absorbed in the amorphous part of the s-PS samples are nearly equally populated, whereas the *trans* conformation largely prevails for the molecules trapped in the cavities of the crystalline δ-form.[22, 24]

Bibliography

1) Ishihara, N.; Seimiya, T.; Kuramoto, M.; Uoi, M. *Macromolecules* **1986**, *19*, 2464.
2) Zambelli, A.; Longo, P.; Pellecchia, C.; Grassi, A. *Macromolecules* **1987**, *20*, 2035.
3) Ishihara, N.; Kuramoto, M.; Uoi, M. *Macromolecules* **1988**, *21*, 3356.
4) Rizzo, P.; Lamberti, M.; Albunia, A. R.; Ruiz de Ballesteros, O.; Guerra, G. *Macromolecules* **2002**, *35*, 5854.
5) Immirzi, A.; De Candia, F.; Iannelli, P.; Vittoria, V.; Zambelli, A. *Macromol. Chem., Rapid Commun.* **1988**, *9*, 765.
6) Guerra, G.; Vitagliano, V. M.; De Rosa, C.; Petraccone, V.; Corradini, C. *Macromolecules* **1990**, *23*, 1539.
7) Guerra, G.; De Rosa, C.; Vitagliano, V. M.; Petraccone, V.; Corradini, C. *J. Polym. Sci., Part B: Ploym. Phys.* **1991**, *29*, 265.
8) De Rosa, C.; Rapacciuolo, M.; Guerra, G.; Petraccone, V.; Corradini, C. *Polymer* **1992**, *33*, 1423.
9) Chatani, Y.; Shimane, Y.; Inoue, Y.; Inagaki, T.; Ishioka, T.; Ijitsu, T.; Yukinari, T. *Polymer* **1992**, *33*, 488.
10) Kobayashi, M.; Nakaoki, T.; Ishihara, N. *Macromolecules* **1990**, *23*, 78.
11) Reynolds, N. M.; Stidham, H. D.; Hsu, S. L. *Macromolecules* **1991**, *24*, 3662.
12) Grassi, A.; Longo, P.; Guerra, G.), *Makromol. Chem., Rapid Commun.* **1989**, *10*, 687.
13) Gomez, M. A.; Tonelli, A. E. *Macromolecules* **1990**, *23*, 3385.
14) De Rosa, C.; Guerra, G.; Petraccone, V.; Corradini, C. *Polym. J.* **1991**, *23*, 1435.
15) De Rosa, C. *Macromolecules* **1996**, *29*, 8460.
16) Cartier, L.; Okihara, T.; Lots, B. *Macromolecules* **1998**, *31*, 3303.
17) Chatani, Y.; Inagaki, T.; Shimane, Y.; Shikuma, H. *Polymer* **1993**, *34*, 4841.
18) De Rosa, C.; Rizzo, P.; Ruiz de Ballesteros, O.; Petraccone, V.; Guerra, G. *Polymer* **1999**, *90*, 2103.
19) De Rosa, C.; Guerra, G.; Petraccone, V.; Pirozzi, B. *Macromolecules* **1997**, *30*, 4147.
20) Puleo, A. C.; Paul, D. R.; Wong, P. K. *Polymer* **1989**, *30*, 1357.

21) Manfredi, C.; Del Nobile, M. A.; Mensitieri, G.; Guerra, G.; Rapacciuolo, M. *J. Polym. Sci., Polym Phys. Ed.* **1997**, *35*,133.
22) Guerra, G.; Manfredi, C.; Musto, P.; Tavone, S.; . *Macromolecules* **1998**, *31*, 1329.
23) Guadagno, L.; Baldi, P.; Vittoria, V.; Guerra, G. *Macromol. Chem. Phys.* **1998**, *199*, 2671.
24) Musto, P.; Manzari, M.; Guerra, G. *Macromolecules* **1999**, *32*, 2770.
25) Cavallo, L.; Milano, G.; Guerra, G. *Eur. J. Inorg. Chem.* **1998**, *1*, 1513.
26) Guerra, G.; Milano, G.; Venditto, V.; Musto, P.; De Rosa, C.; Cavallo, L. *Chem. Mater.* **2000**, *12*, 363.

Chapter 2

Solid State Deuterium NMR

This chapter presents an overview of the interactions involving the nuclear spin states in solids during an NMR experiment, whereby each interaction is represented by a Hamiltonian term. Spin quadrupolar interactions play a very important role for deuterium nuclei and will be treated in detail. Then follows a theoretical description of the computation of the line shapes of the ^{2}H NMR spectra for the static and dynamic case and some examples are reported. Finally, practical problems correlated to the acquisition of the spectra are listed and the pulse sequence used is explained using the operator formalism.

2.1 Nuclear Spin Interactions in Solids

The total Hamiltonian of a nuclear spin system can be represented as the sum of the single terms listed below: $\hat{\mathrm{H}} = \sum \hat{\mathrm{H}}_i$

$\hat{\mathbf{H}}_i$	**Coupling of nuclear spins with:**
$\hat{\mathrm{H}}_Z$	external static magnetic fields
$\hat{\mathrm{H}}_{RF}$	external radio frequency magnetic fields
$\hat{\mathrm{H}}_{CS}$	induced magnetic field generated by the surroundings electron
$\hat{\mathrm{H}}_D$	each other, through direct dipole-dipole interaction
$\hat{\mathrm{H}}_J$	each other, via electron spins
$\hat{\mathrm{H}}_Q$	electric field gradients; it occurs only for nuclei with spin > 1/2

The single interactions are described in the following sections.

2.1.1 $\hat{\mathbf{H}}_{\mathbf{z}}$: *The Zeeman Interaction*

Each NMR active nucleus must possess a spin angular momentum. The nuclear spin angular momentum is a vector:

$$\vec{\mathrm{I}} = \left(\hat{I}_x, \hat{I}_y, \hat{I}_z\right) \qquad [2.1.1]$$

with squared modulus:

$$\left|\vec{\mathrm{I}}^2\right| = \hbar^2\left[I(I+1)\right] \qquad [2.1.2]$$

where I is the spin quantum number and $\hbar = h/2\pi$ (h is Planck constant).
All nuclei having a spin angular momentum $\vec{\mathrm{I}} \neq 0$ possess a nuclear magnetic dipole moment $\vec{\mu}$ coaxial with $\vec{\mathrm{I}}$ and defined as: $\vec{\mu} = \gamma\,\vec{\mathrm{I}}$, where γ is the gyromagnetic ratio. When an external magnetic field $\vec{\mathrm{B}}_0$ is applied, by convention assumed to be aligned along the z axis, it interacts with the magnetic moment. This interaction, that has an order of magnitude of approximately 10^6-10^9 Hz, is called the Zeeman interaction and is at the fundament of nuclear magnetic resonance spectroscopy. The corresponding Hamiltonian is:

$$\hat{\mathrm{H}}_z = -\vec{\mu}\cdot\vec{\mathrm{B}}_0 = -\gamma\,\hbar\,\hat{I}_z\mathrm{B}_0 \qquad [2.1.3]$$

The value of the z component of the spin angular momentum, is defined as $\hat{I}_z = \hbar\, m$ in which the magnetic quantum number $m = (-I, -I+1, \ldots, I-1, I)$. $\hat{I}_z$ has $2I+1$ possible values corresponding to $2I+1$ energy states. In particular if a nucleus with spin $I = 1$ is placed in a homogeneous magnetic field B_0, the threefold degenerate nuclear spin energy level is split into three states, each corresponding to one value of m.

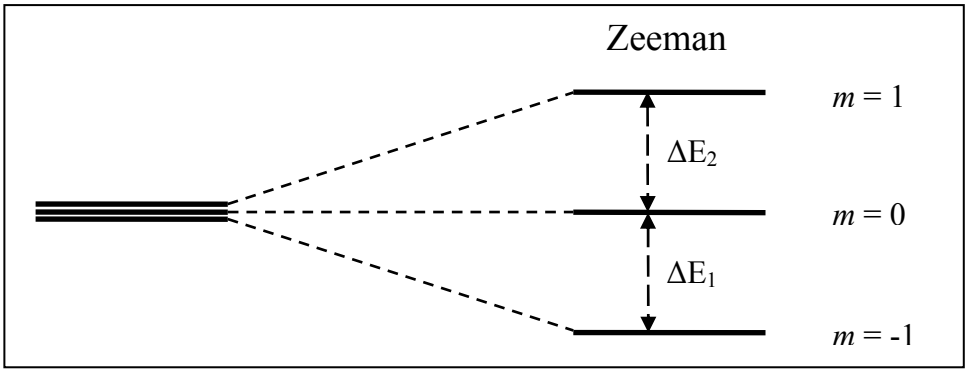

Figure 2.1: Schematic representation of the energy splitting of the spin states resulting from the interaction of a spin $I = 1$ nucleus with the external magnetic field.

The two energy differences between the states have the same value $\Delta E_1 = \Delta E_2 = \Delta E$ that is linear with the external magnetic field:

$$\Delta E = E_{m-1} - E_m = \gamma B_0 \hbar = \hbar \omega_0 \qquad [2.1.4]$$

and the two transitions, allowed according to the selection rule ($\Delta m = \pm 1$), correspond to a radiofrequency ν:

$$\nu_0 = \omega_0 / 2\pi = \Delta E / h \qquad [2.1.5]$$

The resonance frequency ν_0 is called the Larmor frequency and is of the order of MHz. If a radio frequency field B_{rf} oscillating near the resonance frequency ν_0 is applied, transitions will occur. Choosing B_{rf} parallel to the x axis, it can be written as:

$$B_{rf} = (B_1(t) \cos [\omega t + \varphi(t)], 0, 0) \qquad [2.1.6]$$

It is evident that the amplitude and phase of irradiation can be varied, but the carrier frequency ($\omega / 2\pi$) is assumed to be constant. The corresponding Hamiltonian is:

$$\hat{H}_{rf} = -B_1(t) \cos[\omega t + \varphi(t)] \gamma \hbar \hat{I}_x \qquad [2.1.7]$$

If the Zeeman interaction would be the only existing interaction, NMR would not give any information on the system under examination. The structural information originates from the other interactions experienced by nuclei of spin I. These produce characteristic splittings and broadening of the NMR signals as described below.

2.1.2 The Chemical Shift Interaction

The external magnetic field induces in the electron cloud surrounding the nucleus a magnetic moment having a shielding effect on the nucleus. This interaction causes a shift in the resonance frequency of that nucleus, the *chemical shift*, which is proportional to B_0. Since the electron distribution in general is not spherical, the shift depends on the orientation of the molecules with respect to the direction of B_0, i.e. the z direction. The anisotropy of the chemical shift, that causes a broadening of the signal in the solid state, disappears in the liquids where the fast molecular motions average out the anisotropy leaving an isotropic chemical shift. The form of the Hamiltonian for the anisotropic chemical shift is:

$$\hat{\mathrm{H}}_{CS} = \gamma\, \vec{\mathrm{I}} \cdot \hat{\sigma} \cdot \vec{\mathbf{B}}_0 \qquad [2.1.8]$$

where the shielding tensor $\hat{\sigma}$ is a 3 × 3 matrix.

2.1.3 The Dipolar Interaction

Each nucleus generates a local dipolar field and at the same time experiences those produced by the neighboring nuclei. The dipole-dipole Hamiltonian $\hat{\mathrm{H}}_D$ between two spins is given by:

$$\hat{\mathrm{H}}_D = \frac{\mu_0\, \gamma_1\, \gamma_2\, \hbar}{4\,\pi\, r_{12}^3}\left[\vec{\mathbf{I}}_1 \cdot \vec{\mathbf{I}}_2 - \frac{3\left(\vec{\mathbf{I}}_2 \cdot \vec{\mathrm{r}}_{12}\right)\left(\vec{\mathbf{I}}_1 \cdot \vec{\mathrm{r}}_{12}\right)}{r_{12}^2}\right] \qquad [2.1.9]$$

where μ_0 is the permeability constant, r_{12} is the internuclear distance and γ_1 and γ_2 are the two gyromagnetic ratios. It is worth noting that this interaction depends on the magnitude of the magnetic moments and falls off very rapidly with the distance between the nuclei. By changing the expression of the vector $\vec{\mathrm{r}}_{12}$ from the Cartesian coordinates into spherical coordinates (r, θ, φ), and by introducing the Equation 2.1.1 and expressing $\hat{I}_x$ and $\hat{I}_y$ in

terms of raising and lowering operators $\hat{I}_+ = \hat{I}_x + \mathrm{i}\,\hat{I}_y$ and $\hat{I}_- = \hat{I}_x - \mathrm{i}\,\hat{I}_y$, it is possible to write the dipolar Hamiltonian using an expansion known as *dipolar alphabet*:

$$\hat{\mathrm{H}}_D = \omega_\mathrm{D}[\mathrm{A} + \mathrm{B} + \mathrm{C} + \mathrm{D} + \mathrm{E} + \mathrm{F}] \qquad [2.1.10]$$

where

$$\mathrm{A} = (1 - 3\cos^2\theta)\,\hat{I}_{1z}\,\hat{I}_{2z}$$
$$\mathrm{B} = -\frac{1}{4}(1 - 3\cos^2\theta)\,(\hat{I}_{1+}\,\hat{I}_{2-} + \hat{I}_{1-}\,\hat{I}_{2+})$$
$$\mathrm{C} = -\frac{3}{2}(\sin\theta\cos\theta\,\mathrm{e}^{-\mathrm{i}\varphi})\,(\hat{I}_{1+}\,\hat{I}_{2z} + \hat{I}_{1z}\,\hat{I}_{2+})$$
$$\mathrm{D} = -\frac{3}{2}(\sin\theta\cos\theta\,\mathrm{e}^{-\mathrm{i}\varphi})\,(\hat{I}_{1-}\,\hat{I}_{2z} + \hat{I}_{1z}\,\hat{I}_{2-})$$
$$\mathrm{E} = -\frac{3}{4}(\sin^2\theta\;\mathrm{e}^{-2\,\mathrm{i}\varphi})\,\hat{I}_{1+}\,\hat{I}_{2+}$$
$$\mathrm{F} = -\frac{3}{4}(\sin^2\theta\;\mathrm{e}^{2\,\mathrm{i}\varphi})\,\hat{I}_{1-}\,\hat{I}_{2-}$$
$$\omega_D = \frac{\mu_0\,\gamma_1\,\gamma_2\,\hbar}{4\,\pi\,r_{12}^3}$$

For like spins only the A and B terms commute with the operator $\hat{I}_z$ of the Zeeman interaction, therefore only these two terms influence the spectrum. For unlike spins only A commutes with $\hat{I}_z$ and all the other terms in first order do not affect the broadening and the position of the NMR resonance lines.

2.1.4 The Spin-Spin Coupling Interaction

This interaction, which is smaller than the other already considered, (for the common nuclei the values range up to several kHz) arises from an indirect coupling between a pair of spins realized through the electrons in the chemical bonds between them. The Hamiltonian can be written as:

$$\hat{\mathrm{H}}_{SC} = \vec{\mathrm{I}}_1 \cdot \hat{\mathrm{J}} \cdot \vec{\mathrm{I}}_2 \qquad [2.1.11]$$

2.1.5 The Quadrupolar Interaction

Nuclei with $I \geq 1$ have an electric quadrupole moment, expressed as eQ, arising from a not spherical charge distribution inside the nucleus. The nuclear charge distribution must be symmetric with respect to the axis of the nuclear spin, therefore there are two possibilities: a cigar-shape (Figure 2.2a) called prolate spheroid ($eQ > 0$) or a discus-shape (Figure 2.2b) called oblate spheroid ($eQ < 0$). Such distributions can be considered to be the result of a combination of a spherical distribution of positive charges (monopoles) and the quadrupoles shown in Figures 2.2c and d.[1]

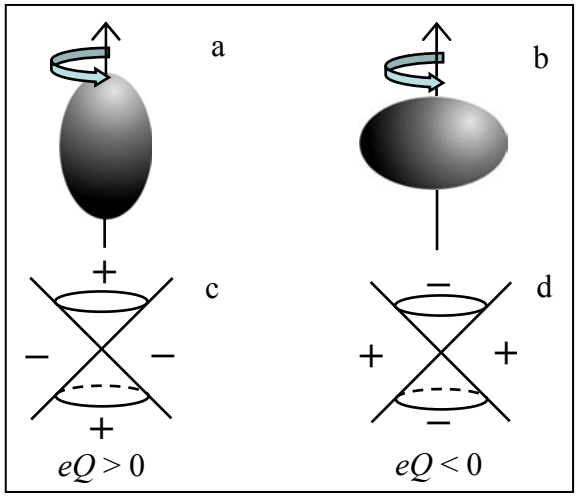

Figure 2.2: Nuclear charge distribution corresponding to: **a**) a positive electric quadrupole (prolate spheroid); **b**) a negative electric quadrupole oblate spheroid; and respective quadrupole moments **c**) and **d**).

The electronic charge distribution around the nucleus generates electric field gradients (EFG) that interact with the nuclear quadrupole moments. The orientation of the spheroid is determined by the minimal interaction energy with the electric field gradients, i.e. by the geometry of the electrical charges surrounding the nucleus. A cubic symmetric environment generates a spherically symmetric EFG and the quadrupolar interaction vanishes. The nucleus is involved in two competing interactions: the external magnetic field acting via the magnetic dipole moment and the electric field gradients interacting with the nuclear quadrupole moment. The quadrupolar Hamiltonian for a single spin **I** can be written as:

$$\hat{H}_Q = \vec{I} \cdot \hat{Q} \cdot \vec{I} \qquad [2.1.12]$$

The second rank quadrupole coupling tensor $\hat{Q}$ is given by the scalar product of the quadrupole momentum eQ and the tensor $\hat{V}$:

$$\hat{H}_Q = \frac{eQ}{2I(2I-1)\hbar} \vec{I} \cdot \hat{V} \cdot \vec{I} \qquad [2.1.13]$$

The elements of the second-rank tensor $\hat{V}$ are the second derivatives of the electric potential, i.e. the electric field gradient at the nuclear site. It is always possible to find a coordinate axis system (XYZ), defined as principal axis system (PAS), in which the off-diagonal elements of the tensor $\hat{V}$ are zero. The diagonal elements satisfy the Laplace equation:

$$\nabla^2 V = V_{XX} + V_{YY} + V_{ZZ} = 0 \qquad [2.1.14]$$

This explains why the quadrupolar Hamiltonian is traceless. Following the convention $|V_{ZZ}| \geq |V_{YY}| \geq |V_{XX}|$,[2] the *asymmetry parameter* η is defined as:

$$\eta = \frac{(V_{XX} - V_{YY})}{V_{ZZ}} \qquad [2.1.15]$$

with $0 \leq \eta \leq 1$. $\eta = 0$ means, obviously, that $\hat{V}$ is symmetric about the principal axis V_{ZZ}. By definition the value of V_{ZZ} is:

$$V_{ZZ} = eq. \qquad [2.1.16]$$

This parameter, expressed in frequency units, is the *anisotropy parameter* δ^*.
According to the value of the quadrupole moment and the local bonding situation, the quadrupolar interactions $\hat{H}_Q$ can range from zero to an order of magnitude of 10^9 Hz. In the presence of the quadrupolar interaction, at first approximation the other abovementioned interactions can be neglected and the complete Hamiltonian can be written as the sum of the Zeeman and quadrupolar interaction only:

$$\hat{H} = \hat{H}_Z + \hat{H}_Q \qquad [2.1.17]$$

2.2 Quadrupolar Interaction for the Deuterium Nucleus

The EFG tensor for a ^{2}H nucleus bound to a carbon atom is in good approximation axially symmetric (η = 0), with the V_{ZZ} axis laying on the C-^{2}H bond (Figure 2.3). This can be explained since the axial symmetry of the charge density distribution for the σ-bonds is reflected in the cylindrical symmetry of the EFG tensor close to the ^{2}H nucleus.

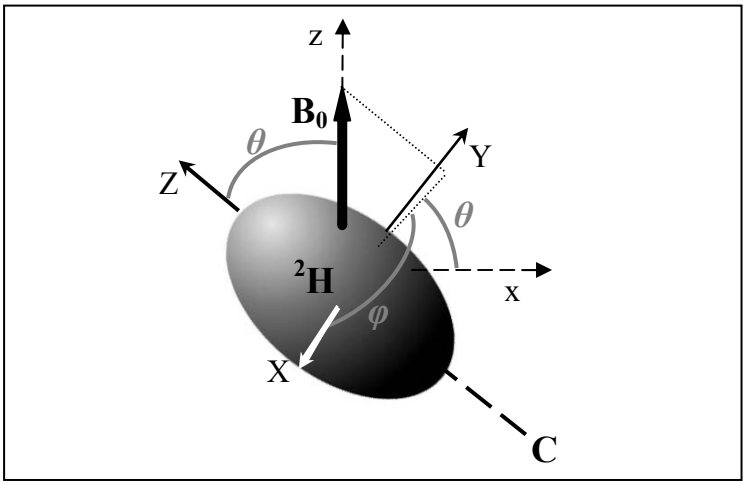

Figure 2.3: Schematic representation of the external magnetic field B_0 and the electric field gradient tensor in the principal axis system for a deuterium bound to a carbon atom.

For the further treatment it is necessary to consider a more general axis system (xyz) with the z axis coinciding with the direction of the external field B_0. The angles θ and φ specify the orientation of the new axis system with respect to the PAS (XYZ) (Figure 2.3). By indicating with V_{ij} the components of the EFG tensor in the xyz axis, the quadrupolar Hamiltonian of deuterium (I = 1) is expressed as:[3]

$$\hat{H}_Q = \frac{3eQ}{2h}\begin{pmatrix} 1/6V_{zz} & \sqrt{1/2}\,V_{-1} & V_{-2} \\ -\sqrt{1/2}\,V_{+1} & -1/3V_{zz} & -\sqrt{1/2}\,V_{-1} \\ V_{+2} & \sqrt{1/2}\,V_{+1} & 1/6V_{zz} \end{pmatrix} \qquad [2.2.1]$$

with $V_{\pm1} = \pm V_{xz} - iV_{yz}$ and $V_{\pm2} = \frac{1}{2}(V_{xx} - V_{yy}) \pm iV_{xy}$.

The solid state NMR spectra of the ^{2}H nucleus are dominated by the quadrupolar interaction. Nevertheless for deuterium the Zeeman Hamiltonian is much larger than the

quadrupolar Hamiltonian and the "high field approximation" holds. Furthermore the total Hamiltonian can be expressed by Equation 2.1.17 with $\hat{H}_Z >> \hat{H}_Q$, hence the changes in the energy levels caused by the quadrupolar interaction can be considered as corrections to the energies of the Zeeman levels and can be calculated by the standard perturbation theory. The energy of the various spin states results from the sum of the contributions of each perturbation order:(2)

$$E_m = E_m^{(0)} + E_m^{(1)} + E_m^{(2)} + \ldots \qquad [2.2.2]$$

As described before, the Zeeman interaction influences the energy levels in a way that all the m-1 → m transitions are equally spaced and the corresponding resonance frequency is:

$$\nu_0 = \frac{E_{m\text{-}1}^{(0)} - E_m^{(0)}}{h} \qquad [2.2.3]$$

According to first-order perturbation theory, the first-order quadrupolar corrections modify the energy levels and:(4)

$$E_m^{(1)} = \langle \Psi_m^0 | \hat{H}_Q | \Psi_m^0 \rangle \qquad [2.2.4]$$

where $|\Psi_m^0\rangle$ are zero-order wave functions, which are eigenfunctions of $\hat{H}_Z$ with energy $E_m^{(0)}$. Equation 2.2.4 shows that only the terms that commute with $\hat{H}_Z$, i.e. the secular part of $\hat{H}_Q$ contribute to $E_m^{(1)}$. The secular part of $\hat{H}_Q$ is composed of the diagonal elements of Equation 2.2.1 which contain only the z component of the EFG tensor in the xyz coordinate system. Therefore the first-order shift of the energy levels due to the quadrupolar interaction assumes the value:(2)

$$E_m^{(1)} = \frac{3\,e\,Q}{4}[m^2 - 1/3\, I(I+1)]V_{zz} \qquad [2.2.5]$$

By expressing V_{zz} as function of V_{ZZ}, θ and φ, and considering that for ^{2}H nuclei $\eta = 0$, Equation 2.2.5 can be rewritten as:

$$E_m^{(1)} = \frac{3}{8} h\, Q_0 (3\cos^2\theta - 1)[m^2 - 1/3\, I(I+1)] \qquad [2.2.6]$$

where $Q_0 = e^2\, q\, Q\, /h = V_{ZZ}\, e\, Q/\, h$ is the quadrupole coupling constant that has units of s^{-1}. Also the second-order corrections modify the energy of the spin states. The changes involve double products of the off-diagonal elements of the Equation 2.2.1, i.e. the non-secular terms in $\hat{H}_Q$ divided by differences between Zeeman energies. The expression resulting for the second-order energy is:

$$E_m^{(2)} = -h\left(\frac{3Q_0^2}{16\nu_0}\right) m \left[\begin{array}{l}(3/2)\cos^2\theta(1-\cos^2\theta)[8m^2 - 4I(I+1)+1] \\ +(3/8)(1-\cos^2\theta)^2(-2m^2 + 2I(I+1) - 1)\end{array}\right] \qquad [2.2.7]$$

From Eq. 2.2.7 is evident that the contribution of $E_m^{(2)}$ to the total energy E_m depends on the ratio Q_0^2/ν_0. The value of the quadrupolar constant for an aliphatic C-^{2}H bond is known: $Q_0 \cong 170\,\text{kH}$.[5] The experiments described in this work are all performed in a high external magnetic field (9.395 T) in which the deuterium Larmor frequency $\nu_0 = 61.4\,\text{MHz}$. By introducing these values, the ratio is $Q_0^2/\nu_0 \approx 471\,\text{Hz}$. The first-order quadrupolar interaction is in the range of 10^4-10^5 Hz, while the second-order energy contribution is much smaller: 10^2 Hz. Therefore the second-order corrections will be neglected and the total energy of each level E_m is given by the sum of $E_m^{(0)}$ and $E_m^{(1)}$. The effect of quadrupolar interaction on the energy of the spin states for a deuterium nucleus is shown in Figure 2.4a. The transition frequencies relative to the first order transitions are:

$$\nu' = \frac{E_{|-1\rangle} - E_{|0\rangle}}{h} = \nu_0 + \frac{3}{8} Q_0 (3\cos^2\theta - 1) \qquad [2.2.8]$$

$$\nu'' = \frac{E_{|0\rangle} - E_{|1\rangle}}{h} = \nu_0 - \frac{3}{8} Q_0 (3\cos^2\theta - 1) \qquad [2.2.9]$$

The corresponding NMR signal results in a doublet symmetric to the Larmor frequency ν_0 with a splitting (Figure 2.4b):

$$\Delta\nu_Q = \nu' - \nu'' = \frac{3}{4} Q_0 (3\cos^2\theta - 1) \qquad [2.2.10]$$

It is worth noting that $\Delta\nu_Q$ depends, through the angle θ, on the spatial orientation of the C-^{2}H bond.

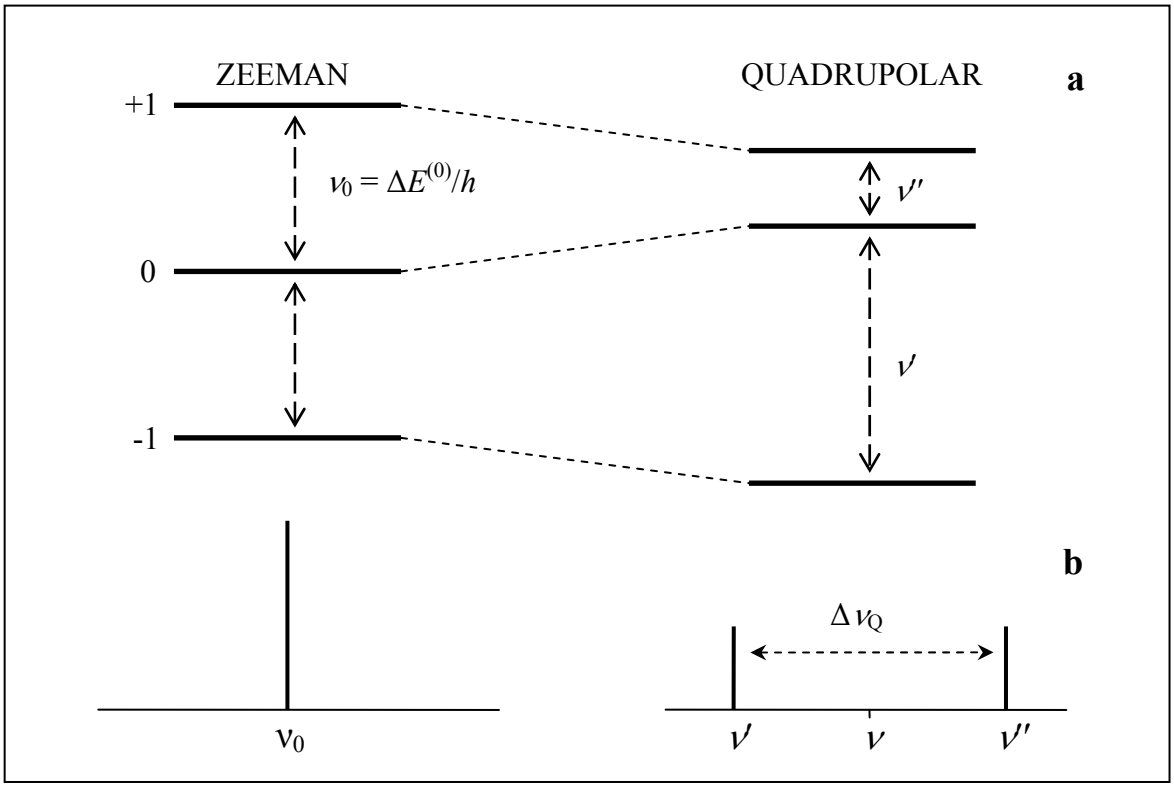

Figure 2.4: **a**) Schematic representation of the energy level of the deuterium spin nucleus resulting from the Zeeman and Quadrupole interaction and **b**) corresponding resonance signals in the ideal case of a single nucleus.

2.3 Deuterium Powder Spectra in the Rigid Limit

A two line spectrum, as that displayed in Figure 2.4b, can only result from the NMR observation of a single crystal in which the axes of the C-^{2}H bonds are all tilted at an unique angle θ with respect to the external field B_0. A powder sample consists of a multitude of small crystallites whose crystal axes are randomly oriented.[6] The orientations of the principal axes V_{ZZ} of the tensors in the powder sample are equally distributed over a sphere. It is more convenient to plot on a sphere the distribution of the orientations of B_0 described by the angles θ and φ in the PAS of each nucleus as shown in Figure 2.5a. The points on this sphere correspond to a specific orientation of B_0 with respect to an axially

symmetric EFG tensor and hence to each point corresponds a doublet in the NMR spectrum.

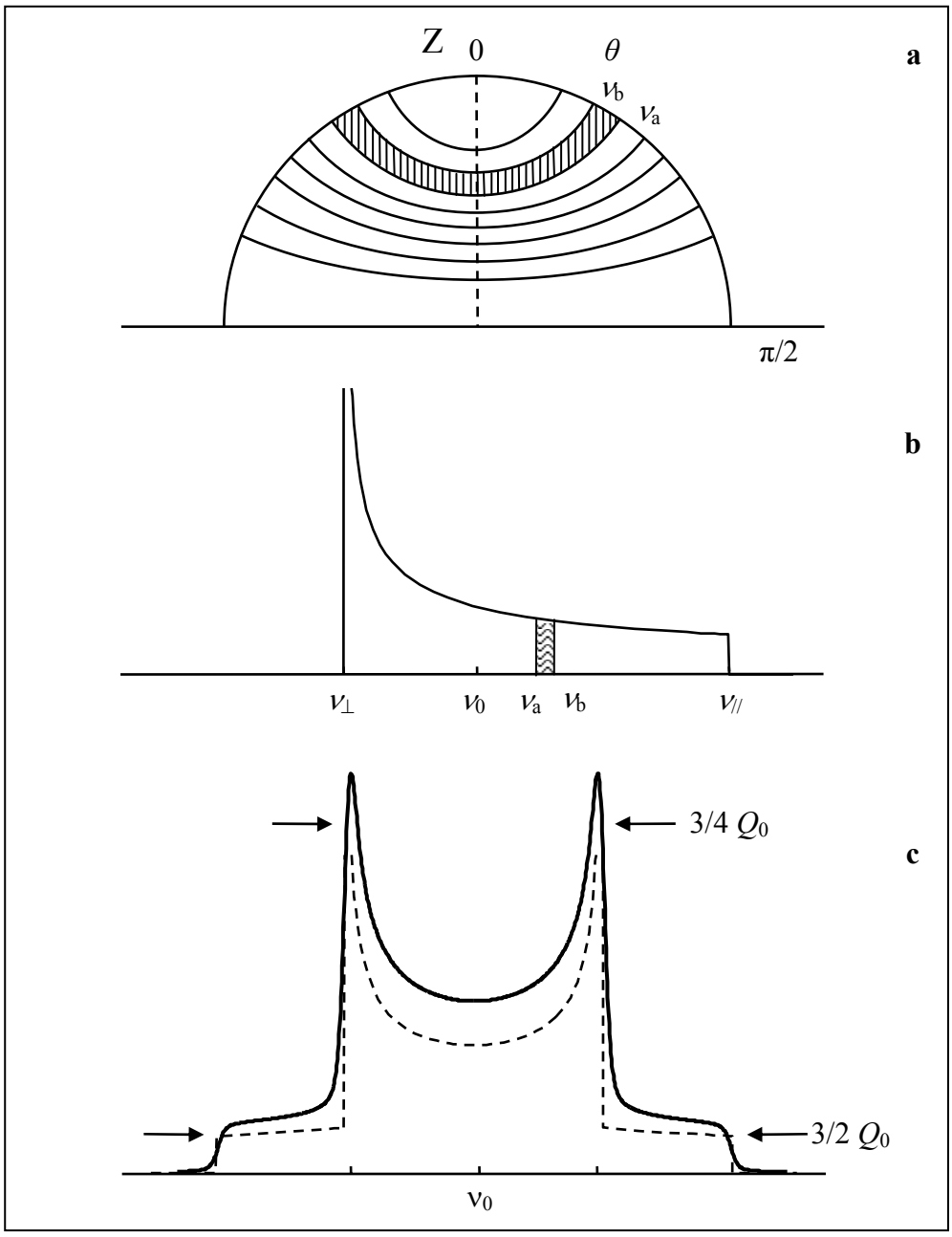

Figure 2.5: **a**) Stereographic projection of curves of constant frequency for an axially symmetric EFG tensor. **b**) ^{2}H powder spectrum calculated for only one of the two single quantum transitions between the spin states. **c**) Pake pattern calculated for the powder spectrum (dashed line) and convolution of the function F(ν) with a Gauss-Lorentz function of the individual resonance lines (solid line).

It is convenient to divide the sphere into latitudes of constant frequency. Since the doublet is disposed symmetrically with respect to the central frequency ν_0, it is possible to calculate the powder pattern considering only one of the two transitions, for example only the frequency $\nu = \nu'$. It is also convenient to assume the central frequency $\nu_0 = 0$, in this case

$$\nu' = +\frac{3}{8}Q_0(3\cos^2\theta - 1) = \nu \qquad [2.3.1]$$

The NMR spectrum results by the superposition of all the single signals from each nucleus. The intensity of the signal $f(\nu)$, depends on the probability to find the nucleus at the orientation θ, with respect to the external field, that causes a splitting $h\nu$ between the energy levels. The intensity for $\nu_a \leq \nu \leq \nu_b$ can be calculated as the area between the two curves of constant frequency ν_a and ν_b:[6, 7]

$$\int_{\nu_a}^{\nu_b} f(\nu)\, d\nu = c \int_{\theta_a}^{\theta_b} \sin\theta \, d\theta \qquad [2.3.2]$$

c is a normalization factor that can be chosen in such a way that $\int_{-\infty}^{+\infty} f(\nu)\, d\nu = 1$ and θ_a and θ_b specify the orientation of B_0 for which the curves of constant frequencies ν_a and ν_b are obtained. The integration variable θ of the second term can be substituted with a function of ν by solving the Equation 2.3.1 for θ:

$$\theta = \arccos\left(\sqrt{\frac{8\nu}{9Q_0} + \frac{1}{3}}\right) \qquad [2.3.3]$$

Differentiating this equation and substituting the resulting expression for $\sin\theta \, d\theta$ into Equation 2.3.2 yield:

$$\int_{\nu_a}^{\nu_b} f(\nu)\, d\nu = \frac{4}{3\sqrt{3Q_0}} \int_{\nu_a}^{\nu_b} \frac{d\nu}{\sqrt{1 + (8\nu / 3Q_0)}} \qquad [2.3.4]$$

Equation 2.3.4 refers to the case of two generic integration limits ν_a and ν_b. By equating the integrands it results:

$$f(\nu) = \frac{4}{3\sqrt{3}\,Q_0}\frac{1}{\sqrt{1+(8\nu/3Q_0)}}, \qquad -\frac{3}{8}Q_0 \le \nu \le \frac{3}{4}Q_0 \qquad [2.3.5]$$

The function expressed in the Equation 2.3.5 is represented in the Figure 2.5b. The function presents discontinuities at the frequencies labeled as $\nu_{//} = 3/4\ Q_0$ and $\nu_{\perp} = -3/8\ Q_0$ which correspond respectively to B_0 parallel ($\theta = 0$) or perpendicular ($\theta = 90°$) to the principal axis of symmetry of the EFG tensors.

Figure 2.5b shows the shape calculated by taking into account only one of the two transitions occurring: $\nu = \nu'$. Since $\nu'' = -\nu' = -\nu$ the complete function for both the transitions can be calculated by the sum $F(\nu) = f(\nu) + f(-\nu)$. The ^2H NMR spectrum of a deuterated polycrystalline material will consist of properly weighed superimposed doublets which result in a typical pattern, the Pake powder spectrum shown in Figure 2.5c (dashed line). Experimental spectra do not show the sharp features of the line shape exhibited in Figure 2.5b, but they are smoothed by several factors like residual dipolar interaction, vibrational motions, sample inhomogeneities.[8] It is suitable to convolute the function $F(\nu)$ with a Gaussian-Lorentzian broadening function to get a more realistic simulated pattern as displayed in Figure 2.5c (solid line).

This pattern is calculated for deuterium nuclei (for which holds $\eta = 0$) in absence of motion, i.e. the so-called rigid limit axial powder spectrum. It is symmetric with respect to the Larmor frequency ν_0 and is composed by an internal doublet spaced by a frequency $\Delta\nu_R = 2\,|\nu_{\perp}| = \frac{3}{4}\ Q_0$ and two pedestals at $\pm\ \frac{3}{4}\ Q_0$. Since the constant Q_0 contains the principal asymmetry parameter V_{ZZ} $\left(Q_0 = \frac{eQ}{h}V_{ZZ}\right)$ and from Equations 2.1.14 and 2.1.15 results that for $\eta = 0$ $|V_{XX}| = |V_{YY}| = |V_{ZZ}|/2$, the components of the EFG tensor are directly related to the frequencies characterizing the rigid limit powder spectrum. In fact $|V_{ZZ}| = \frac{h}{eQ}Q_0 = \frac{4}{3}\frac{h}{eQ}\Delta\nu_R = \frac{\Delta\nu_R}{k}$ with $k = \left|\frac{3}{4}\frac{eQ}{h}\right|$.

In general, for $\eta = 0$ the anisotropy parameter $\delta^* = k\,V_{ZZ}$ coincides with the frequency $|\nu_{//}| = 2|\nu_{\perp}| = \Delta\nu_R$, that is the splitting between the resonance arising from the perpendicular components (highest doublet peaks), i.e. $\delta^* = \Delta\nu_R$.

2.4 Influence of Fast Molecular Motions on Deuterium Powder Spectra

The contribution of the quadrupolar interaction to the NMR spectrum is sensitive to molecular dynamics: the deuterium line shape varies according to the kind of motion and the correlation time.[9, 2] The rate of molecular reorientations is referred to the spectroscopic time scale. A motion is fast if the correlation time τ_c satisfies the condition: $\tau_c \ll \tau_{NMR} \approx Q_0^{-1} \approx 10^{-6}$ s. If we take into account a single C-^{2}H bond involved in a fast reorientation, then a dynamical exchange among the different positions occupied by the C-^{2}H bond during the motion occurs. The final EFG tensor experienced by the nucleus is then the average of all tensors of the positions occupied during the motion. As a consequence, even if the single tensors are axially symmetric, the average EFG tensor can have a less than cylindrical symmetry, hence the average asymmetry parameter can be: $\overline{\eta} \neq 0$. The first order quadrupolar perturbation can then be calculated by using the more general form of the Equation 2.2.4:[2]

$$E_m^{(1)} = \frac{1}{2} h \,\overline{\delta}^* \,(3\cos^2 \Theta - 1 + \overline{\eta} \sin^2 \Theta \cos 2\Phi)\left[m^2 - \frac{1}{3} I(I+1) \right] \qquad [2.4.1]$$

The angles Θ and Φ specify the orientation of B_0 with respect to the PAS of the average EFG tensor. $\overline{\delta}^* = k\,\overline{V}_{ZZ}$ is the average anisotropy parameter and $\overline{V}_{ZZ}$ is the principal element of the diagonal matrix representing the average EFG tensor. The average asymmetry parameter is defined as $\overline{\eta} = \frac{\overline{V}_{XX} - \overline{V}_{YY}}{\overline{V}_{ZZ}}$. The first-order perturbation of the single quantum transitions will result in a NMR doublet symmetric to a central frequency that is assumed to be $\nu_0 = 0$. The resulting frequencies are:

$$\overline{\nu}' = +\frac{1}{2}\overline{\delta}^*(3\cos^2 \Theta - 1 + \overline{\eta} \sin^2 \Theta \cos 2\Phi) \qquad [2.4.2]$$

$$\overline{\nu}'' = -\frac{1}{2}\overline{\delta}^*(3\cos^2 \Theta - 1 + \overline{\eta} \sin^2 \Theta \cos 2\Phi) \qquad [2.4.3]$$

Also in the case of $\overline{\eta} \neq 0$ it is possible to calculate the intensity of the signal as function of one of the two frequencies. Analogous to the case $\eta = 0$ we consider only one transition $\overline{\nu} = \overline{\nu}'$ and calculate the line shape $f(\overline{\nu})$. The function for the complete spectrum $F(\overline{\nu})$ is

given by superimposing the mirror-symmetric powder pattern $f(-\bar{\nu})$. The line shape for the powder spectrum in the case $\bar{\eta} \neq 0$ has been calculated following the same procedure presented in the previous chapter. A complete description can be found in Ref. 7 of which only the final results will be reported here. The function $f(\bar{\nu})$ assumes different shapes for two different frequency ranges:

If $\nu_2 \leq \bar{\nu} \leq \nu_3$:

$$f(\bar{\nu}) = \pi^{-1}\left[(\nu_3 - \nu_2)(\bar{\nu} - \nu_1)\right]^{-1/2} K\left\{\arcsin\left[\frac{(\nu_3 - \bar{\nu})(\nu_2 - \nu_1)}{(\nu_3 - \nu_2)(\bar{\nu} - \nu_1)}\right]^{1/2}\right\} \qquad [2.4.4]$$

If $\nu_1 \leq \bar{\nu} \leq \nu_2$:

$$f(\bar{\nu}) = \pi^{-1}\left[(\nu_3 - \bar{\nu})(\nu_2 - \nu_1)\right]^{-1/2} K\left\{\arcsin\left[\frac{(\nu_3 - \nu_2)(\bar{\nu} - \nu_1)}{(\nu_3 - \bar{\nu})(\nu_2 - \nu_1)}\right]^{1/2}\right\} \qquad [2.4.5]$$

where by convention $|\nu_3| \geq |\nu_2| \geq |\nu_1|$. K(arcsin k) is the complete elliptic integral of the first kind. For a powder the frequency $|\nu_3| = \bar{\delta}^* = k\,\bar{\nabla}_{ZZ}$ is obtained by introducing $\Theta = 0$ in the Equation 2.4.2. It is defined as the resonance frequency of all the crystallites that yield an EFG tensor with the principal axis $\bar{\nabla}_{ZZ}$ oriented parallel to the external field B_0. The other two frequencies are defined as: $|\nu_1| = \frac{1}{2}\bar{\delta}^*(1+\bar{\eta}) = k\,\bar{\nabla}_{XX}$ and $|\nu_2| = \frac{1}{2}\bar{\delta}^*(1-\bar{\eta}) = k\,\bar{\nabla}_{YY}$. An example of the spectrum calculated by using the Eq. 2.4.4 and 2.4.5 in case $\bar{\eta} = 0.4$ for one and for both transitions is reported in Figures 2.6a and b respectively.

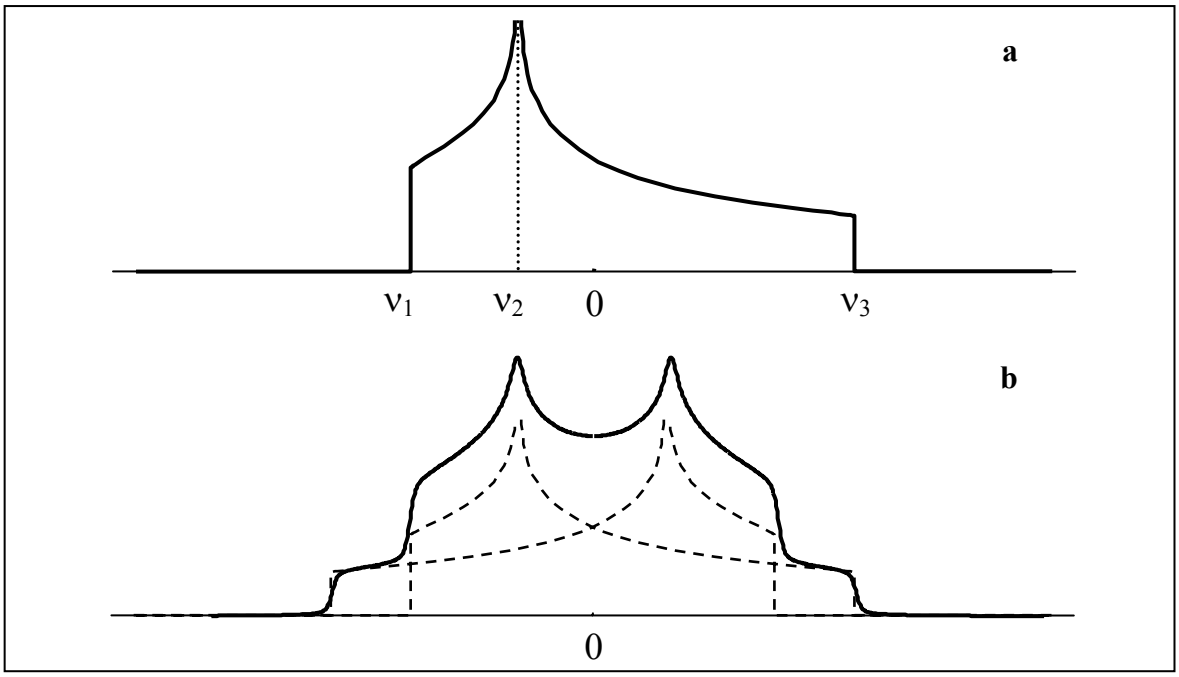

Figure 2.6: Powder pattern calculated in case the average asymmetry parameter has the value $\overline{\eta} = 0.4$ **a**) for the transition corresponding to the frequency ν. **b**) Representation of the function F(ν) (dashed line) and convolution of F(ν) with a Gauss-Lorentz function of the individual resonance lines (solid line).

Some particular reorientations of the deuterated molecules or molecular groups, i.e. a free uniaxial rotation or jumps between N sites about a C_N symmetry axis with $N \geq 3$, yield an average tensor that is axially symmetric.

If $\overline{\eta} = 0$, two of the components of the EFG tensor have the same value: $\left|\overline{V}_{XX}\right| = \left|\overline{V}_{YY}\right| = \frac{\left|\overline{\nu}_{//}\right|}{2k} = \frac{\left|\overline{\nu}_{\perp}\right|}{k}$. Therefore the average anisotropy parameter, as for the rigid limit case, $\overline{\delta}^* = k\left|\overline{V}_{ZZ}\right| = \left|\overline{\nu}_{//}\right| = \left|\nu_3\right|$ correspond to the frequency splitting of the internal doublet $\overline{\delta}^* = \Delta\nu_Q$. The pattern will hold the Pake shape, but the splitting $\overline{\delta}^*$ of the internal doublet will be reduced with respect to the rigid limit case (δ^*). The reduction gives information on the axis of rotation as will be explained in the forthcoming section.

In the limit of isotropic motion, as in liquids, the quadrupole interaction is averaged to zero and the Pake doublet will collapse into a narrow Lorentzian component at the frequency ν_0.

In case of the coexistence of deuterium nuclei with different dynamical behavior, the ^{2}H NMR spectrum results by the superposition of the different contributions.

2.5 Simulation of Fast Motions

It is possible to derive information about the dynamics occurring in solid powder samples by simulating the molecular reorientation that averages the EFG tensor of the crystallites, in such a way that the experimental results can be reproduced. The calculation of how motions modify the EFG tensor (expressed in Hz), experienced by the nucleus will be illustrated using the parameters $\bar{\eta} = \frac{\nu_1 - \nu_2}{\nu_3} = \frac{\bar{V}_{XX} - \bar{V}_{YY}}{\bar{V}_{ZZ}}$ and $\bar{\delta}^* = |\nu_3|$.

In the assumption of fast molecular reorientation the line shape can be simulated by considering a dynamical exchange among *N* different positions occupied by the C-^{2}H bond during the motion. First of all it is convenient to choose a coordinate system in which all the EFG tensors can be added. If we consider, for example, a uniaxial molecular reorientation, a proper coordinate system is chosen with one axis coincident with the molecular rotation axis. It is possible to relate the elements of the EFG tensor in the principal axis system (PAS) to those in the reference frame using the appropriate rotation matrices. The frame of reference is correlated to the PAS through rotations by the triplet of Euler angles: α, β and γ. A generic triplet of Euler angles used to characterize the relative orientation of two coordinate axis systems a and b is given in Figure 2.7.

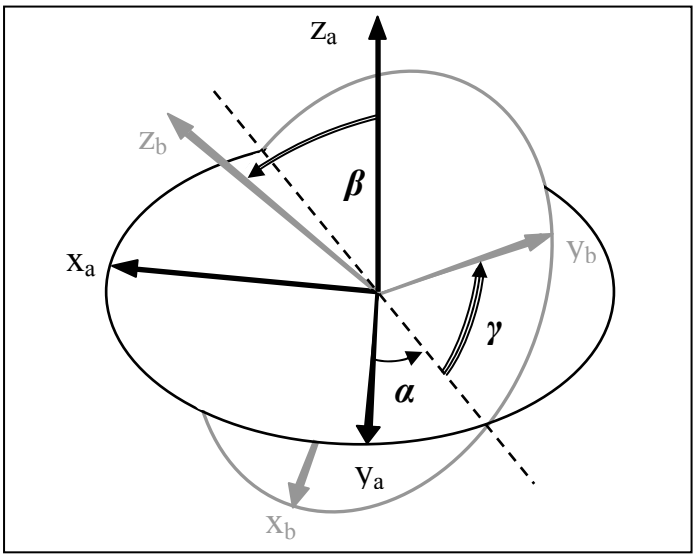

Figure 2.7: Graphical representation of Euler angles (α,β,γ) in the Rose convention.

The procedure to accomplish an axis system transformation using the Euler angles[10] is shown in three steps in Figure 2.8. The first step is a rotation by the angle α about the z

axis of the starting frame, to define the axes x' and y', the second step is a rotation by an angle β about y' to get x" and z" and finally γ defines a rotation angle about z". Anticlockwise rotations are considered to be positive.

The matrix representing the electric field gradient tensor, for a deuterium nucleus, in the PAS, with the components expressed in frequency units, is:

$$k^*\hat{V}_{PAS} = \begin{pmatrix} \mp\frac{1}{2}\delta^* & 0 & 0 \\ 0 & \mp\frac{1}{2}\delta^* & 0 \\ 0 & 0 & \pm\delta^* \end{pmatrix} \qquad [2.5.1]$$

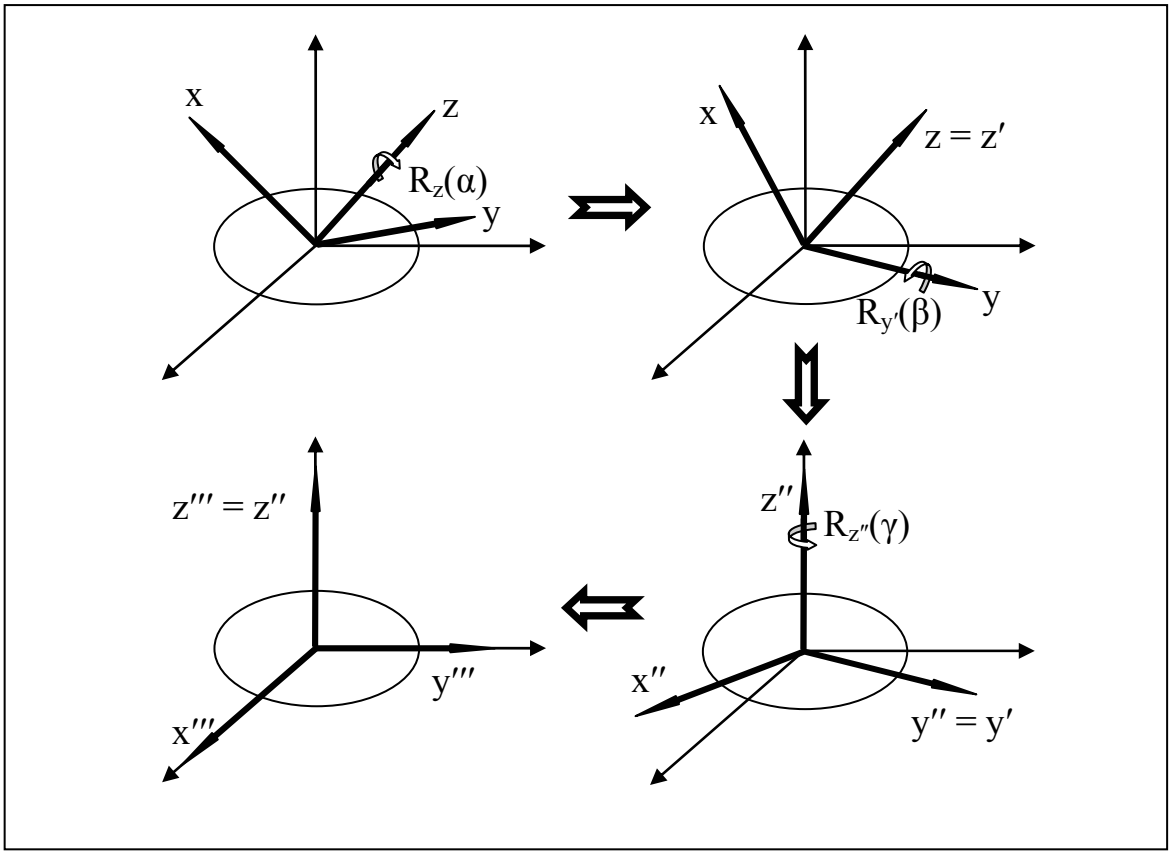

Figure 2.8: Three steps process for bringing an arbitrarily oriented coordinate axis systems (x,y,z) to a desired orientation (x‴,y‴,z‴) by using the Euler angles (α,β,γ) defined according to the convention of Rose.[10]

The tensor $\hat{V}_l$ expresses the tensor $\hat{V}_{PAS}$ in the chosen coordinate axis system and is given by the transformation:

$$\hat{V}_l = \tilde{R}(\alpha,\beta,\gamma)\,\hat{V}_{PAS}\,\tilde{R}^{-1}(\alpha,\beta,\gamma) \qquad [2.5.2]$$

where the rotation matrix $\tilde{R}$ is defined as:

$$\tilde{R}(\alpha,\beta,\gamma) = R_z^T(\gamma)\,R_y^T(\beta)\,R_z^T(\alpha) \qquad [2.5.3]$$

$$\tilde{R}(\alpha,\beta,\gamma) = \begin{pmatrix} \cos\gamma & \sin\gamma & 0 \\ -\sin\gamma & \cos\gamma & 0 \\ 0 & 0 & 1 \end{pmatrix}\begin{pmatrix} \cos\beta & 0 & -\sin\beta \\ 0 & 1 & 0 \\ \sin\beta & 0 & \cos\beta \end{pmatrix}\begin{pmatrix} \cos\alpha & \sin\alpha & 0 \\ -\sin\alpha & \cos\alpha & 0 \\ 0 & 0 & 1 \end{pmatrix} \qquad [2.5.4]$$

Fast molecular motions are then taken into account by dividing the motion into N-1 steps and calculating the electric field tensor in the common axis system for each step. By adding all these tensors and dividing by N, the average tensor is found. For instance when an active rotation (for the definition of active and passive rotation (see Appendix A) of the molecule over an angle ε_u about an axis u is considered, the EFG tensor in the reference frame is calculated for each position s_n, (with $1 \le n \le N$), which correspond to a rotation over $\varepsilon_{u(n)} = \frac{(n-1)\varepsilon_u}{N-1}$ about the u-axis, (Figure 2.9) via Equation 2.5.5:

$$\hat{V}_n = R(\varepsilon_{u(n)})\,\hat{V}_l\,R^{-1}(\varepsilon_{u(n)}) \qquad [2.5.5]$$

where $R(\varepsilon_u)$ is the rotation matrix for a rotation ε_u about the u-axis.

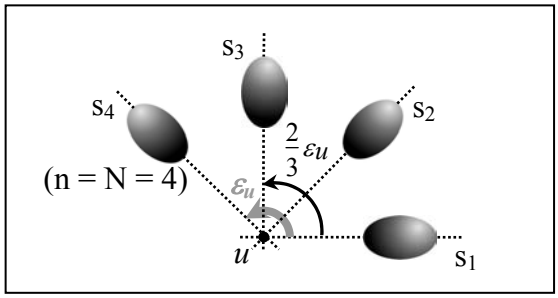

Figure 2.9: Representation of a EFG tensor during a rotation of a ^{2}H atom about an axis u by an angle ε_u in N-1 = 3 steps. Each position s_n results from a rotation by an angle $\frac{n-1}{3}\varepsilon_u$.

After adding the corresponding matrix elements of all $k\,\hat{\mathrm{V}}_n$ and dividing by *N*, an averaged tensor is obtained, which by diagonalization yields:

$$k\,\hat{\bar{\mathrm{V}}}_{PAS} = \begin{pmatrix} \mp\frac{1}{2}\bar{\delta}^*(1+\bar{\eta}) & 0 & 0 \\ 0 & \mp\frac{1}{2}\bar{\delta}^*(1-\bar{\eta}) & 0 \\ 0 & 0 & \pm\bar{\delta}^* \end{pmatrix} \qquad [2.5.6]$$

The diagonal components ν_1, ν_2 and ν_3, are the frequencies of the spectral discontinuities. The NMR spectrum for the reorientational model considered is calculated by introducing these three values in the Equations 2.4.4 and 2.4.5.

For free uniaxial rotation and for jumps between *N* sites about a C_N symmetry axis with $N \geq 3$, the average tensor is axially symmetric ($\bar{\eta} = 0$) and the $\bar{\mathrm{V}}_{ZZ}$ component of the averaged tensor coincides with the rotation axis. In this case Equation 2.5.6 becomes:

$$k\,\hat{\bar{\mathrm{V}}}_{PAS} = \begin{pmatrix} \mp\frac{1}{4}\delta^*(3\cos^2\beta - 1) & 0 & 0 \\ 0 & \mp\frac{1}{4}\delta^*(3\cos^2\beta - 1) & 0 \\ 0 & 0 & \pm\frac{1}{2}\delta^*(3\cos^2\beta - 1) \end{pmatrix} \qquad [2.5.7]$$

The features $\nu_1 = \nu_2 = \nu_\perp$ and $\nu_3 = \nu_{//}$ and consequently the splitting between the resonances arising from the perpendicular components $\Delta\nu_Q$, are scaled down by a factor dependent on the angle β that the C-^{2}H bond forms with the rotation axis. This reduction is expressed for the averaged asymmetry parameter $\bar{\delta}^* = \Delta\nu_Q$ as:

$$\bar{\delta}^* = \frac{1}{2}\delta^*\,(3\cos^2\beta - 1) \qquad [2.5.8]$$

Since a fast free uniaxial rotation yields a Pake pattern, from the observation of the spectral parameter $\Delta\nu_Q$ and by Equation 2.5.8, it is possible to determine the tilt angle β.

2.6 Examples of Motion

An example of how deuterium NMR spectroscopy gives information about the molecular motion is now discussed. To this purpose a ^{2}H bound to an aromatic carbon is considered. Two reorientations will be separately analysed: a 180° jump from site s_1 to site s_2 about an C_2 symmetry axis as shown in Figure 2.10 and a free uniaxial rotation about the same axis.

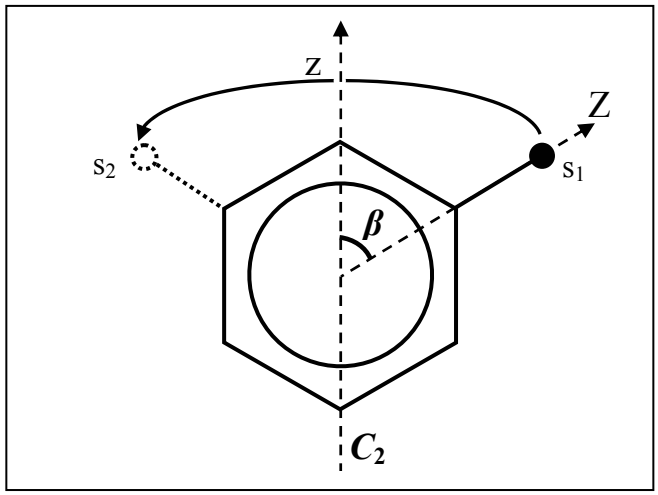

Figure 2.10: Schematic representation of an aromatic deuterium rotating about the C_2 symmetry axis from site s_1 to site s_2.

2.6.1 The Static Case

For an aromatic deuterium the static anisotropy parameter is δ^*_{ph} = 137 kHz[11] and the spectral features of the static spectrum are $\nu_1 = \nu_2 = \pm$ 68.5 kHz and $\nu_3 = \mp$137 kHz (Figure 2.11a). These three values constitute the three components of the diagonal matrix $k\,\hat{V}_{PAS}$ expressed in Equation 2.5.1.

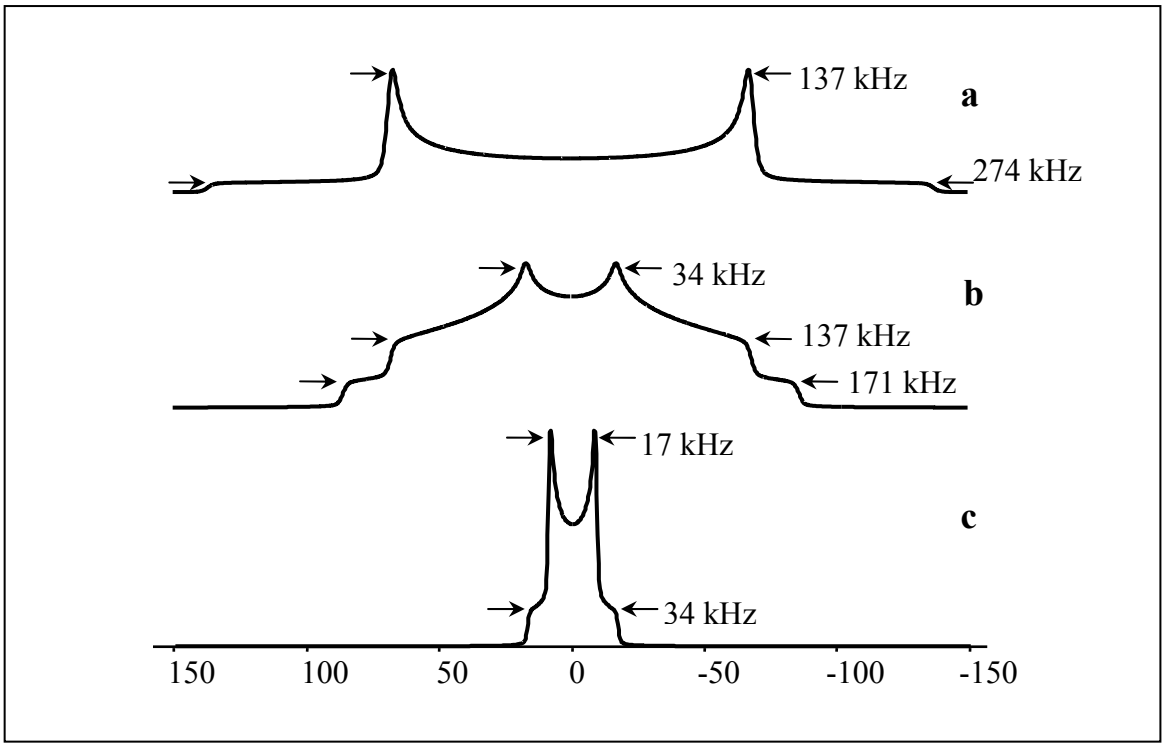

Figure 2.11: Simulated spectra of a ^{2}H of a phenyl group for: **a**) the static case; **b**) a 180° jump of an aromatic deuteron about the C_2 axis defined in Figure 2.10; **c**) a free rotation about the C_2 symmetry axis.

2.6.2 Two-Site Jump

As described before, the first step to the simulation of the line shape consists in the calculation of the matrix $k\,\hat{\mathrm{V}}_1$. Because of the axial symmetry of the EFG tensor, only one component of the Euler triplet, i.e. the angle β, is relevant for the coordinate transformation from the PAS (XYZ) to a new axis system (xyz). By choosing the Y-axis as the rotation axis the matrix $\widetilde{R}$ is:

$$\widetilde{R} = (0, \beta, 0) = \begin{pmatrix} \cos\beta & 0 & -\sin\beta \\ 0 & 1 & 0 \\ \sin\beta & 0 & \cos\beta \end{pmatrix} \qquad [2.6.1]$$

$\widetilde{R}$ is calculated for $\beta = 60°$ and the result is introduced in the Equation 2.5.2 to give the tensor $k\,\hat{\mathrm{V}}_1$.

Then, in the xyz axes system the tensor is rotated by 180° about the z axis. The transformation matrix *R* becomes:

$$R = (0, 0, \varepsilon_z) = \begin{pmatrix} \cos\varepsilon_z & -\sin\varepsilon_z & 0 \\ \sin\varepsilon_z & \cos\varepsilon_z & 0 \\ 0 & 0 & 1 \end{pmatrix} \qquad [2.6.2]$$

Equation 2.6.2 for $\varepsilon_z = 180°$ is substituted in the Equation 2.5.5 and the tensor relative to the deuterium in the site s_2 ($k\,\hat{V}_2$) is also determined. The average of the two tensors, expressed as a diagonal matrix gives the values of the three frequencies $\nu_1 \cong \mp 17$ kHz, $\nu_2 \cong \mp 68.5$ kHz and $\nu_3 \cong \pm 85.5$ kHz ($\overline{\eta} \cong 0.6$ and $\overline{\delta}^* \cong 85.5$). The line shape, calculated as described in Chapter 2.4, is displayed in Figure 2.11b.

2.6.3 Free Uniaxial Rotation

In this case the phenyl ring sweeps out a cylinder and the simulated spectrum (Fig. 2.11c) holds the Pake pattern, i.e. $\overline{\eta} = 0$. According to Equation 2.5.8 the spectral parameters are scaled down by: $\overline{\delta}^* = \frac{1}{2}\delta^*_{ph}\,(3\cos^2\frac{\pi}{3} - 1) = \frac{1}{8}\delta^*_{ph} \cong 17$ kHz.

This example clearly outlines that by comparison of the calculated with the experimental spectral features ^{2}H NMR spectroscopy is very effective to detect the type of motion occurring.

2.7 Experimental Aspects of Deuterium NMR Spectroscopy

The simulated pattern of deuterium nuclei displayed in Figures 2.11a and b show that the experimental spectra are expected to extend over a wide range of frequencies. Several practical problems arise when such broad spectra have to be recorded and sometimes spectral distortions are experimentally observed. The difficulties in the acquisition of such broad spectra are related to the following experimental difficulties:

- The pulses have to be very short and, consequently, high-power has to be used, to uniformly excite the complete frequencies range. Due to the finite length t_n of the n^{th} rf pulse[12] a precession of the nuclear spins due to quadrupolar interaction during the rf pulse can take place for those components $f(\nu)$ of the line shape that are sufficiently far from the Larmor frequency $\omega_0 = 2\,\pi\,\nu_0$. This leads to distortions of the spectrum which can not always be experimentally eliminated.
- The signal decay is very fast and a fast digitizer is required. Furthermore a great part of the signal can get lost in the dead time of the receiver after the strong pulse.
- The pulses have to be perfectly set to 90°.

A great contribution to minimize the distortion effects arising from the experimental limits to these requirements is given by the use of the two pulse quadrupolar echo sequence,[13, 14] and a proper phase cycling, both described in the next section.

2.7.1 Quadrupolar Echo Sequence

The quadrupolar-echo pulse sequence is related to the Hahn-echo sequence used to measure T_2 values. A schematic representation of the Hahn-echo pulse sequence with the vector model is presented in Figure 2.12. Unfortunately this vector model can not be used to describe the behaviour of the spins for nuclei with spin I =1 as there are three states available. A treatment of the quadrupolar-echo pulse sequence using the operator formalism will now be given. In order to understand the following quantum-mechanical treatment, a short introduction of the quantum-mechanical operators recurring in the text is now necessary. For a detailed treatment of this matter the books of Abragam,[2] Ernst[15] and Haeberlen[7] are recommended.

The state of the spins is described by a density operator $\hat{\rho}(t)$, while the interaction that modifies the state of the system, is expressed by a Hamiltonian. The general equation that describes the change of the density operator under the effect of the Hamiltonian $\hat{\mathrm{H}}$ is the Liouville-von Neumann equation:

$$\frac{\mathrm{d}}{\mathrm{dt}}\hat{\rho} = -\mathrm{i}\left[\hat{\mathrm{H}}, \hat{\rho}\right] \qquad [2.7.1]$$

By comparison with the Schrödinger equation $\frac{d}{dt}\Psi = -i\hat{H}\Psi$ Equation 2.7.1 can be considered as the "Schrödinger equation" for the density operator. If $[\hat{H}, \hat{\rho}] = 0$, i.e. the Hamilto operator commutes with the density operator, the density operator $\hat{\rho}(t)$ remains constant with time. If the system is perturbed by an Hamiltonian $\hat{H}$ independent of time: $\frac{\partial \hat{H}}{\partial t} = 0$, the solution of Equation 2.7.1 is the "sandwich" expression:

$$\hat{\rho}(t) = e^{-\frac{i}{\hbar}\hat{H}t}\ \hat{\rho}(t_0)\ e^{\frac{i}{\hbar}\hat{H}t} \qquad [2.7.2]$$

The system, characterized by the density operator $\hat{\rho}(t_0)$ at a time t_0, evolves in time to a new state $\hat{\rho}(t)$ calculated through the operator:

$$\hat{U}(t) = e^{-\frac{i}{\hbar}\hat{H}\tau} \qquad [2.7.3]$$

called "propagator".

The quadrupolar-echo sequence (Figure 2.13) can be explained by observing the time evolution in the intervals t_n - t_{n-1}.

For the case of axially symmetric electric field gradients the quadrupolar Hamiltonian is expressed by the equation:

$$\hat{H}_Q^{(1)} = \frac{1}{2}h\,\overline{\delta}\,(3\cos^2\Theta - 1)\left[\hat{I}_z^2 - \frac{1}{3}I(I+1)\right] \qquad [2.7.1]$$

Substituting the value I =1 and assuming $\nu_q = \frac{1}{2}\overline{\delta}\,(3\cos^2\Theta - 1)$ and $\omega_q = 2\,\pi\,\nu_q$:

$$\hat{H}_Q^{(1)} = \hbar\,\omega_q\left(\hat{I}_z^2 - \frac{2}{3}\right) \qquad [2.7.2]$$

The equilibrium density operator $\hat{\rho}(t_0)$ is:[16]

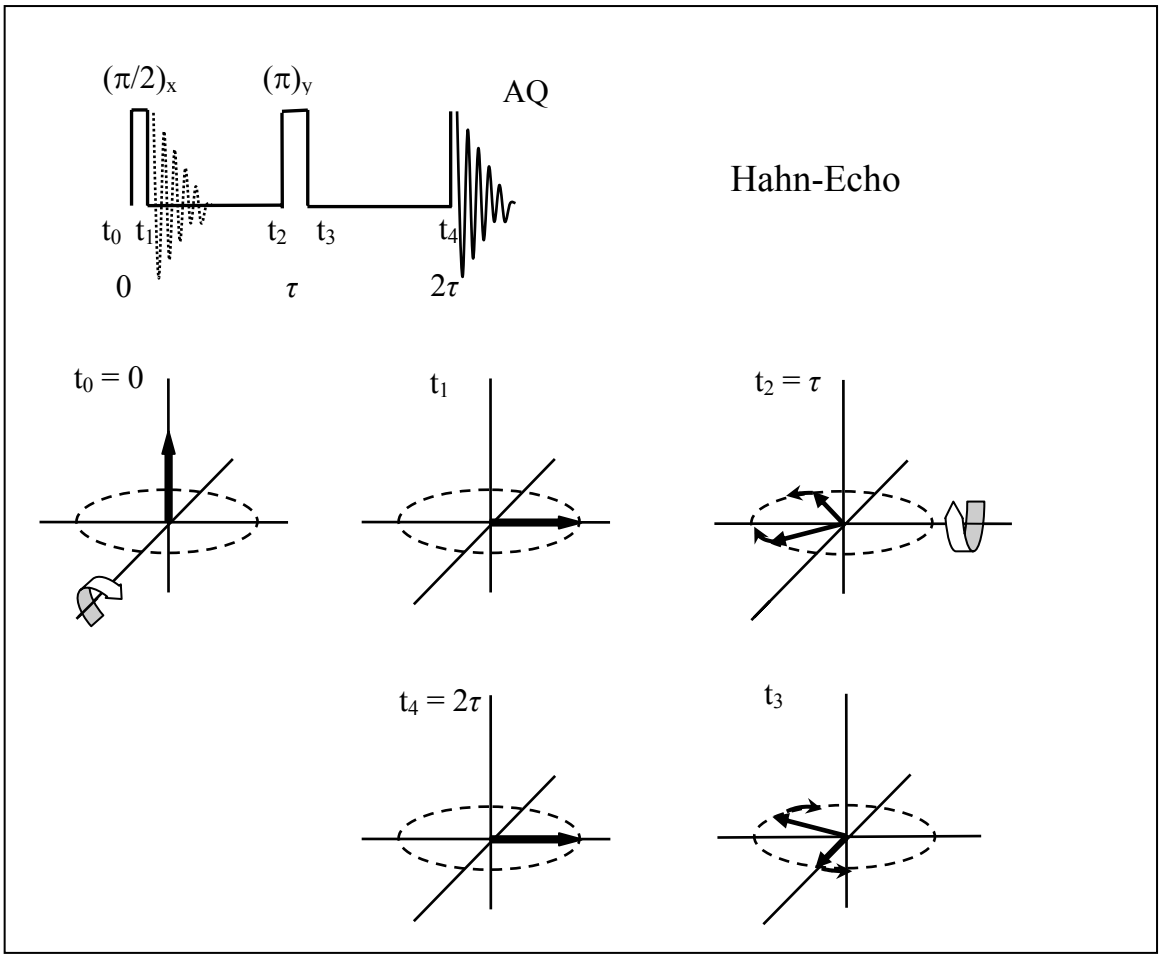

Figure 2.12: Schematic representation of the Hahn-echo pulse sequence and illustration of its effect on the spins with the vector model.

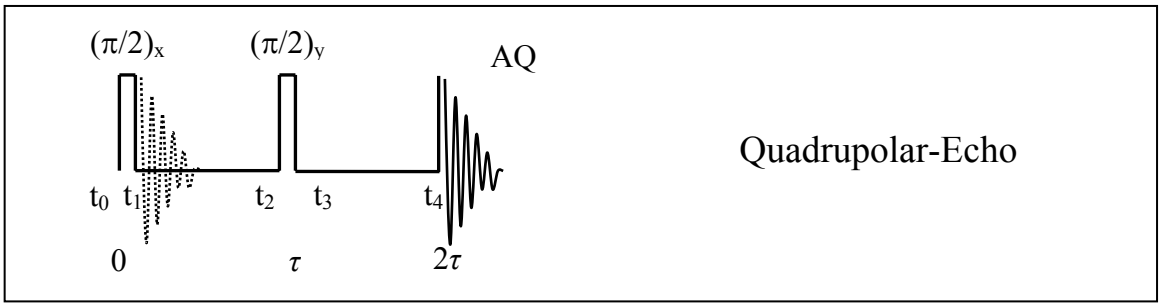

Figure 2.13: Schematic representation of the quadrupolar-echo pulse sequence

$$\hat{\rho}(t_0) = \hat{I}_z \qquad (\text{for } \gamma B_0 \gg \overline{\delta}^*) \qquad [2.7.3]$$

Given the RF Hamiltonian $H_{RF}= -\gamma h\, B_1 \hat{I}_x$ ($\gamma B_1 >> \bar{\delta}^*$), after the first 90° pulse of length $\tau_p = \frac{\pi}{2\gamma B_1}$ the density operator becomes:

$$\hat{\rho}(t_1) = e^{-\frac{i}{\hbar}\hat{H}_{RF}\tau_p}\ \hat{\rho}(t_0)\, e^{\frac{i}{\hbar}\hat{H}_{RF}\tau_p} = e^{i\frac{\pi}{2}\hat{I}_x}\ \hat{I}_z\ e^{-i\frac{\pi}{2}\hat{I}_x} = \\ = \hat{I}_z \cos\left(-\frac{\pi}{2}\right) - \hat{I}_y \sin\left(-\frac{\pi}{2}\right) = \hat{I}_y \qquad [2.7.4]$$

Equation 2.7.4 was calculated referring to the general expression:

$e^{i\phi\hat{A}}\ \hat{B}\, e^{-i\phi\hat{A}} = \hat{B}\cos(a\,\phi) - \hat{C}\sin(a\,\phi)$, where $\left[\hat{A},\hat{B}\right] = i\,a\,\hat{C}$.

During the first free evolution interval t_n - t_{n-1} = τ the sandwich propagator expression assumes the form:

$$\hat{\rho}(t_2) = e^{-\frac{i}{\hbar}\hat{H}_Q^{(1)}\tau}\ \hat{\rho}(t_1)\, e^{+\frac{i}{\hbar}\hat{H}_Q^{(1)}\tau} = e^{-i\omega_q\left(\hat{I}_z^2 - \frac{2}{3}\right)\tau}\ \hat{I}_y\ e^{+i\omega_q\left(\hat{I}_z^2 - \frac{2}{3}\right)\tau} \qquad [2.7.5]$$

This expression can be worked out using the commutator[17] $\left[\hat{I}_z^2 - \frac{2}{3}, \hat{I}_y\right] = -i\,(\hat{I}_z\hat{I}_x + \hat{I}_x\hat{I}_z)$, then the density operator is expressed as:

$$\hat{\rho}(t_2) = \hat{I}_y\cos(\omega_q\tau) - (\hat{I}_z\hat{I}_x + \hat{I}_x\hat{I}_z)\sin(\omega_q\tau) \qquad [2.7.6]$$

At the time $t = t_3$ just after the second 90° pulse along y, the density operator becomes:

$$\hat{\rho}(t_3) = e^{\frac{i\pi}{2}\hat{I}_y}\ \hat{\rho}(t_2)\, e^{-\frac{i\pi}{2}\hat{I}_y} = \\ = \hat{I}_y\cos(\omega_q\tau) - \sin(\omega_q\tau)\left\{e^{\frac{i\pi}{2}\hat{I}_y}\ (\hat{I}_z\hat{I}_x + \hat{I}_x\hat{I}_z)\, e^{-\frac{i\pi}{2}\hat{I}_y}\right\} \qquad [2.7.7]$$

The commutator required in this case is $\left[\hat{I}_y, \hat{I}_z\hat{I}_x + \hat{I}_x\hat{I}_z\right] = -2i\,(\hat{I}_z^2 - \hat{I}_x^2)$ and Equation 2.7.7 can be further evaluated:

$$\hat{\rho}(t_3) = \hat{I}_y\cos(\omega_q\tau) - \sin(\omega_q\tau)\left\{(\hat{I}_z\hat{I}_x + \hat{I}_x\hat{I}_z)\cos(\pi) - (\hat{I}_z^2 - \hat{I}_x^2)\sin(\pi)\right\} = \\ = \hat{I}_y\cos(\omega_q\tau) + (\hat{I}_z\hat{I}_x + \hat{I}_x\hat{I}_z)\sin(\omega_q\tau) \qquad [2.7.8]$$

The commutators required to calculate the reduced density operator after the evolution time $t = 2\tau$ are $\left[\hat{I}_z^2 - \frac{2}{3}, \hat{I}_y\right] = -i\,(\hat{I}_z\hat{I}_x + \hat{I}_x\hat{I}_z)$ and $\left[\hat{I}_z^2 - \frac{2}{3}, \hat{I}_z\hat{I}_x + \hat{I}_x\hat{I}_z\right] = i\,\hat{I}_y$. The density operator at the time $t = t_4$ assumes the value:

$$\begin{aligned}\hat{\rho}(t_4) &= \mathrm{e}^{-i\omega_q\left(\hat{I}_z^2-\frac{2}{3}\right)2\tau}\left\{\hat{I}_y\cos(\omega_q\tau) + (\hat{I}_z\hat{I}_x + \hat{I}_x\hat{I}_z)\sin(\omega_q\tau)\right\}\mathrm{e}^{+i\omega_q\left(\hat{I}_z^2-\frac{2}{3}\right)2\tau} = \\ &= \cos(\omega_q\tau)\left\{\hat{I}_y\cos(\omega_q\tau) - (\hat{I}_z\hat{I}_x + \hat{I}_x\hat{I}_z)\sin(\omega_q\tau)\right\} + \\ &+ \sin(\omega_q\tau)\left\{(\hat{I}_z\hat{I}_x + \hat{I}_x\hat{I}_z)\cos(\omega_q\tau) + \hat{I}_y s\sin(\omega_q\tau)\right\} = \\ &= \hat{I}_y\end{aligned} \qquad [2.7.9]$$

After a delay τ following the second $\pi/2$ pulse the magnetization refocuses along the y axis, independent of the value of ω_q. The advantage of using this pulse sequence is that the acquisition has to start a time τ after the last pulse, thereby avoiding that data points at the beginning of the FID can get lost during the receiver dead time. Since these initial data points determine the pattern at the outer limits of the spectrum, the echo sequence removes this source of distortion. An example of the dramatic improvement in the spectral line shape is given in Figure 2.14.

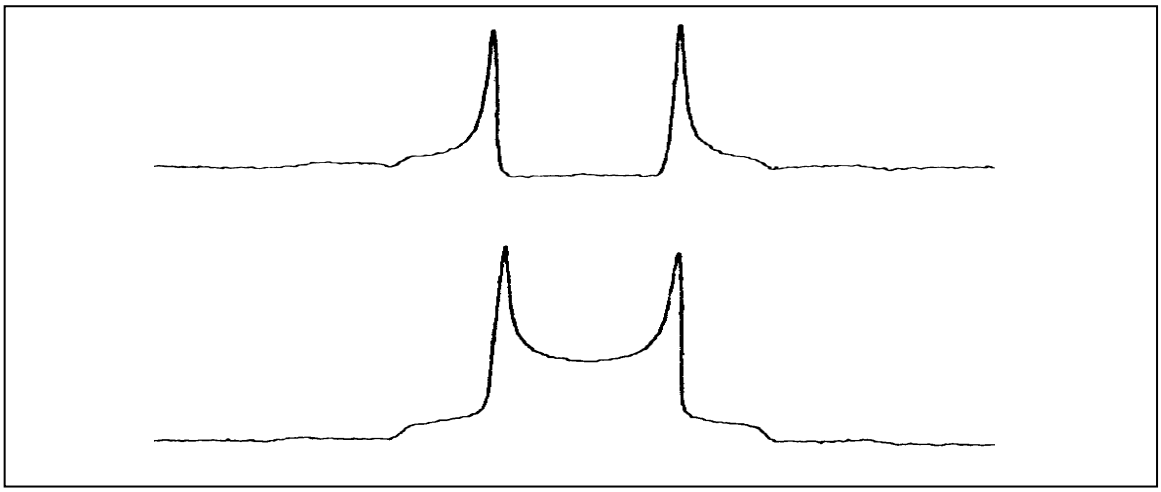

Figure 2.14: Comparison between two spectra of perdeuterated plexiglass acquired **a**) after a 90° pulse and **b**) after a quadrupolar-echo sequence (Ref. 11 p.84).

Calculations for a quadrupolar echo sequence in which the second pulse is $-(\pi/2)$ brings the same result, i.e. the echo is independent of the sign of the second pulse. This can be used to eliminate spurious signals. In fact if the pulse lengths are not exactly 90° there is a residual magnetization along the z axis after the first pulse, which is flipped into the *xy* plan by the second $\pi/2$ pulse. In a phase cycle the use of alternate phases of the second pulse cancels the contribution to the signal due to this undesired magnetization, while the quadrupolar echo signals add up. An example of a phase cycling procedure aimed to suppress unwanted signals and double-quantum coherence-transfer artefacts is proposed by Ronemus *et al*.[18]

Bibliography

1) Harris, R. K. *Nuclear Magnetic Resonance Spectroscopy*; Longman Scientific & Technical, 1987.
2) Abragam, A. *The Principles of Nuclear Magnetism*. Eds. Marshall, W. C.; Wilkinson, D. H., Claredon Press, Oxford, 1961.
3) Vega, A. J. *Encyclopedia of Nuclear Magnetic Resonance*. Grant, D. M., Harris, R. K. Eds.; John Wiley & Sons, New York; Vol. 6, p. 3869-3888.
4) Gerstein, B. C.; Dybowski, C. R. *Transient Techniques in NMR of Solids. An Introduction to Theory and Practice*. Academic Press. 1985.
5) Schmidt-Rohr, K.; Spiess, H. W. *Multidimensional Solid State NMR and Polymers*. Academic Press, 1994.
6) Spiess, W. H. NMR Basic Principles and Progress. Eds. Diehl, P.; Fluck, E.; Kosfeld, R., Springer Verlag, Berlin, 1978, Vol. 15.
7) Haeberlen, H. High Resolution NMR in Solids. Selective Averaging, Academic Press, New York, 1976.
8) McBrierty, V. J.; Packer, K. J. *Nuclear Magnetic Resonance in Solid Polymers*. Cambridge University Press, 1993.
9) Mehring, M., In *NMR Basic Principles and Progress*; Diehl, P., Fluck, E., Kosfeld, R., Eds.; Springer-Verlag: West Berlin, 1976; Vol. 11, p. 30.
10) Rose, M. E. *Elementary Theory of Angular Momentum*. Wiley, New York, 1957.

11) Fyfe, C. A. In *Solid State NMR for Chemists*; C.F.C. Press: Guelph, 1983.
12) Bloom, M.; Davis, J. H.; Valic, M. I. *Can. J. Phys.* **1980**, *58*, 1510.
13) Davis, J. H.; Jeffrey, K. R.; Bloom, M.; Valic, M. I.; Higgs, T. P. *Chem. Phys. Lett.* **1976**, *42*, 390.
14) Boden, N.; Levine, Y. K. *J. Magn. Reson.* **1978**, *30*, 327.
15) Ernst, R. R.; Bodenhausen, G.; Wokaun, A. *Principles of Nuclear Magnetic Resonance in One and Two Dimensions* Oxford University Press, **1987**.
16) Veeman, W. S. Lecture notes.
17) Kimmich, R. *NMR Tomography Diffusometry Relaxometry.* Springer-Verlag, Berlin Heidelberg. 1997.
18) Ronemus, A. D.; Vold, R. L.; Vold, R. R. *J. Magn. Reson.* **1986**, *70*, 416.

Chapter 3

Experimental Section

This section describes the sample preparation procedure, followed by the results of the quantitative analysis to determine the sample composition and finally the acquisition parameter of the NMR spectra. The samples were prepared by treating the syndiotactic polystyrene, in the γ and in the δ semicrystalline forms, separately with six different perdeuterated solvents. These are aromatic molecules (benzene-d_6 and toluene-d_8) and halogenated molecules (1,2-dichloroethane-d_4, dichloromethane-d_2, chloroform-d and 1,2-dibromoethane-d_4).

3.1 Preparation of the Samples

Syndiotactic polystyrene in the clathrate form including toluene (δ_{Tol}) was synthesized by using a homogeneous catalyst consisting of $CpTiCl_3$ and methylalumoxane (MAO) in toluene at 50° C.

Samples of s-PS in the empty δ form, were obtained by treatment of the s-PS clathrate form, δ_{Tol}, arising from the polymerization process, with refluxing acetone in a Kumagawa extractor for 5 h, followed by drying at 60 °C for 6 h. The acetone insoluble fraction, consisting of highly syndiotactic polystyrene, is 92 wt.-% of the starting polymer.

s-PS γ was obtained by annealing a sample of the δ_{Tol} sealed *in vacuo* in a glass vial for 3 h at 140 °C.

The perdeuterated solvents were purchased from Cambridge Isotopes and used as received.

Different procedures were used for the preparation of the aromatic and of the halogenated samples. The two methods will be exposed separately in the following sections.

3.1.1 Samples Including Aromatic Molecules

The s-PS samples including benzene-d_6 and toluene-d_8 were prepared using the following procedure. The polymer powder in both the δ and the γ form was mechanically sieved and the fraction with grain size in the range 80-60 Mesh was used for the NMR experiments.

The s-PS powder (1 g) was stirred in an aqueous solution of the appropriate deuterated compound at a concentration in the range 376 ÷ 8100 ppm for a time from 17 h to 30 h at room temperature. The precise conditions are reported in Table 3.1. The powder was separated by filtration and dried at room temperature. The semicrystalline form of each sample was then confirmed by wide-angle-X-ray powder diffraction (WAXS) analysis. A part of these measurements was performed in the department of Physical Chemistry at the University of Salerno and a part in the Department of Inorganic Chemistry at the University of Duisburg by Dr. Westphal. The concentration of deuterated molecules in the s-PS clathrates or swollen s-PS γ samples was determined by comparison of the integrated intensity of the ^2H NMR resonances corresponding to these molecules with those of tetrahydrofurane-d_8 used as internal standard. The NMR samples were prepared by dissolving 60 mg of the clathrated sample in 0.11 ml of $CHCl_3$ solutions containing THF-d_8 (0.17 M).

Table 3.1. Synthesis of the δ-chlatrates and γ swollen s-PS samples

Sample	Concentration of the deuterated compound in the aqueous solution (ppm)	Stirring time (h)	Concentration of the deuterated molecules in the sample [a] (wt.-%)
δ_{Ben}	1660	30	10.2 1.8 [b]
γ_{Ben}	1660	30	4.0
δ_{Tol}	376	17	5.2
γ_{Tol}	515	30	4.3

a) Determined with the NMR method described in the Experimental Section.
b) After evaporating for 13 h at room temperature

3.1.2 Samples Including Halogenated Molecules

Eight samples including halogenated molecules were prepared: the two semicrystalline forms of s-PS, δ and γ, were exposed to the vapors of respectively 1,2-dichloroethane-d_4, dichloromethane-d_2 and chloroform-d for 24 h and 1,2-dibromoethane-d_4 for 48 h as showed in the schematic representation in Figure 3.1.

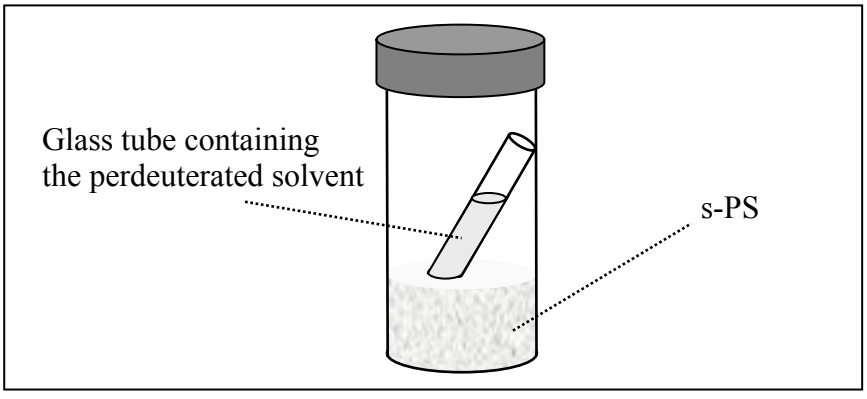

Figure 3.1: Schematic representation of the experimental conditions used to prepare the halogenated samples by sorption from the vapors of the solvent.

The excess of solvent was then evaporated at room temperature for few hours. With respect to the procedure described in the previous section, this method presents the

advantage of requiring a smaller amount of solvent and the possibility to recover from the glass tube the solvent not evaporated. This advantage becomes the more relevant the more expensive the used solvents are, e.g. for 1,2-dichloroethane-d_4.

The percentage of solvent included in each sample was determined via ^2H NMR spectroscopy of the solutions: a weighed amount of the polymer hosting deuterated molecules was dissolved in $CHCl_3$ and the relative intensity of the ^2H signals was determined using an appropriate internal standard. In general chloroform-d was used as reference substance, but for the s-PS samples including $CDCl_3$ the chosen internal standard was benzene-d_6. These measurements were performed on a Bruker DRX 500 spectrometer at 76.75 MHz resonance frequency. The values found for the eight samples are reported in the Table 3.2.

Table 3.2. Concentration of halogenated molecules in δ-chlatrates and γ-swollen s-PS samples.

Sample	Concentration of the deuterated molecules in the sample (wt.-%)
δ_{DCE}	8.9
γ_{DCE}	3.3
δ_{DCM}	8.2
γ_{DCM}	3.2
δ_{CF}	16.4
γ_{CF}	8.3
δ_{DBE}	11.5
γ_{DBE}	7.8

3.2 Acquisition and Processing of the ^2H NMR Spectra

The ^2H NMR measurements on solid samples were performed on a Bruker ASX 400 spectrometer operating at 61.42 MHz with a 7 mm sample tube. The spectra were acquired

using a quadrupole echo pulse sequence, as described in the section 2.7, where an interval $\tau = 40$ μs separates the two 90° pulses of length 4.3 μs. Although these pulses are rather long, the basic results and conclusions of this work are not compromised by a possible small distortion of deuterium line shape.

An appropriate phase cycling procedure was used to suppress artifacts.[1] Spectra were acquired with a 1 MHz spectral width, accumulation of 6 k to 40 k scans and a 2 s recycle time. The temperature was controlled with a flow of N_2 gas and stabilized, with a precision of ± 1° C, with a temperature unit control.

3.3 Simulations

MATHEMATICA® program were developed for simulations of the spectral line shapes. The effective deuterium electric field gradient tensor in case of specific molecular motions was calculated according to the procedure described in the Chapter 2.

Bibliography

1) Ronemus, A. D.; Vold, R. L.; Vold, R. R.; *J. Magn. Reson*. **1986**, *70*, 416.

Chapter 4

^{2}H NMR Investigation

The experimental ^{2}H NMR spectra of the samples investigated are now presented. Each deuterated solvent was analyzed as a guest molecule included in the γ and in the δ form of syndiotactic polystyrene. In the γ semicrystalline form the molecules are hosted only in the amorphous phase, while in the δ form, they are prevalently included in the crystalline cavities to give clathrates.

4.1 Samples Investigated

A schematic description of the preparation of the samples investigated is given in Figure 4.1. Samples of syndiotactic polystyrene (s-PS) were prepared according to the literature procedure (see Chapter 3): typically the s-PS recovered from the reactor is in the toluene δ clathrate form, δ_{Tol}, toluene being the polymerization solvent employed. The "emptied δ-form", δ, was thus obtained by treatment of the δ-clathrate with refluxing acetone as shown in the left part of the scheme in Figure 4.1. Subsequently, δ-clathrates with benzene-d_6 (δ_{Ben}), toluene-d_8 (δ_{Tol}), 1,2-dichloroethane-d_4 (δ_{DCE}), dichloromethane-d_2 (δ_{DCM}), chloroform-d (δ_{CF}), and 1,2dibromoethane-d_4 (δ_{DBE}) were prepared according to the methods described in the Chapter 3. The concentration of the deuterated guest molecules (2 - 16 wt.-%) was determined by integration of the appropriate ^{2}H NMR resonances observed in the solution spectrum of the polymer sample dissolved in $CHCl_3$ containing a weighted amount of a properly chosen internal standard (see Chapter 3). The approximate content of deuterated molecules in the δ-form is reported in brackets in Figure 4.1.

The crystalline phase of s-PS can not exclusively be filled with these solvents because the deuterated molecules are also trapped in the amorphous part. In order to differentiate the ^{2}H signals of the molecules adsorbed in the crystalline phase from those in the amorphous phase of the polymer, a series of s-PS samples in the γ-form hosting the same molecules were prepared (see right side of the scheme in Figure 4.1). The γ semicrystalline form shows a chain conformation similar to the δ-form, but contains no cavities in the crystalline phase and molecules can be hosted only in the amorphous part. The X-ray analysis confirms that the γ samples are not converted to δ-clathrates after treatment with the deuterated solvents.

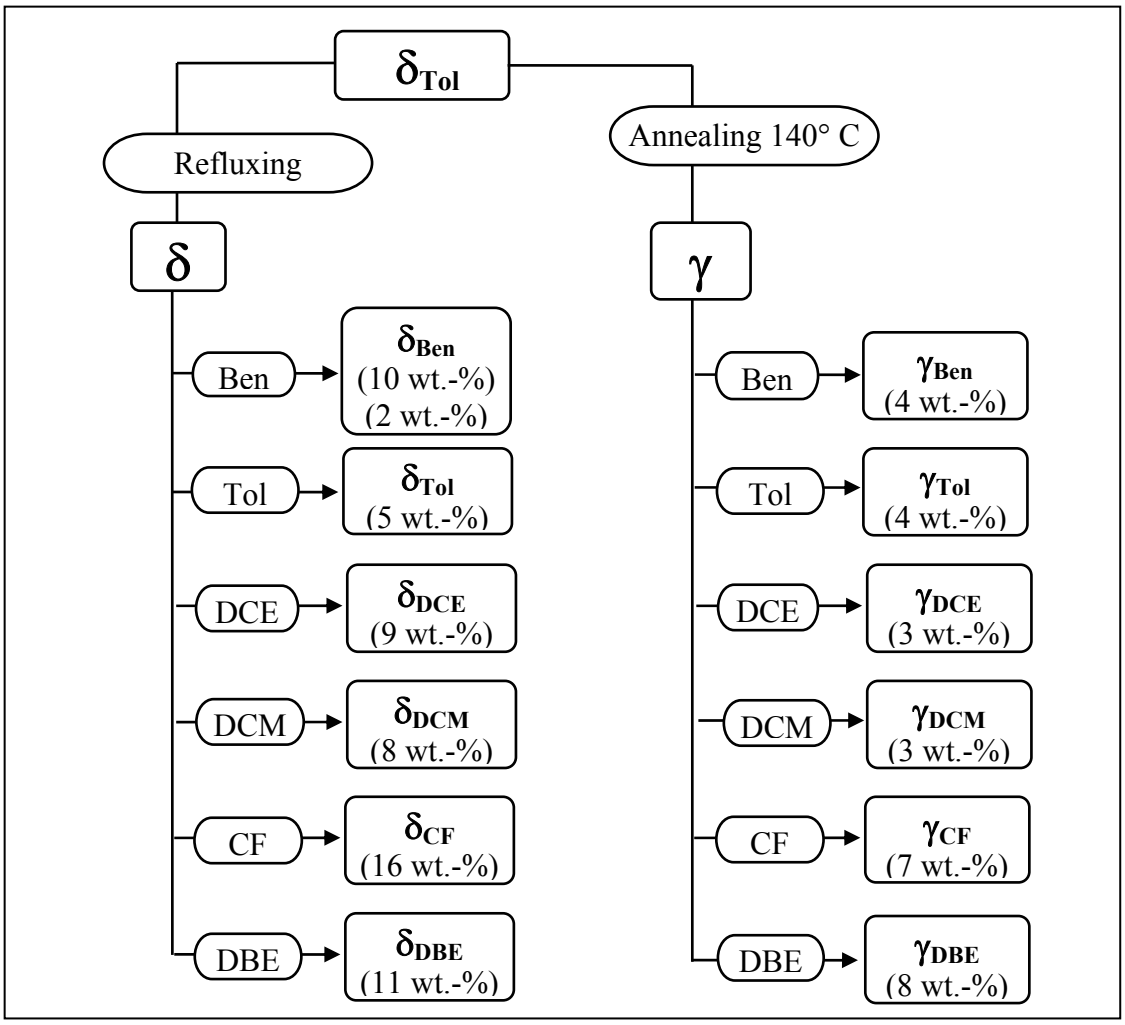

Figure 4.1: Schematic representation of the preparation procedure of the different samples.

In the following sections the results of the NMR analysis of each deuterated solvent included in the two semicrystalline forms are presented.

4.2 Investigation of Aromatic Molecules Hosted in s-PS

4.2.1 Benzene-d_6 ^{2}H NMR Spectra

Solid state ^{2}H NMR spectra (T = 298 K) of benzene included in γ_{Ben} (4.3 wt.-%) and in δ_{Ben} (10.2 wt.-% and 1.8 wt.-%) samples are depicted respectively in Figures 4.2 a, b and c.

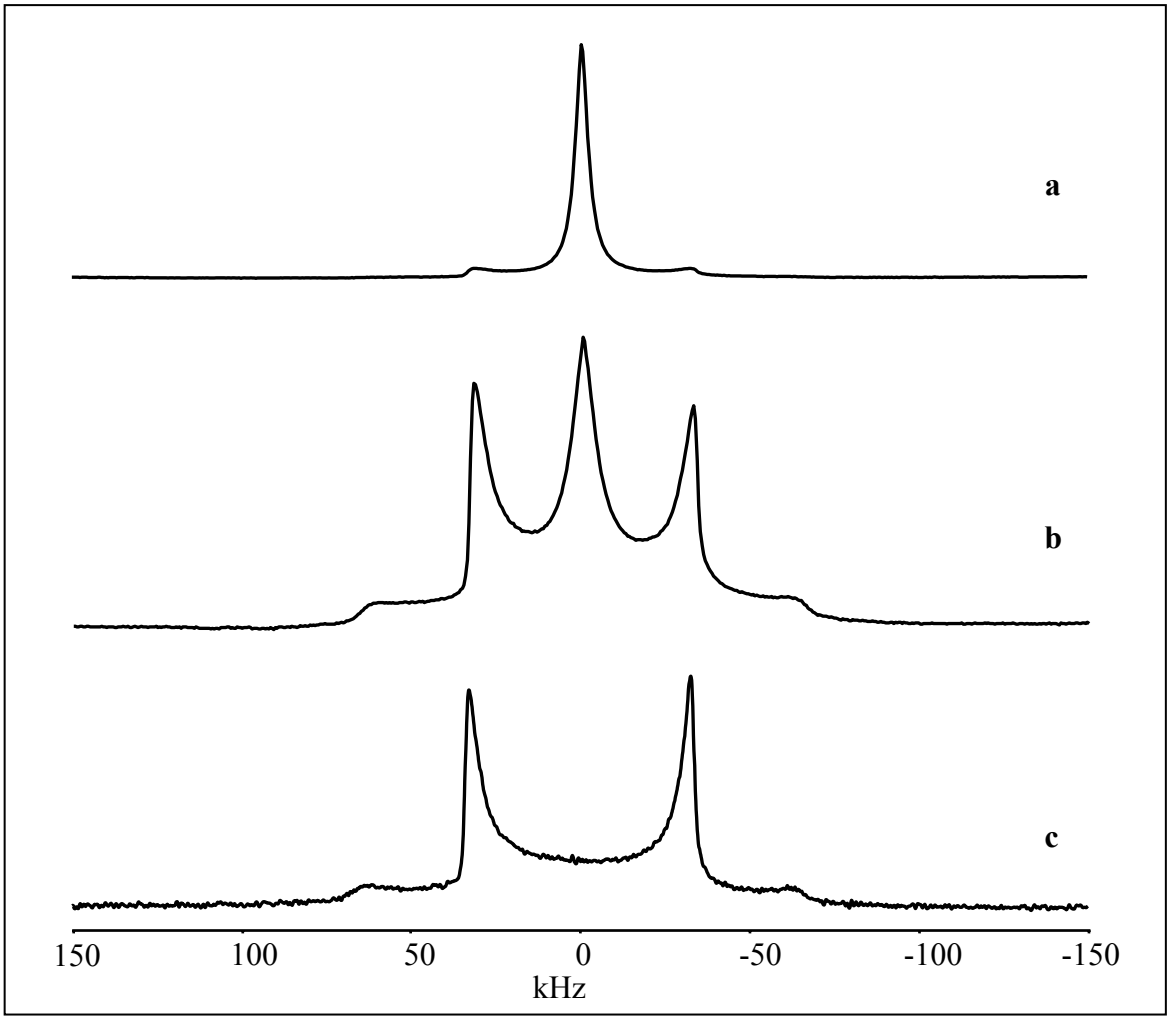

Figure 4.2: Solid state ^{2}H NMR spectra at 298 K of: **a**) γ_{Ben} (4.0 wt.-% of guest molecules); **b**) δ_{Ben} (10.2 wt.-% of guest molecules) and **c**) δ_{Ben} (1.8 wt.-% of guest molecules).

The spectrum of γ_{Ben} where the benzene is exclusively included in the amorphous phase, Figure 4.2a, shows the prevalence of a single line, centred at Larmor frequency ν_0 with a full width at half maximum $\nu_{1/2} \approx 4.0$ kHz that is two orders of magnitude greater than that

expected for the molecules in liquid state. This result reveals that for a large number of included molecules the typical quadrupolar pattern which one would expect in the case of rigid benzene molecules is averaged by motions that are either fast with respect to the ^2H NMR timescale τ_{NMR} (10^{-6} – 10^{-5} s) but at room temperature not completely isotropic, or isotropic but not sufficiently fast. Furthermore, it is possible to distinguish a doublet of lower intensity spaced by 67 kHz. By comparison with the spectrum in Figure 4.2b, the doublet can be considered as a part of a quadrupole pattern attributed to a small rigid fraction of molecules. A much higher concentration of deuterated molecules in γ_{Ben} causes an increase only of the single line intensity in the NMR spectrum. The ^2H NMR spectrum of the more concentrated sample δ_{Ben} (Figure 4.2 b) clearly exhibits a Pake shape pattern with two horns and two shoulders spaced 67 kHz and 134 kHz, respectively. This line shape, according to the theory illustrated in section 2.5, suggests that the benzene molecules in the δ s-PS cavities execute a fast uniaxial reorientational motion. In addition, this spectrum of δ_{Ben} exhibits a signal centred at ν_0 with a line width $\nu_{1/2} \approx 7$ kHz accounting for molecules having a higher degree of reorientational freedom. Considering the high concentration of benzene-d_6 in the sample (10.2 wt.-%), we can attribute this signal to those molecules located in the amorphous phase. In the ^2H NMR spectrum of the less concentrated sample, (1.8 wt.-% of benzene-d_6) (Figure 4.2c) the singlet has disappeared and only the Pake pattern is observed as in Figure 4.2b. Apparently at low concentration the guest molecules are preferably absorbed in the crystalline cavities.

4.2.2 Toluene-d_8 ^2H NMR Spectra

In Figure 4.3 the solid state ^2H NMR spectra of γ_{Tol} (Figure 4.3a) and δ_{Tol} (Figure 4.3b) at 298 K are pictured. The ^2H NMR spectrum of γ_{Tol} at room temperature exhibits a broad triangular signal with $\nu_{1/2} \approx 7$ kHz corresponding to the pseudo-isotropic reorientation of the toluene molecules in the amorphous phase of the polymer. A low intensity doublet with $\Delta\nu_Q = 37$ kHz is also detected and accounts for the presence of a small fraction of molecules constrained in motion showing the same spectral features prevailing in the pattern of the crystalline δ_{Tol} form (Figure 4.3b).

The ^2H NMR spectrum of δ_{tol} exhibits a superposition of signals, each signal accounts for deuterons with different mobility. It is possible to clearly distinguish a broad singlet

centred at ν_0 and a Pake-like pattern consisting of two internal lines spaced $\Delta\nu_Q$ = 37 kHz and two shoulders separated by 72 kHz. Besides this line shape the spectrum presents another doublet with a splitting of 136 kHz that can be attributed to another quadrupolar powder pattern of which the perpendicular edges, expected at 272 kHz, can not be detected as result of the instrumental limitations.

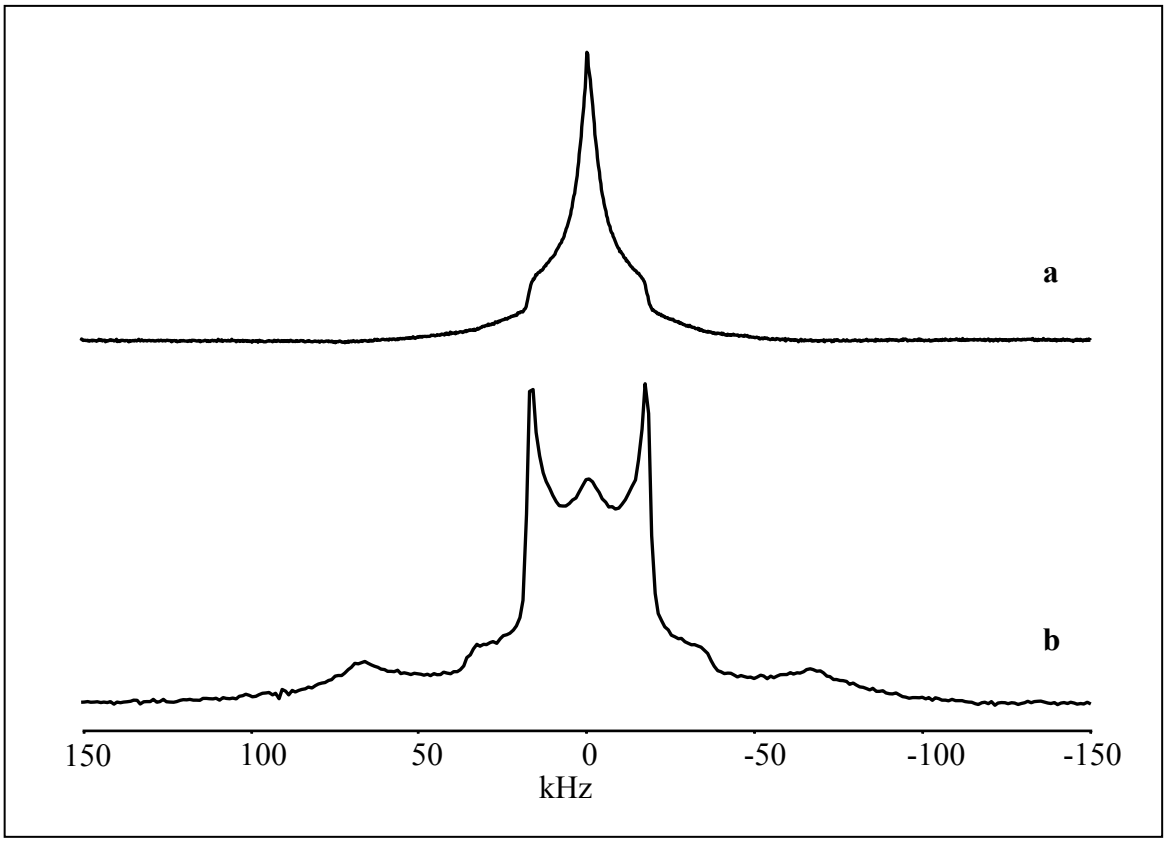

Figure 4.3: Solid state ^{2}H NMR spectra at 298 K of: **a)** γ_{Tol} (4.3 wt.-% of guest molecules); **b)** δ_{Tol} (5.2 wt.-% of guest molecules).

4.3 Investigation of Halogenated Molecules Hosted in s-PS

4.3.1 ^2H NMR Spectra of 1,2-Dichloroethane-d_4

The ^2H NMR spectra at 298 K of s-PS in the γ and δ form, including 1,2-dichloroethane-d_4, are depicted in Figure 4.4a (γ_{DCE} with 3.3 wt.-% DCE) and Figure 4.4b (δ_{DCE} with 8.9 wt.% DCE). Analogously to the result observed for the aromatic molecules previously investigated, the spectrum of γ_{DCE} with DCE exclusively included in the amorphous phase, (Figure 4.4 a) shows in good approximation a single line centred at ν_0 with a line width $\nu_{1/2}$ = 12 kHz. Even if there is evidence of a small fraction of molecules with a limited mobility, most of the 1,2-dichloroethane-d_4 show a nearly isotropic motional behavior. Investigation of γ_{DCE} with a much higher concentration of deuterated molecules always shows a single line. The spectrum of the δ_{DCE} sample (Figure 4.4b) is composed by a signal centred at ν_0 as in Figure 4.4 a, and a quadrupole pattern whose spectral features, marked in Figure 4.4 a as $\Delta\nu_1$ = 36 kHz, $\Delta\nu_2$ = 78 kHz and $\Delta\nu_3$ = 114 kHz. The deconvolution of the spectra is deferred to the next chapter.

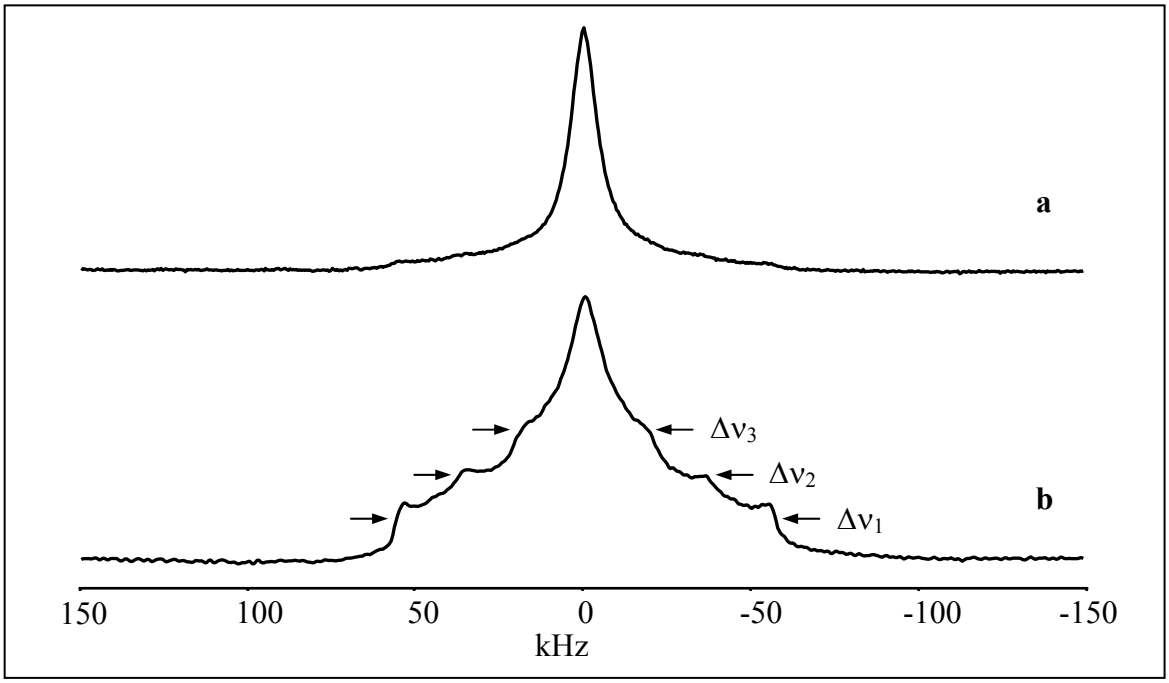

Figure 4.4: Solid state ^2H NMR spectra at 298 K of: **a**) γ_{DCE} (3.3 wt.-% of guest molecules); **b**) δ_{DCE} (8.9 wt.-% of guest molecules).

The symmetrical single line at the center of the spectrum in Figure 1b can be attributed to the DCE molecules in the amorphous phase of δ_{DCE}, just like in γ_{DCE}, while the complex pattern, is ascribed to the DCE clathrated molecules. This pattern differs from the quadrupole shape as observed for benzene and toluene and consequently can not arise from a simple fast reorientational motion of the molecules about an axis. The interpretation of this pattern is not immediate and further investigations were necessary to find the motion responsible for this experimental result. In order to help the interpretation of the line shapes, spectra of DCE hosted in the γ and in the δ forms were recorded at temperatures in the range between 143 and 333 K (Figure 4.5). For γ_{DCE} a rigid quadrupole pattern is observed at 143 K with a rigid limit Pake doublet separation of $\Delta\nu_R$ = 120 kHz (Figure 4.5). At higher temperatures the rigid Pake-type pattern gradually decreases to disappear at about 273 K where the shape of the signal changes into a single line at frequency ν_0 with $\nu_{1/2}$ = 25 kHz. By a further increase of the temperature the line narrows to a value of 5 kHz at 333 K, as shown in the top spectrum in Figure 4.5. This result proofs that at higher temperatures the DCE molecules in the amorphous domains in γ s-PS do not have a preferential reorientional motion and therefore the reorientation is almost isotropic.

The spectra of DCE in δ s-PS over the same temperature range are shown in Figure 4.6. By comparing the spectra of γ_{DCE} and δ_{DCE} it is clear that the central peak of the spectra in Figure 4.6 can be assigned to the DCE molecules in the amorphous s-PS domains. At corresponding temperatures the line width of DCE in the amorphous domains of γ_{DCE} is somewhat smaller than in δ_{DCE}, indicating a slight difference in the motional correlation time and/or isotropy of the motion in the amorphous domains.

In contrast to γ_{DCE} the spectra of δ_{DCE} show in addition to the amorphous peak at least one quadrupole pattern. In the low temperature range from 143 up to 273 K the quadrupole pattern seems to keep a Pake pattern, only the amplitude of the splitting slightly reduces from 120 kHz at 143 K to 114 at 273 K. The 5 % reduction observed can be attributed to small amplitude fluctuation of the C-D bonds of the molecule hosted in the crystalline phase. As the temperature is raised over 273 K additional spectral features appear. This suggests the arising of molecular motions involving reorientation with larger amplitude, which cause asymmetry of the average EFG tensor. These features do not vary much in the high temperature range investigated. Possible motions which generate these patterns will be discussed in the next chapter. A clear conclusion at this point is that even at 333 K the

DCE molecules in the crystalline cavities are still motionally hindered, this in contrast to the molecules in the amorphous domains.

In order to elucidate the motion in which the clathrated DCE molecules are involved at room and higher temperatures, clathrates with three other halogenated solvents are investigated. The three paragraphs that follow describe the results of the investigation of DCM, CF and DBE respectively. The first two solvents were chosen to observe the dynamics of molecules with a shorter distance between the two chlorine atoms and the latter to observe the effect of the size of the halogens on the motion.

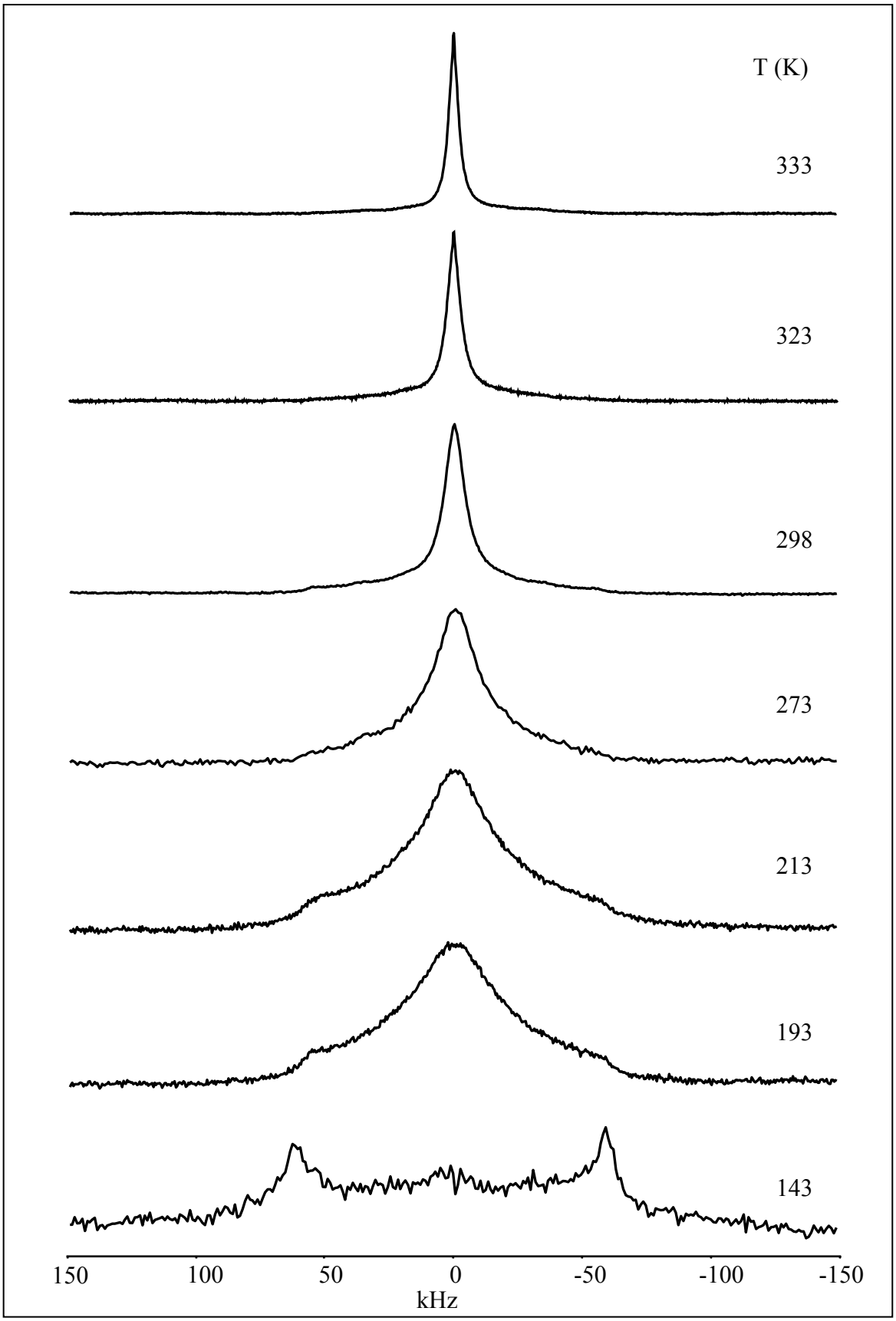

Figure 4.5: ^{2}H NMR spectra, acquired in the temperature range between 143 and 333 K, of DCE included in s-PS in γ form.

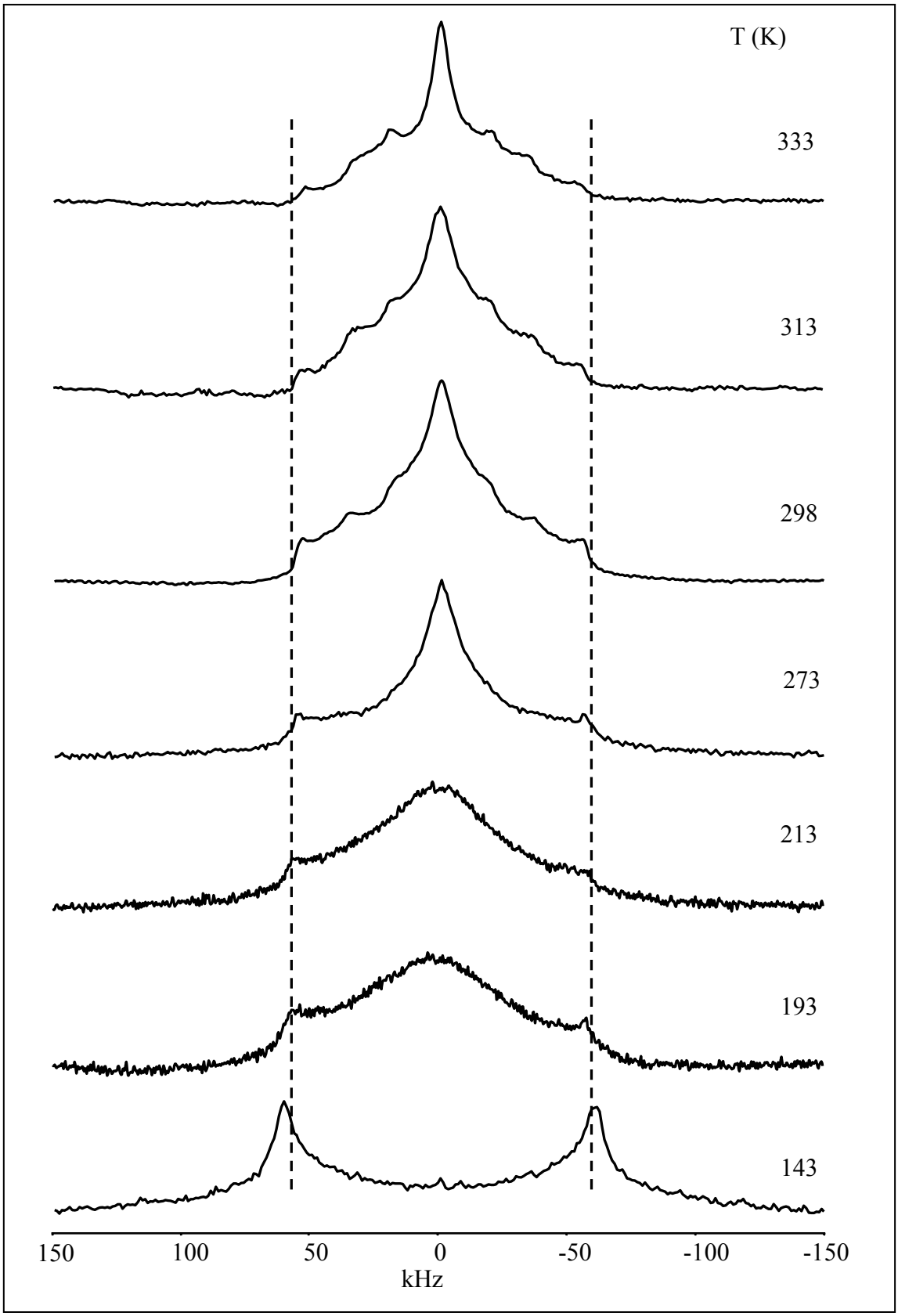

Figure 4.6: ^{2}H NMR spectra, acquired in the temperature range between 143 and 333 K, of DCE included in s-PS in δ form.

4.3.2 Dichloromethane-d_2 ^2H NMR Spectra

Figure 4.7 shows the ^2H NMR spectra of dichloromethane-d_2 (DCM) in the γ and δ form of s-PS: γ_{DCM} with 2.7 wt.-% DCM at 298 K (Fig. 4.7a) and δ_{DCM} with 8.2 % DCM at 298 K (Fig. 4.7b) and at 253 K (Fig. 4.7c). The γ_{DCM} spectrum presents only a single line with line width $\nu_{1/2}$ = 8 kHz.

Also here as for DCE the dichloromethane-d_2 in the γ and in the amorphous phase of the δ form reorient almost isotropically. In the crystalline phase a motionally induced quadrupole asymmetry can be observed. In fact both spectra of δ_{DCM} present discontinuities, at 298 K with the frequencies: ν_1 = ± 19 kHz, ν_2 = ± 37 kHz ν_3 = ± 56 kHz, and at 253 K at ν_1 = ± 19 kHz, ν_2 = ± 39 kHz ν_3 = ± 58 kHz. The interpretation of these patterns will be presented in the next chapter.

By comparing the spectra for DCE and DCM it is clear that the dynamics of the two molecules in the corresponding phases must be very similar, except the motion for DCM starts already at a lower temperature.

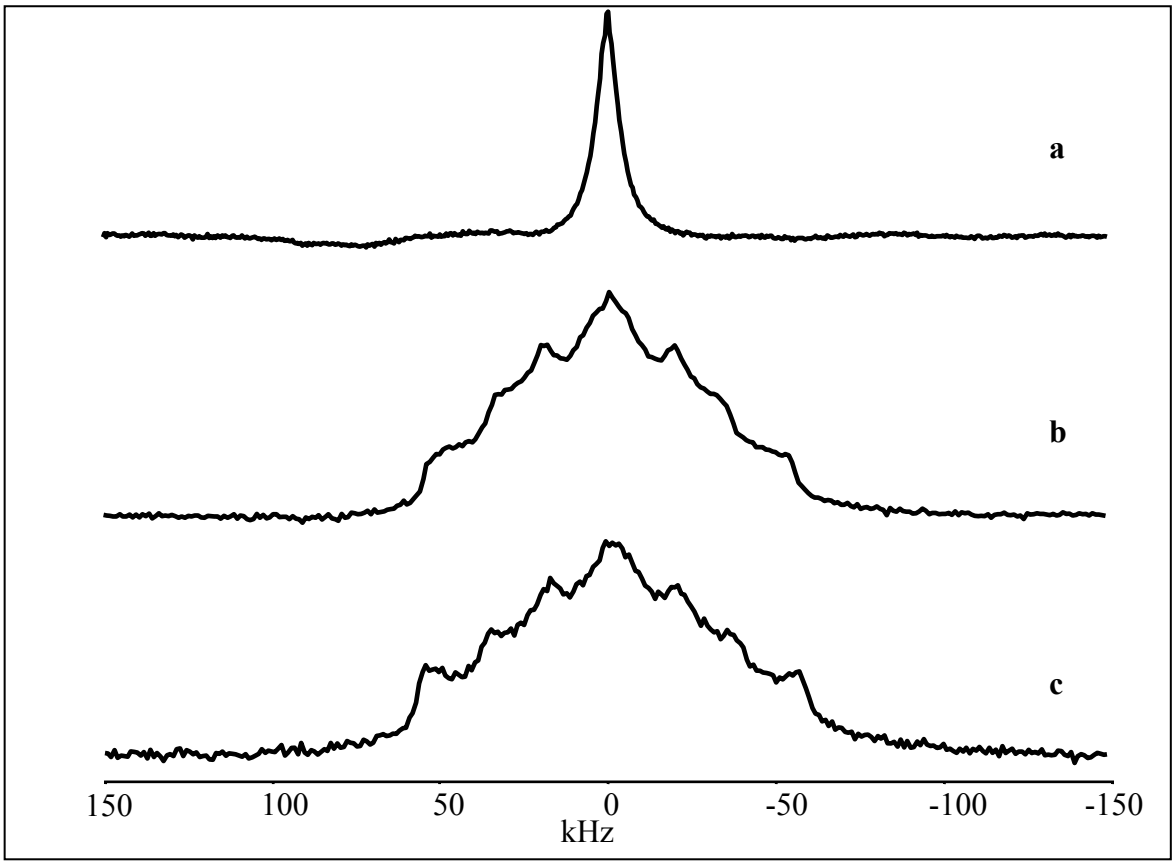

Figure 4.7: Solid state ^2H NMR spectra of: **a**) γ_{DCM} (2.7 wt.-% DCM) at 298 K, **b**) δ_{DCM} (8.2 wt.-% DCM) at 298 K and **c**) at 253 K.

4.3.3 ^2H NMR Spectra of Chloroform-d

The spectrum of 8.3 wt.-% chloroform included in γ s-PS (γ_{CF}) results in a single line with a full width at half maximum of $\nu_{1/2}$ = 8.5 kHz representative of an anisotropic motion (Figure 4.8a). The spectra in Figures 4.8b and c of δ_{CF}, with 16.4 wt.-% chloroform at 298 K and 313 K represent the sum of the line shapes of deuterons with two different mobilities. The single line evidences that a fraction of chloroform-d included in the δ_{CF} sample can reorient isotropically. This high molecular freedom is ascribed to the molecules in the amorphous phase. The other fraction, that must be clathrated in the polymer, shows an anisotropic motion that does not modify the shape of the rigid limit spectrum but causes a reduction of the internal splitting from 120 kHz to 110 kHz. The comparison of the two δ_{CF} spectra proofs that the temperature increase does not activate new modes of motion, but the decrease of the quadrupolar pattern intensity with respect to that of the single line shows that the molecules leave the cavities.

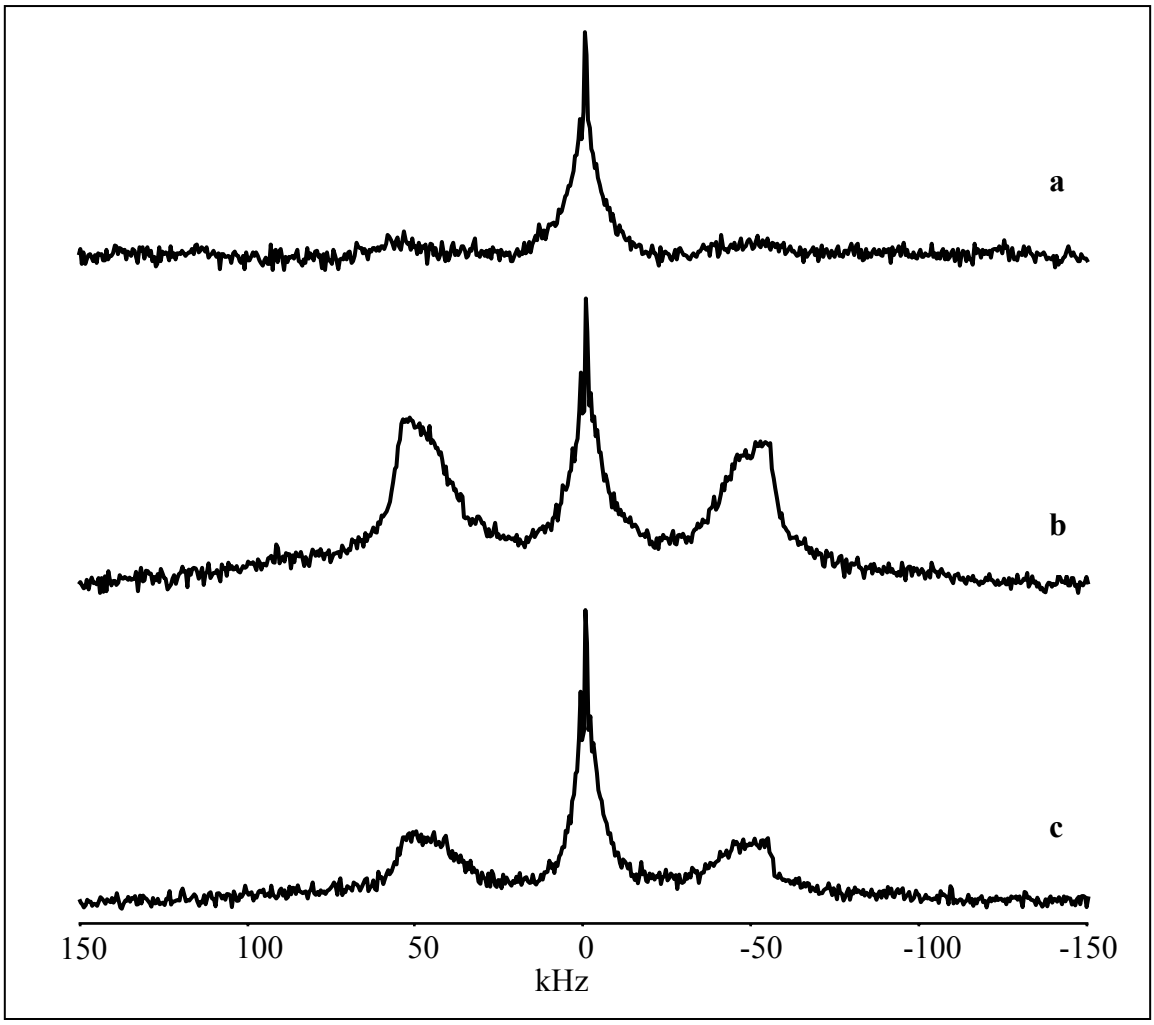

Figure 4.8: ^{2}H NMR spectra of **a**) γ_{CF} (8.3 wt.-% CF) at 298 K and of δ_{CF} (16.4 wt.-% CF); **b**) at 298 K and **c**) at 313 K.

4.3.4 ^{2}H NMR Spectra of 1,2-Dibromoethane-d_4

The ^{2}H NMR spectra of 1,2-dibromoethane-d_4 at 298 K in the γ_{DBE} sample including 7.8 % DBE and of δ_{DBE} with 11.5 % DBE are compared in Figures 4.9a and 4.9b, while Figures 4.9c and 4.9d show the spectra of δ_{DBE} respectively at 313 and 333 K.

Also in this case the molecules included in the amorphous phase show a nearly isotropic reorientation giving rise to a single signal with $\nu_{1/2}$ = 9.5 kHz.

The molecules hosted in the crystalline part of δ_{DBE} show a rigid pattern with a splitting of 120 kHz and a central band similar to but somewhat broader than the one observed in the pure amorphous γ_{DBE}. At higher temperature the line shape does not change but a decrease of the intensities of the rigid pattern is evident.

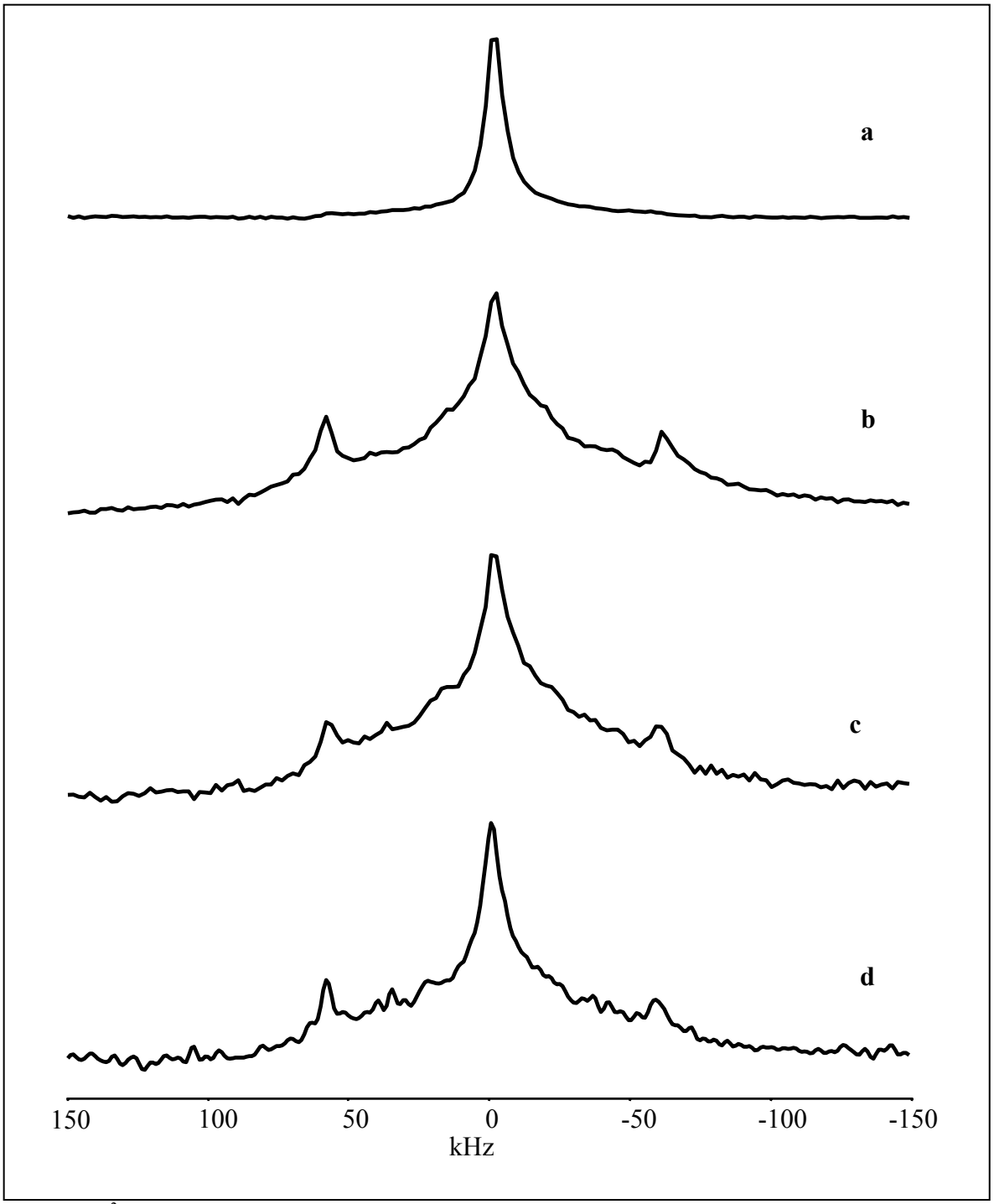

Figure 4.9: ^{2}H NMR spectra of **a**) γ_{DBE} (7.8 wt.-% DBE) at 298 K and spectra of δ_{DBE} (11.5 wt.-% DBE) at **b**) 298 K, **c**) 313 K and **d**) 333 K.

Chapter 5

Simulation of ^{2}H NMR Spectra and Discussion

From the results shown in the previous chapter it is evident that, in the fast motional range, the molecules trapped in the amorphous phase of the δ and the γ probes show mainly isotropic reorientation yielding a single unstructured line in the NMR spectrum. The experimental data of the clathrated molecules show anisotropic motions even in the high temperature range. In the forthcoming analysis of the results we focus on the motion of the clathrated molecules and try to find the dynamical process experienced by the deuterium atoms that generate the observed spectral features. A model for the molecular dynamics is proposed for all the molecules investigated.

5.1 Analysis of the NMR Spectra of Aromatic Molecules Clathrated in s-PS

5.1.1 Benzene-d_6

We commence the interpretation of the results with benzene-d_6 included in the δ samples. The difference between the spectrum in Figure 5.1a of the concentrated benzene sample and the spectrum in Figure 5.1b of the less concentrated sample is obviously caused by a contribution of an amorphous signal around ν_0.

In the ^{2}H NMR spectrum of the less concentrated sample, (1.8 wt.-% of benzene-d_6) obtained by evaporating the solvent at room temperature, (Figure 5.1b) the singlet has disappeared and only the Pake pattern of Figure 5.1a is observed ($\overline{\eta} = 0$) . The attribution of this signal to the clathrated molecules is supported by literature data which show a faster desorption from the amorphous phase with respect to the crystalline phase in analogous systems.[1]

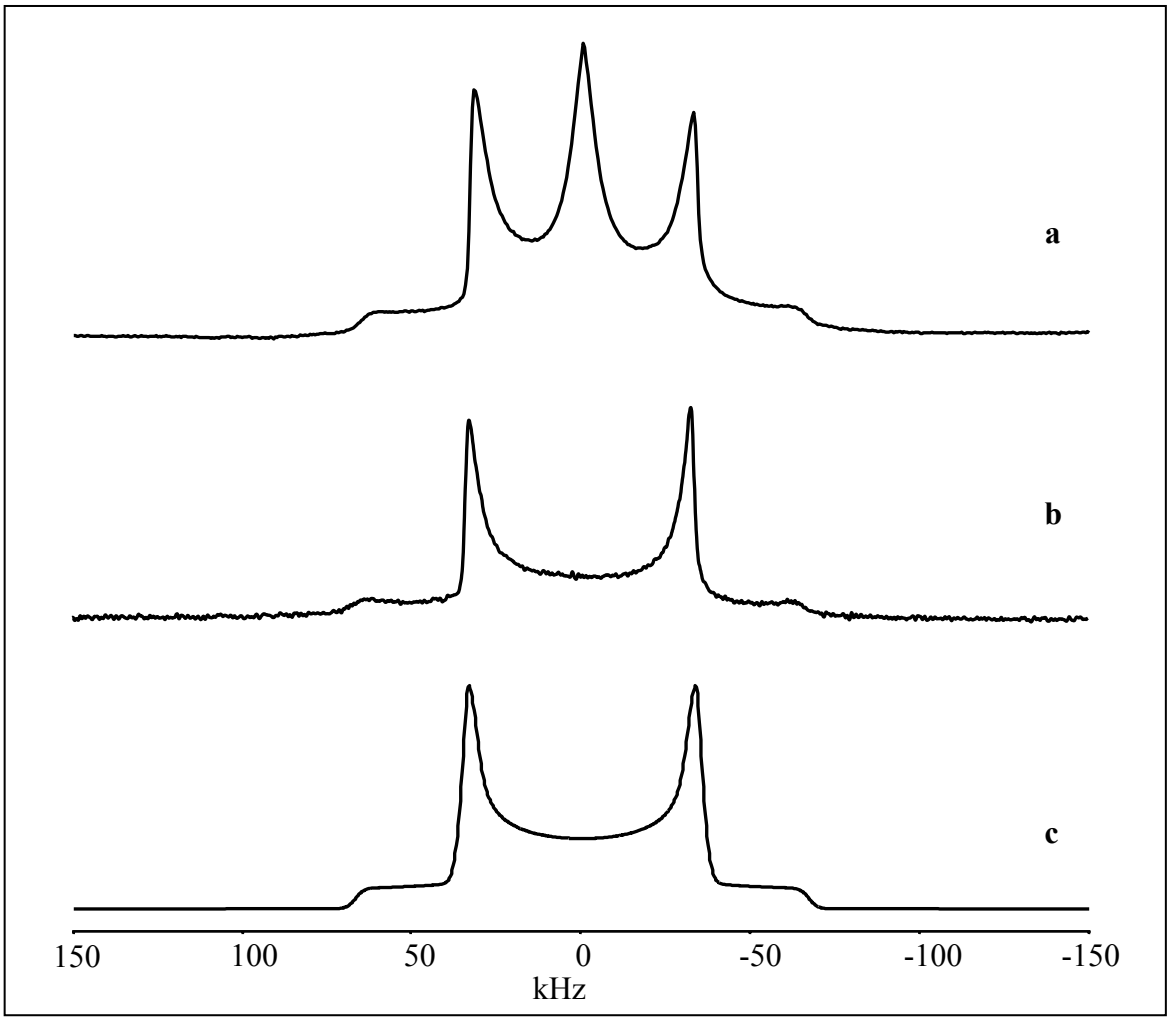

Figure 5.1: Solid state ^{2}H NMR spectra at 298 K of: **a**) δ_{Ben} (10.2 wt.-% of guest molecules); **b**) δ_{Ben} (1.8 wt.-% of guest molecules). **c**) Simulated spectrum relative to the reorientation of benzene molecules as described in the text.

The quadrupole pattern of Figure 5.1b shows a doublet separation of $\Delta\nu_Q$ = 67 kHz that corresponds to approximately one half of the value expected for the rigid-limit powder spectrum ($\Delta\nu_R$ = 137 kHz).[2] This reduction of the splitting can be simulated by assuming

a fast reorientation about the C_6 symmetry axis orthogonal to the aromatic ring as shown in Figure 5.2. This motion was modelled as described in section 2.5 assuming that for an uniaxial reorientation the average anisotropy parameter $\overline{\delta}^* = \Delta\nu_Q$ only depends on the Euler angle β between the rotation axis and the direction of the C-^{2}H bond. In fact, according to Equation 2.5.8, if $\beta = 90°$ the parameter $\overline{\delta}^*$ is reduced to exactly one half of the anisotropy parameter $\delta^* = 137$ kHz expected for benzene in the rigid limit case.

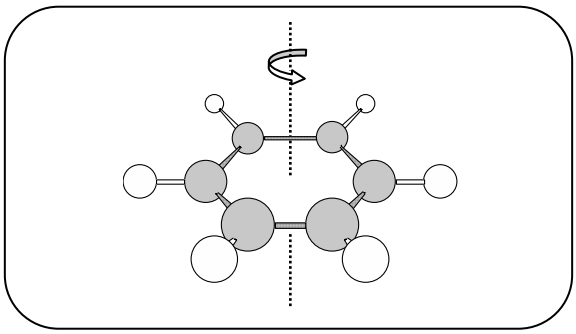

Figure 5.2: Model proposed for the dynamics of the benzene-d_6 clathrated in s-PS δ-form: in-plane rotational motion about the C_6 symmetry axis.

In this case $\overline{\eta} \approx 0$ and the spectrum of Figure 5.1c is calculated as explained in section 2.4 for $\overline{\delta}^* = \frac{1}{2}\delta^*$. The simulated spectrum shows the splitting between the resonances arising from the perpendicular components of 68.5 kHz that, in good approximation, fits with the experimental observations ($\Delta\nu_Q$ = 67 kHz). As discussed before the slight reduction of the experimental splitting can be explained by small angle librational motion of the rotation axis. A similar wobbling motion of the rotation axis was observed for pure benzene-d_6 at 200 K[3] and for benzene-d_6 molecules trapped in the cavities of the ZSM-5 zeolite at 193 K[4] for which the experimental splitting are respectively $\Delta\nu_Q$ = 71 kHz and $\Delta\nu_Q$ = 66 kHz. These values are very close to the $\Delta\nu_Q$ of the spectrum in Figure 5.1b and confirm the validity of the dynamical model we proposed. The rotation of benzene about its six-fold axis only suggests a strong interaction of the benzene molecules with the cavities. On the basis of the packing model proposed for the emptied δ form[5] (presented in section 5.2.7), we can assume that the benzene molecules are sandwiched between the aromatic ring of the phenyl groups of the s-PS chains in a sort of stacking complex that mainly permits the rotation of the molecules about the C_6 axis orthogonal to the aromatic ring (see Figure 5.1.3)

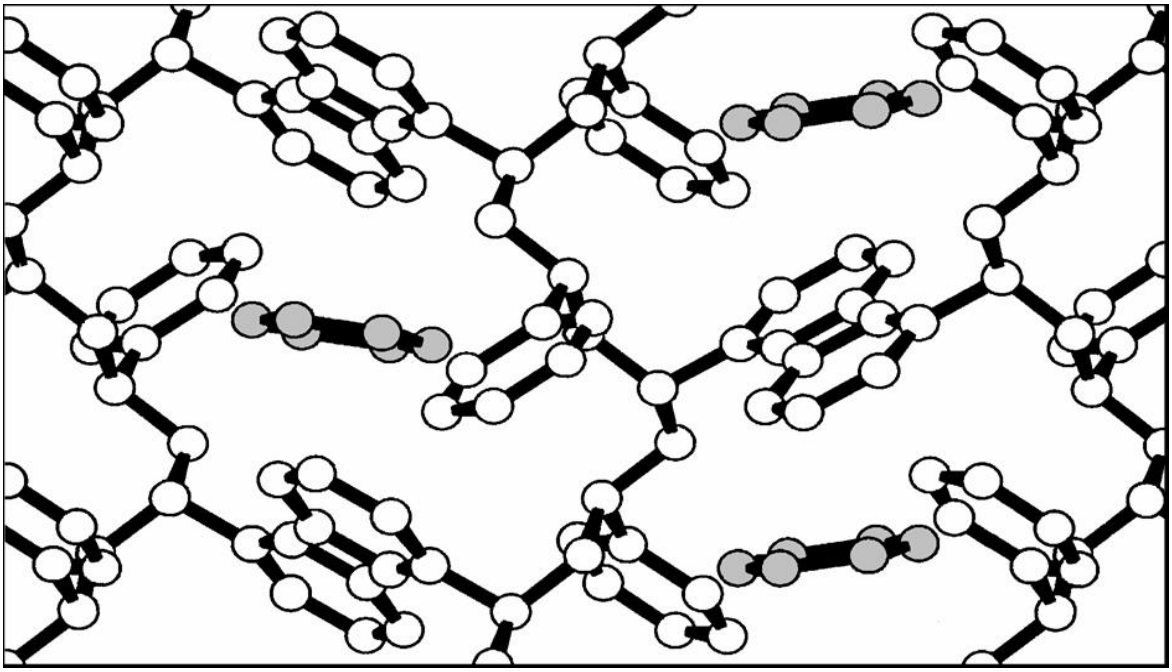

Figure 5.3: Stick and ball model representing the location of the benzene molecules in the cavities of the s-PS δ form. The cavities were designed according to the X-ray structure of the δ form reported in the literature.[4]

5.1.2 Toluene-d_8

The spectrum of toluene clathrated in s-PS, displayed in Figure 5.4e, is simulated by superposing three spectral contributions. The first, shown in Figure 5.4a, is a Lorentz line shape resonant at the Larmor frequency ν_0 with full width at half maximum of $\nu_{1/2}$ = 13 kHz, representing the contribution of deuterated toluene in the amorphous phase. The following line shape (Figure 5.4b) is a rigid limit axial powder pattern calculated assuming an anisotropy parameter $\eta = 0$ and δ^* =137 kHz, a value generally observed for rigid aromatic deuterons. This can be attributed to the deuterons of the phenyl ring of the clathrated toluene-d_8 molecules which appear to be rigid. It is worth noting that the same splitting was recently observed for rigid aromatic deuterons in $[N(CH_3)_4][Cd_3(CN)_7]$ toluene-d_8 clathrate at 128 K.[6]

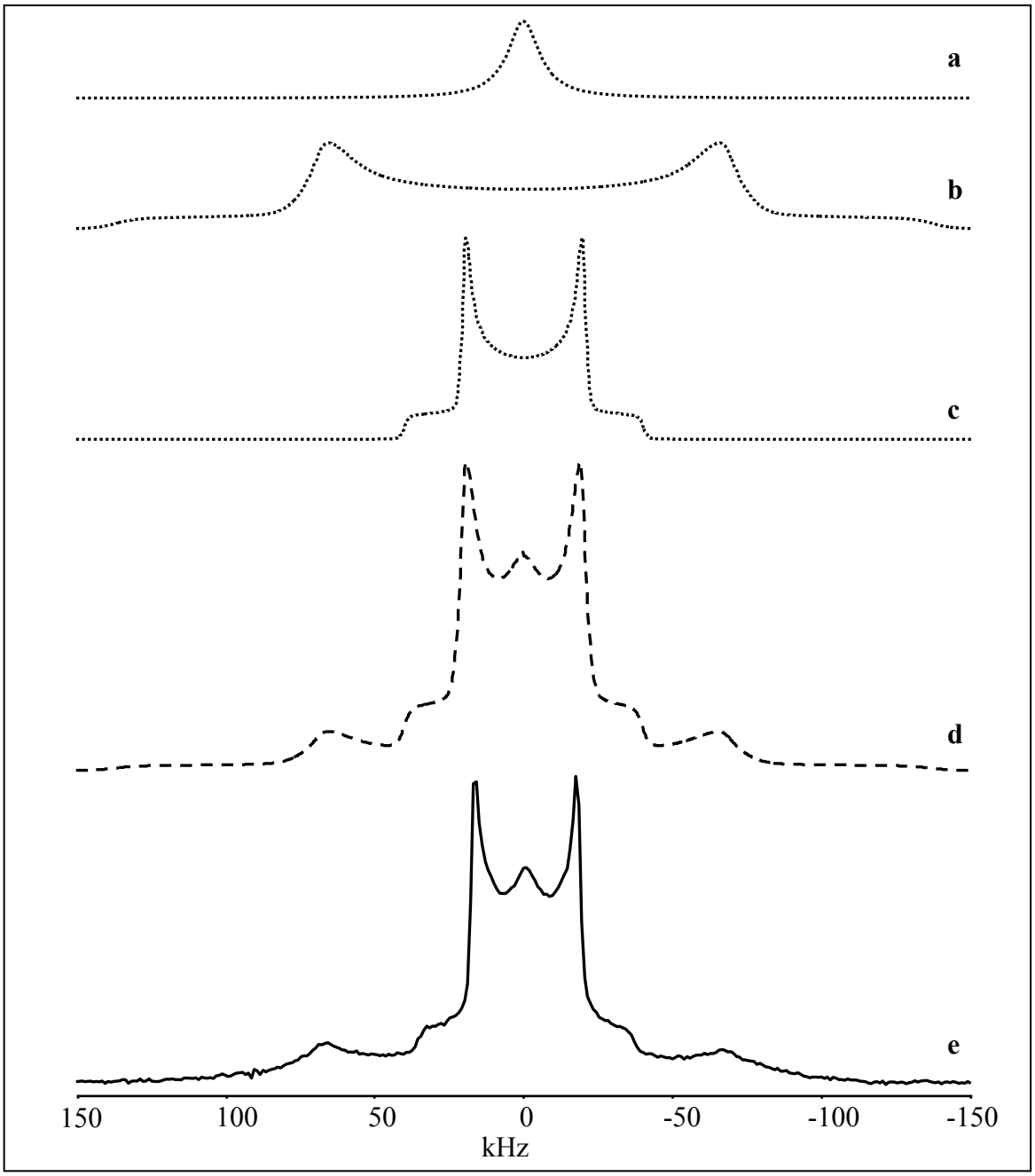

Figure 5.4: ^{2}H NMR spectra calculated for **a**) a Lorentzian line with $\nu_{1/2}$ = 13 kHz; **b**) a quadrupole Pake pattern with η =0 and δ* =137 kHz and **c**) a quadrupole Pake pattern with $\overline{\eta} = 0$ and $\overline{\delta}^* = 37\,\text{kHz}$. **d**) Combination of the pattern **a**) **b**) and **c**). **e**) Experimental solid state ^{2}H NMR spectra at 298 K of δ_{Tol} (5.2 wt.-% of guest molecules).

The third pattern (Figure 5.4c) presents a Pake shaped line from the toluene methyl groups, scaled down by assuming a fast reorientation of the methyl group about the C_2 symmetry axis of the molecule as shown in Figure 5.5. The quadrupole constant for aliphatic

deuterium nuclei $Q_{0\text{-}Al}$ = 160 kHz and the anisotropy parameter averaged by the uniaxial motion proposed, calculated by Equation 2.5.8 for $\beta = 109.4°$, has the value $\overline{\delta}^* = 40\,\text{kHz}$. Similar results were previously reported for the methyl groups of toluene-d_3 ($\overline{\delta}^* = 34\,\text{kHz}$) and *p*-xylene-$d_6$ ($\overline{\delta}^* = 36\,\text{kHz}$) clathrated in ZSM-5 zeolite at 193 K and 143 K, respectively,[4] and toluene-d_3 ($\overline{\delta}^* = 37.5\,\text{kHz}$) included in polycyano-polycadmates at 140 K.[6] In all these cases the motion is interpreted using the model mentioned above. The spectrum in Figure 5.4d represents a combination of the three line shapes in a way that the sum fits the experimental spectrum (solid line) depicted at the bottom (Figure 5.4e). A quantitative evaluation of the intensity of the amorphous and crystalline contribution to the spectrum is not possible because of the distortions due to the experimental limitations. One of these, the loss of intensity, affects the Pake shape signal more pronounced by intensities that resonate at frequencies far from the Larmor frequency $\nu_0 = 0$. This is mainly caused by too long pulses (4.3 μs) that are not able to uniformly irradiate the whole frequency range. An extensive description of how the experimental acquisition parameters influence the NMR signals is given in section 2.7.

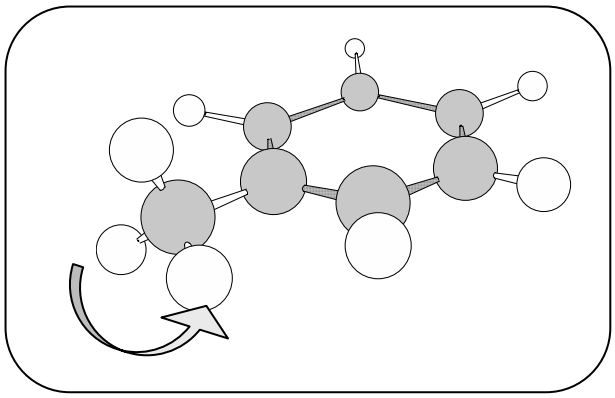

Figure 5.5: Model proposed for the dynamics of the toluene-d_8 clathrated in s-PS δ-form: no motion of the aromatic ring and rapid reorientation of the C^2H_3 about the C_2 molecular symmetry axis.

The steric interaction of the toluene -C^2H_3 group with the s-PS crystalline cavities is able to stop the rapid rotational motion observed in the clathrates with benzene, thus the fast rotation of the methyl group is the only molecular motion detectable for toluene on the NMR time scale.

5.2 Analysis of the NMR Spectra of Halogenated Molecules Clathrated in s-PS

The shape of the ^{2}H NMR spectra of the halogenated molecules clathrated in s-PS is in some cases different from the Pake pattern previously observed for benzene and toluene. In particular for DCM and DCE above 273 K molecular motions produce a complex pattern where the correlation between the characteristic spectral frequencies and the dynamics is not immediate. For this reason the spectral data for these two halogenated molecules can not be interpreted as easily as for benzene and toluene. The results obtained for the other halogenated molecules and the information about the shape of the cavities are needed to elucidate the geometry and mechanism of motion. In particular the structural differences between the investigated halogenated molecules will be correlated to the differences between the line shapes. Therefore in the forthcoming discussion the spectra are analyzed not following the sequence used in the previous chapter but they are discussed in such a sequence to help the interpretation of the molecular dynamics.

5.2.1 Chloroform-d

The spectra of δ_{CF} at both the temperatures investigated (313 and 298 K) are reproduced again in Figures 5.6a and 5.6b (solid lines). Besides the single signal at the Larmor frequency, the presence of an axially symmetric powder pattern is clearly distinguishable, even if the parallel components (shoulder) of the pattern are lost in the noise. Notwithstanding the relatively high percentage of chloroform in the polymer (16.4 wt.-%) and the large number of scans (10360 at 313 K and 22352 at 298 K) used to record the spectra, the signal to noise ratio is quite low due to the low deuterium content per molecule. Both patterns show a reduction of the splitting between the resonances arising from the perpendicular components (highest doublet peaks) from 120 kHz, expected in absence of motion, to 110 kHz. Even at 313 K, large amplitude reorientations are hindered inside the cavities, in agreement with the results of recent FTIR investigations of these systems that reveal an interaction of the chlorine with the phenyl rings of the polymer.[7]

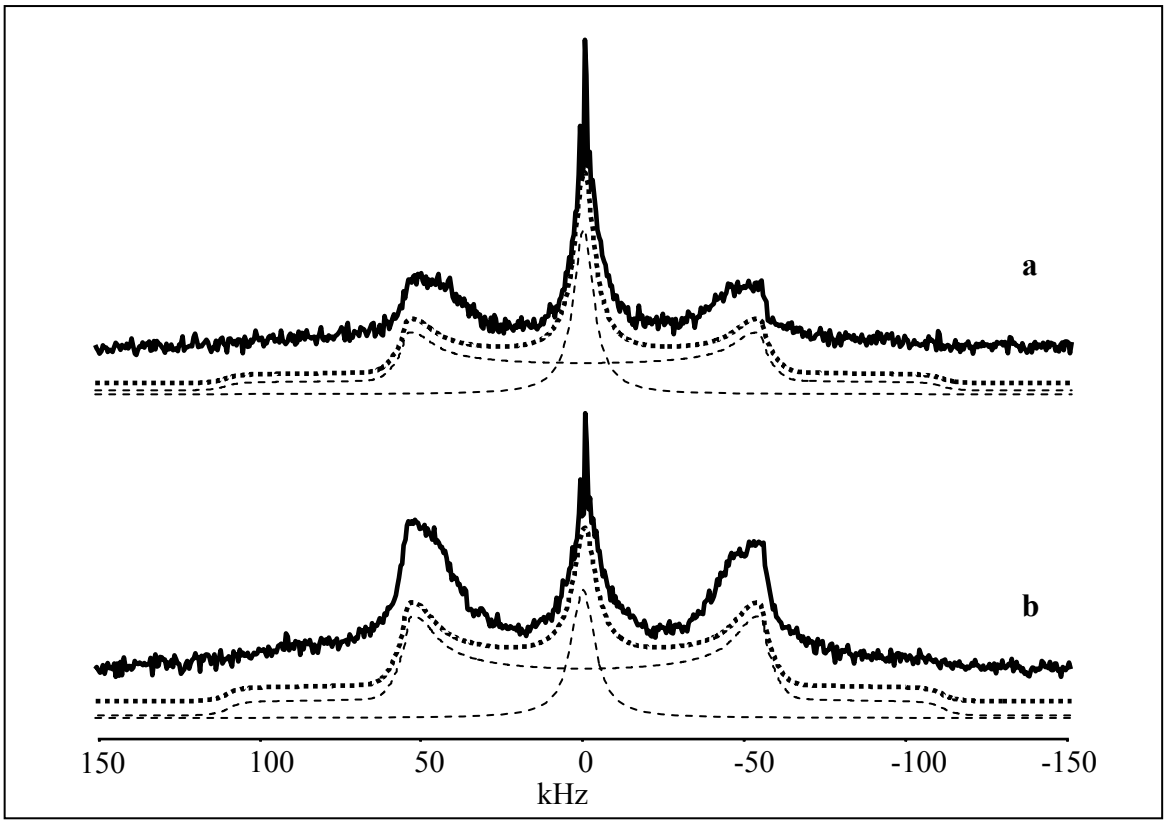

Figure 5.6: Experimental (solid lines) and simulated (dotted lines) spectra and their deconvolution (dashed lines) of the δ_{CF} sample at **a**) 313 K and **b**) 298 K.

A motion that does not alter the orientation of the C-^{2}H bond does not affect the deuterium spectrum. Consequently the reduction of the splitting from 120 to 110 kHz can not be the outcome of a translation of the molecules inside the cavities, nor of a reorientation of the molecule about the C-^{2}H bond as shown in Figure 5.7. In fact for chloroform-d involved in the rotation shown in Figure 5.7 the principal component of the EFG tensor would be situated on the rotation axis and a static pattern would be observed.[4]

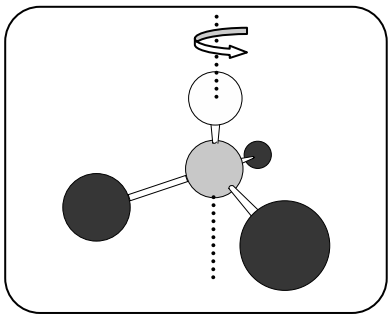

Figure 5.7: Chloroform-d rotating about the C-^{2}H bond.

The motional averaging observed must be the outcome of another motion that involves a reorientation of the C-^{2}H bond and consequently of the plane containing the three chlorines. Since only a small effect on the deuterium spectra is observed, i.e. a reduction of only 10 kHz of the value of $\overline{\delta}^*$, it is reasonable to assume that the C-^{2}H bond rotates about axes which make a small angle with the C-^{2}H bond. This could be a rapid wobbling motion of the chloroform C_3 symmetry axis within a cone of a given small apex angle or a rotation about a fixed axis which makes a small angle with C-^{2}H bond, like shown in Figure 5.8.

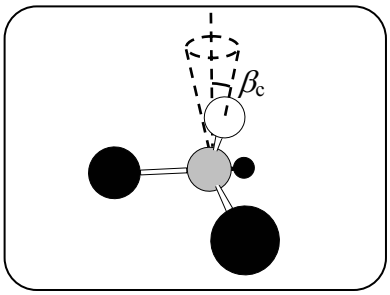

Figure 5.8: Model proposed for the dynamics of the chloroform-d clathrated in s-PS δ form by assuming that the C-^{2}H bond is tilted at a fixed angle β_c with respect to the rotation axis.

It is possible to simulate the experimental spectra shown in Figure 5.6 by assuming that the C-^{2}H bond is tilted at a fixed angle $\beta_c = 13°$ with respect to the rotation axis as displayed in Figure 5.6 (dashed lines). The complete pattern was simulated by adding a Lorentzian line of $\nu_{1/2} = 8.5$ kHz at 298 K and $\nu_{1/2} = 7$ kHz at 313.

5.2.2 1,2-Dichloroethane-d_4

By comparing the spectra in Figures 4.5 and 4.6 it is clear that the symmetrical peak at the center of the spectra of δ_{DCE} in Figure 4.6 is due to DCE molecules in the amorphous domains of δ s-PS. The temperature dependence of this line shows the steady decrease of motional correlation time and/or the increase of the rotation angle with the temperature. Below 273 K there is evidence of an axial powder pattern with a splitting that gradually changes from 120 kHz, observed at 143 K, up to 114 kHz at 273 K. This reduction must be caused by a fast small amplitude wobbling motion of the molecule. Above 273 K new

reorientation modes set in, which cause a complicated new pattern. The frequencies belonging to the discontinuities of this pattern do not change much by a further increase of the temperature, suggesting that the motion is already fast at the NMR timescale at 298 K. Spectra of the δ_{DCE} crystalline phase in the temperature range between 298 and 333 K are calculated by assuming that the three discontinuities in the spectrum belong to one unique pattern. The computation was performed by substituting the spectral values reported in Table 5.1 in Equations 2.4.4 and 2.4.5 as values for ν_1, ν_2 and ν_3 ($|\nu_1| = ½\,\Delta\nu_1$, $|\nu_2| = ½\,\Delta\nu_2$, $|\nu_3| = ½\,\Delta\nu_3$). The simulated and experimental spectra at 333, 313 and 298 K are shown in Figures 5.9a, 5.9b and 5.9c respectively and the corresponding quadrupole parameters $\overline{\delta}^*$ and $\overline{\eta}$ are reported in Table 5.1. The computed spectra reproduce the experimental results well.

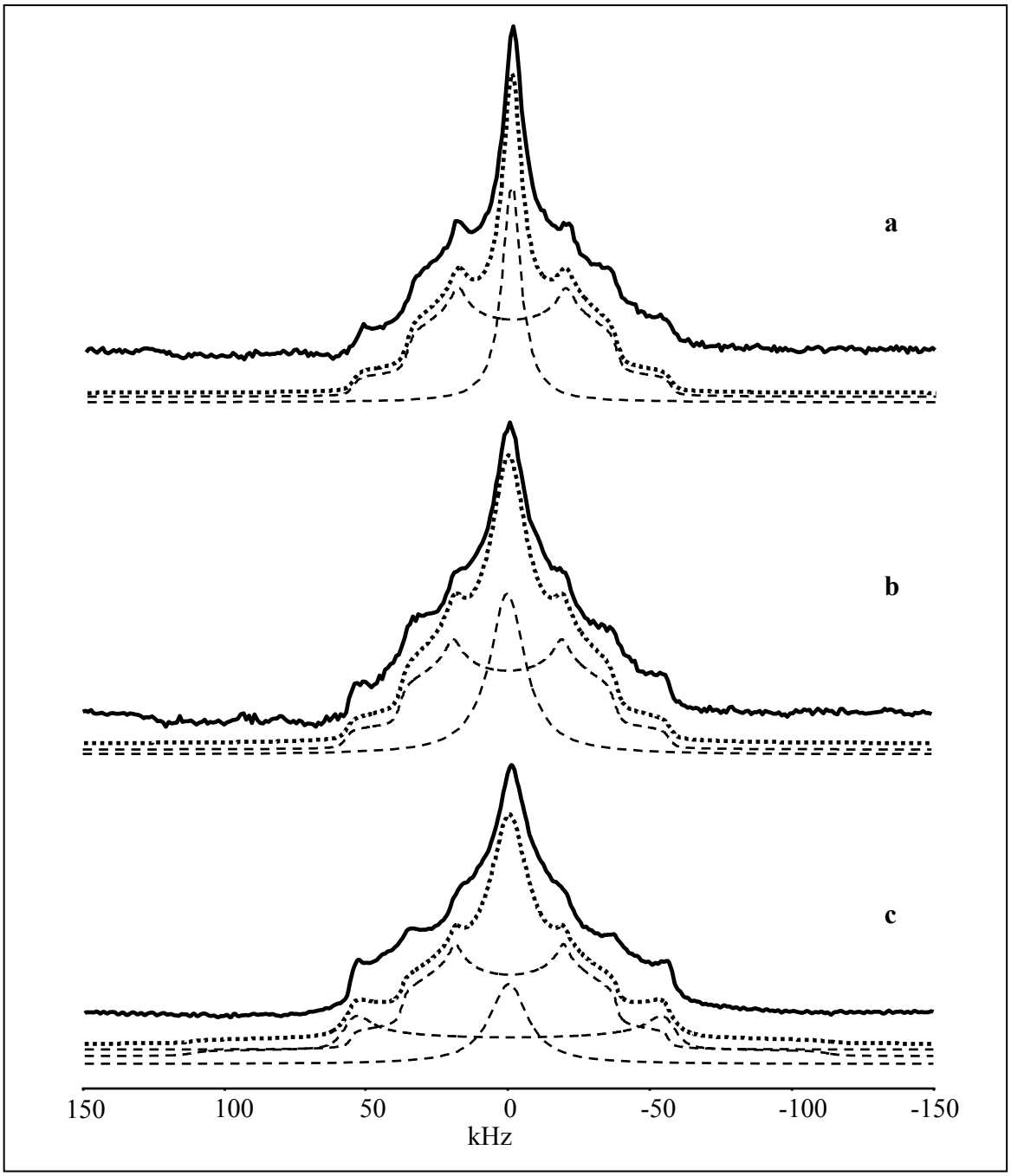

Figure 5.9: Experimental (solid lines) and simulated (dotted lines) spectra and their deconvolution (dashed lines) of the δ_{DCE} sample at **a**) 333 K, **b**) 313 K and **c**) 298 K.

Table 5.1. Spectral features observed for the DCE and DCM molecules included in the crystalline phase of δ s-PS, at different temperatures together with $\overline{\eta}$ and $\overline{\delta}$ of the corresponding spectra.

Sample	*Temperature (K)*	*Spectral features:* $\Delta\nu_1$ - $\Delta\nu_2$ - $\Delta\nu_3$ (in kHz)	$\overline{\eta}$	$\overline{\delta}^*$
δ_{DCE}	298	36 - 78 - 114	0.36	57
δ_{DCE}	313	38 - 76 - 114	0.33	57
δ_{DCE}	333	38 - 74 - 112	0.32	56
δ_{DCM}	298	38 - 74 - 112	0.32	56
δ_{DCM}	253	38 - 78 - 116	0.34	58

In general the experimental patterns of the δ_{DCE} samples are well described by a combination of two simulated spectra, one consisting of a broad Lorentz line with full width at half maximum of $\nu_{1/2} \approx 16$ kHz at 298 K, $\nu_{1/2} \approx 13$ kHz at 313 K and $\nu_{1/2} \approx 9$ kHz at 333 K, representing the amorphous contribution and a quadrupole pattern with $\overline{\delta}^*$ and $\overline{\eta}$ as listed in Tab.5.1, except for the spectrum at 298 K. Here the shoulders at $|\nu_3| = 57$ kHz in the experimental spectrum are higher than in the simulated spectrum. A good agreement of the simulated spectrum with that recorded at 298 K is reached if a third component is introduced with an axially symmetric EFG tensor with $\overline{\delta}^* \approx 57\,\text{kHz}$. The averaged anisotropy parameter of this third component is smaller than $\delta^* \approx 120\,\text{kHz}$ expected for the rigid limit case. This suggests that for DCE in the crystalline phase at room temperature there are two fractions executing different motions. One fraction of molecules yield an averaged axially symmetric EFG tensor characterized by $\overline{\delta}^* = 57$ kHz and $\overline{\eta} \approx 0$. The other fraction produces a spectrum with $\overline{\delta}^* = 57$ kHz and $\overline{\eta} \approx 0.36$. As consequence of heating above 298 K the axial powder pattern disappears and the asymmetry parameter of the remaining quadrupolar line shape slightly decreases. This latter observation can be explained by a small increase of the motional amplitude at higher temperatures.[8] It is important to note, however, that being able to simulate the spectra does not mean that the

motion leading to these spectra is also understood. A discussion of the molecular dynamics able to explain the NMR results of δ_{DCE} sample in the high temperature range is deferred to other sections. We prefer first to discuss the experimental data of the DCM and DBE molecules and then by comparing the results, we propose a solution in agreement with all the observations.

5.2.2 Dichloromethane-d_2

The spectra of DCM at 298 and 253 K are simulated by introducing the values of Tab. 5.1 in the Equations 2.4.4 and 2.4.5 and the results are reported in Figure 5.10a and 5.10b. The dynamical features $\Delta\nu_1$, $\Delta\nu_2$ and $\Delta\nu_3$ and the values of the parameters $\overline{\delta}^*$ and $\overline{\eta}$ are close to those observed for DCE, suggesting that the deuterium atoms of both clathrated molecules are involved in the same motion. Also in this case, analogously to the DCE spectra, the increase of the temperature in the range investigated is accompanied by a small reduction of the asymmetry parameter from $\overline{\eta} = 0.34$ to $\overline{\eta} = 0.32$, evidencing a slight change in the motion between 253 and 298 K. The simulation of the complete spectra involves the contribution of a Gauss-Lorentz line and of an axial pattern calculated by assuming $\overline{\delta}^* = 57\,\text{kHz}$. The latter line shape suggests the presence of a fraction of molecules involved in a small angle librational motion.

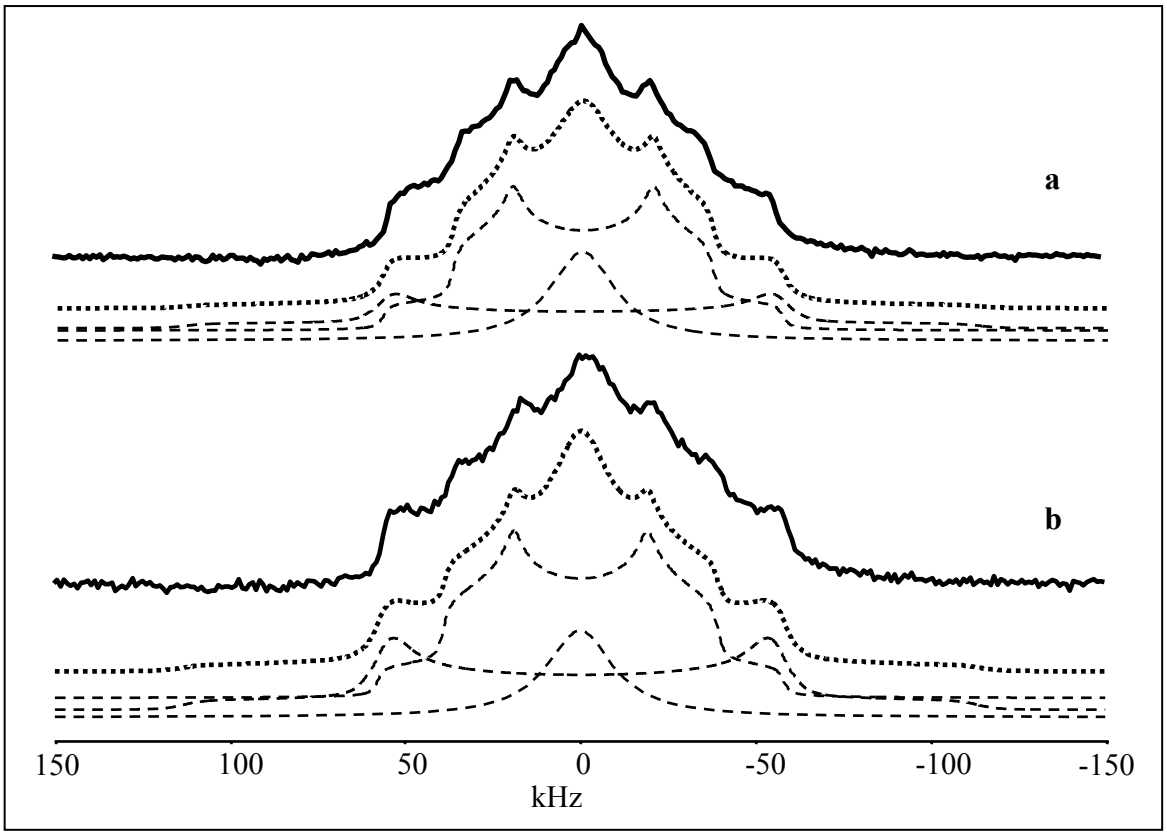

Figure 5.10: Experimental (solid lines) and simulated (dotted lines) spectra and their deconvolution (dashed lines) of the δ_{DCM} sample at **a**) 298 K and **b**) 253 K.

5.2.3 1,2-Dibromoethane-d_4

For completeness, the DBE spectra are deconvoluted as displayed in Figure 5.11. All the computed spectra are the result of the superposition of a narrow Lorentzian line, a broad Gauss-line ($\nu_{1/2}$ = 50 kHz) and a quadrupolar pattern with an asymmetry parameter $\overline{\eta} \approx 0$ and an anisotropy parameter that coincides with the rigid limit case $\overline{\delta}^* = \delta^* = 60\,\text{kHz}$. The powder pattern indicates that 1,2-dibromoethane-d_4 clathrated in the s-PS δ form shows a static behavior: in contrast to DCE and DCM the rigid pattern also persists in the high temperature range (up to 333 K). The larger hindrance and the higher polarizability of the bromine atoms in comparison to chlorine, apparently prevent the clathrated DBE molecules from any large amplitude motion.

The reason for the presence of the broad Gaussian line in each spectrum is not clear. It could evidence the existence of a distribution of anisotropic motional modes rather than a

single mode that would result in a quadrupolar pattern or could be the outcome of a slow motion ($10^{-5} \leq \tau_c \leq 10^{-4}$).

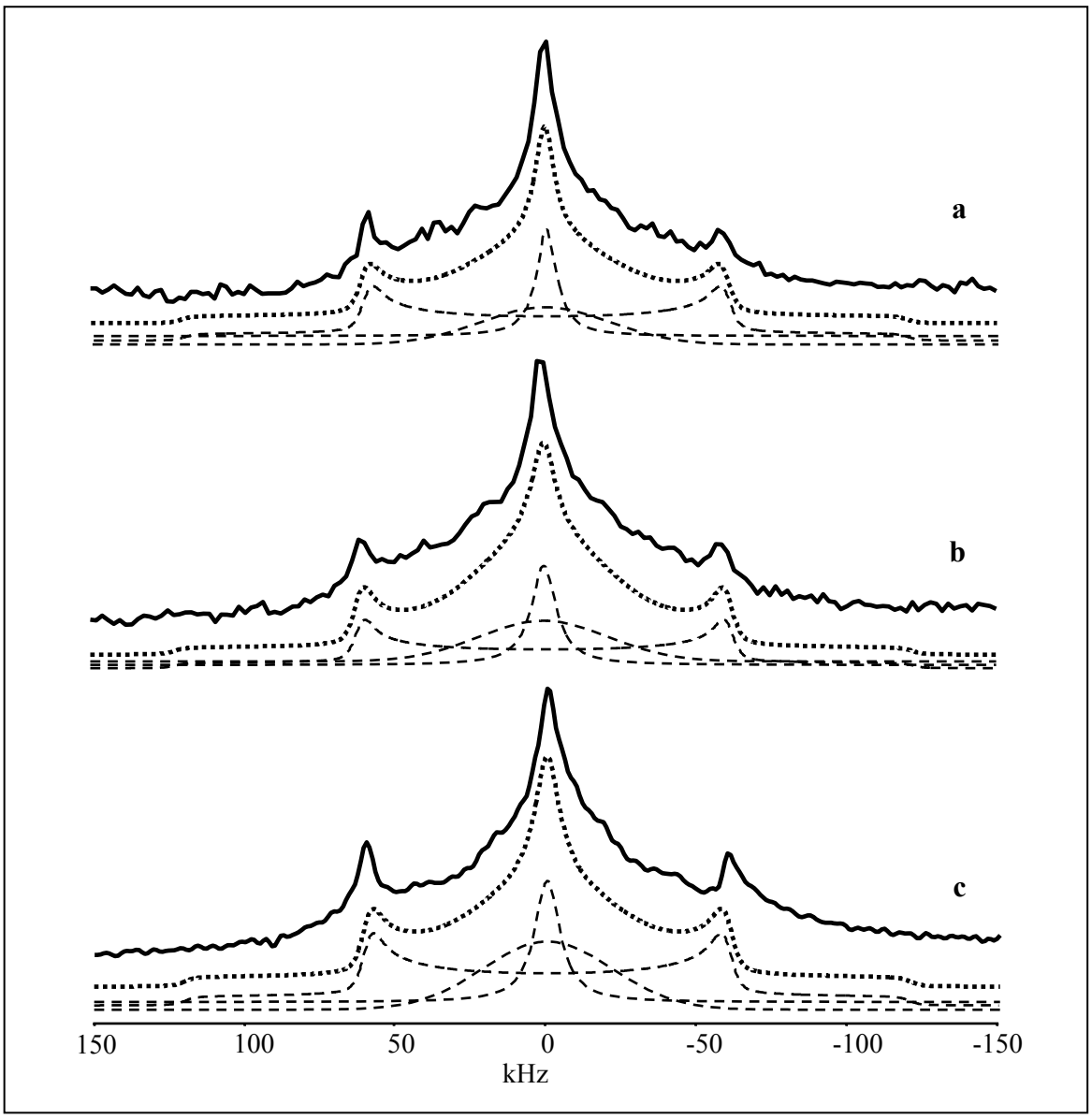

Figure 5.11: Experimental (solid lines) and simulated (dotted lines) spectra and their deconvolution (dashed lines) of the ^{2}H NMR spectra of 1,2-dibromoethane-d_4 of δ_{DBE} (11.5 wt.-% DBE) at **a**) 333 K, **b**) 313 K and **c**) 298 K.

5.2.4 Simulation of Trans-Gauche Interconversion for 1,2-Dichloroethane-d_4

We begin the analysis of the spectra of the chlorinated molecules by the investigation of the dynamical behavior of DCE. We try to answer the following question: can the fast motion observable in the ^{2}H NMR high temperature spectra be the outcome of an exchange between the *trans* and the *gauche* conformations? The problem we want to understand is to what extent the interaction with the polymer can stabilize preferentially one of the two energetically more favorable conformations of the isolated molecule. Investigation of this polymeric clathrate by means of FTIR spectroscopy reveals that the cavities seem to selectively host the *trans* conformer. In fact, for a low concentration of guest molecules absorbed in the δ form, the relative absorbance intensities of two probe peaks, one for each conformer, suggests that at least 90 % of the population is in the *trans* conformation.[1, 9, 10]
We now examine the possibility of a dynamical exchange between the two conformers. Fig. 5.12a shows the result of a ^{2}H NMR simulation for fast rotational jumps over 120° (three-site jumps) about the C-C axis (which yields the same spectrum as a fast free rotational diffusion about the same axis), while the result for a fast two-site jump of 120° between *trans* and one of the *gauche* conformations is reported in Fig. 5.12b. There is an evident discrepancy between the patterns of Figures 5.12a and b with that of Figure 5.12c resulting from the deconvolution of the experimental spectrum at 298 K. This pattern can not be reproduced, even if we recalculate the spectra for the rotational-jumps models considering an unequal distribution of the population between the conformers. The difference between these calculated results and the experimental data is the reason to discard the possibility of *trans-gauche* interconversions. The NMR data alone do not reveal that only one conformation exists in the δ s-PS cavities, but taking into account the FTIR observations recalled above, we assume that the DCE molecules clathrated in s-PS are in the *trans* conformation.
By comparison of the 1,2-dichloroethane with the 1,2-dibromoethane molecule we suppose that the latter molecule is even more stable in the *trans* conformation than the 1,2-dichloroethane, both for steric and electrostatic reasons.
Further in the text we will regard the DCE as well as the DBE molecules in the crystalline cavities of the s-PS δ form as molecules executing a motion in the rigid *trans* conformation.

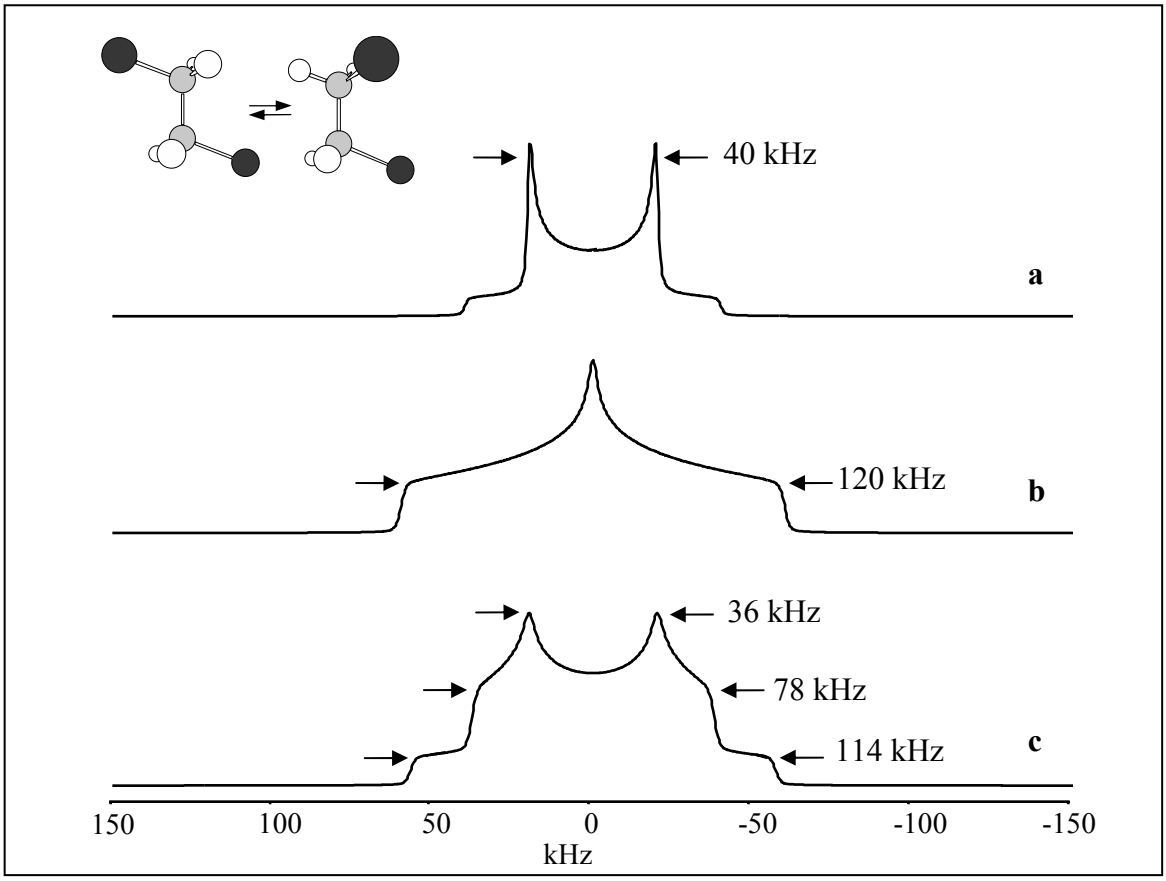

Figure 5.12: Simulated spectra calculated by assuming **a**) discrete jumps between three equivalent sites about an axis passing through the two carbon atoms, corresponding to the *trans* and the two *gauche* conformations and **b**) discrete jumps between two equivalent sites the *trans* one of the two *gauche* conformations. **c**) Calculated pattern resulting from the deconvolution of the δ_{DCE} spectrum at 298 K.

5.2.5 Reorientation about the Cl-Cl Axis

The next step to the elucidation of the dynamics of DCE and DCM molecules is based on simple observations on the molecular structures and the corresponding mobility. A comparison between the size of the cavity of δ s-PS and the size of the included halogenated molecules together with the size of the chlorine atoms leads to the conclusion that the interaction with the cavity prevents a large amplitude motion of the bulky chlorine atoms. We therefore first consider a rotation of the molecule about the Cl-Cl axis. In particular we choose the rotation axis coincident with the molecular axis of inertia. In this case the DCM and DCE would sweep out the cylinders depicted in Figure 5.13. The

corresponding C-^{2}H bonds would undergo a reorientation at similar angles with the rotation axis for all chlorinated molecules, generating similar ^{2}H NMR spectral features as is observed experimentally. For comparison, in Figure 5.13 is also shown the cylinder calculated for a corresponding rotation of DBE.

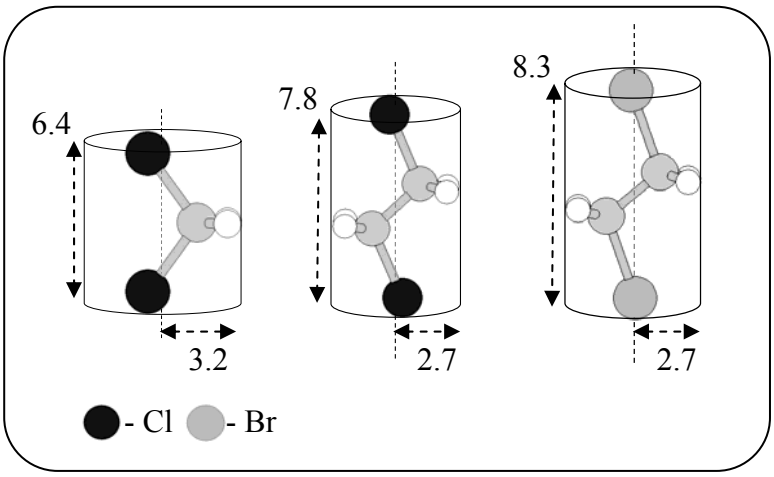

Figure 5.13: Cylinders generated by the rotation about the axis of inertia of dichloromethane-d_2, 1,2-dichloroethane-d_4 and 1,2-dibromoethane-d_4.

If this rotation would be the reorientation mode executed by the clathrated molecules, then discrepancies arise with the experimental observations. DCM exhibits an anisotropic fast motion already at 253 K, while for DCE it is activated only above 273 K. By comparing the dimension of the cylinders, the bigger radius required for the reorientation of DCM should represent a higher obstacle to this rotational motion than for the DCE molecule. Furthermore, no motion was observed for DBE, while the cylinder radius for this molecule is the same as that of DCE. This reasoning brings us to the conclusion that the molecular dynamics of DCE and DCM inside the cavities can not involve a reorientation of the carbons only but that also the Cl-Cl axis must move to a certain extent.

5.2.6 Oscillation about an Arbitrary Axis.

In this section we examine another general motional process. We consider a rotation of the C-^{2}H bond over an angle ω_α around an axis which makes an angle ω_β with the bond (Figure 5.14). The angles are varied between 0° and 360° for ω_α and between 0° and 180° for ω_β.

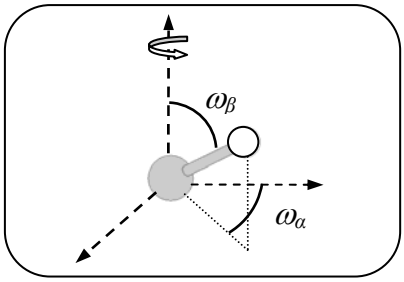

Figure 5.14: Orientation of a C-^{2}H bond that oscillate by an angle ω_α about an axis tilted of an angle ω_β with respect to the rotation axis.

The spectra are calculated for each combination of the two parameters varied in steps of 2°. The points shown in the diagram of Figure 5.16 represent the combination of ω_α and ω_β for which the spectral features of DCE at 298 K are obtained (Table 5.1). A similar diagram results from the fit of the DCM spectrum.

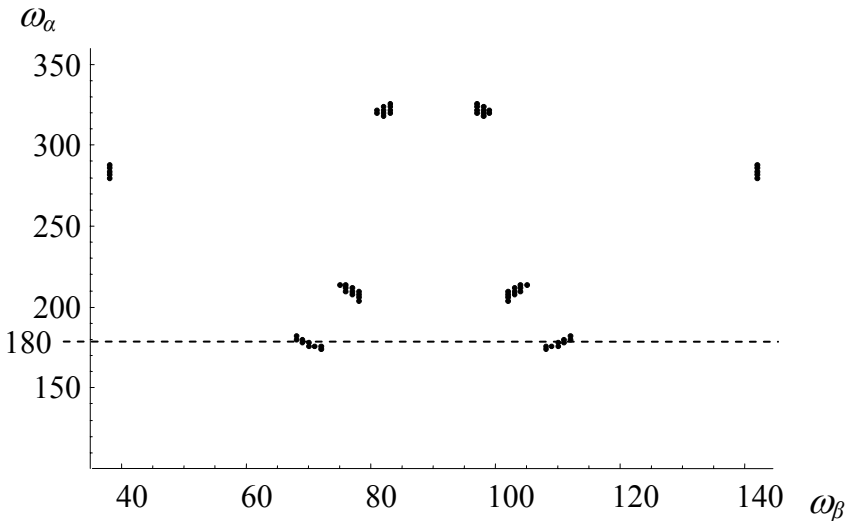

Figure 5.15: Combination of the angles ω_α (oscillation amplitude) and ω_β (tilt angle) able to reproduce the set of the spectral features for DCE at 298 K reported in Table 5.1.

It is evident that only large angle oscillations can reproduce the observed spectral parameters. All these "successful" combinations involve a rotation by at least nearly 180°. DCE in the *trans* conformation and DCM molecules are symmetric with respect to a plane containing the carbon and chlorine atoms. Since only one NMR pattern is observed the deuterium atoms of each molecule must show the same reorientation, consequently the oscillation axis must lie on the molecular plane of symmetry and contain the center of gravity of the molecule. In particular from the diagram presented in Figure 5.15 it results

that for DCE an agreement with the experimental results would be given for an oscillation about $\omega_\beta \approx 70°$. In this case the rotation axis contains the C-C bond and would involve the corresponding oscillation of the bulky chlorines, as shown in Figure 5.16, that is hindered by the small dimension of the cavity described in the next section.

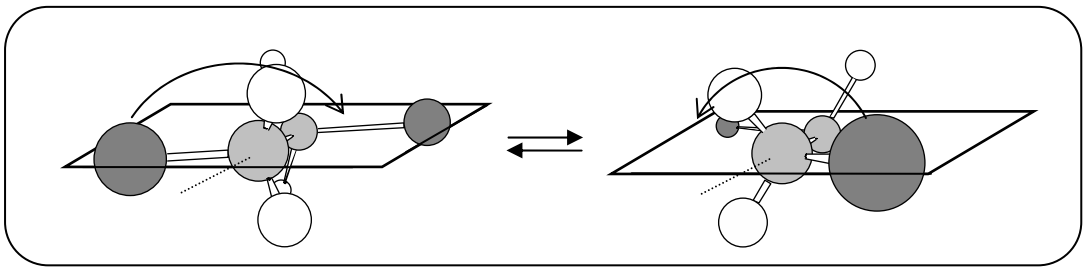

Figure 5. 16: Oscillation by 180° of the DCE molecule about an axis passing through the two carbon atoms.

In the hypothesis that this rotation could occur inside the cavity, the symmetry of the molecule and the symmetry of the crystalline cavities (section 5.2.7) would suggest that after a free rotation over 180° there would be no obstacle to complete the rotation over 360°. Such complete uniaxial rotation is not observed from the spectra therefore we believe these large oscillations do not have physical consistence.

5.2.7 The Polymeric Crystalline Cavity: a Short Review

Before preceding our discussion it is important to summarize the results from X-ray diffraction studies as well as the results of theoretical studies aimed to determine the free volume of the empty cavities of the s-PS δ form. The parameters of the unit cell were determined from the reflections observed in the X-ray diffraction pattern: a = 17.4 Å, b = 11.85 Å, c = 7.7 Å and γ = 117°.[5, 11] The values of the parameters b and γ slightly vary depending on the kind of guest molecules. The structure of the empty δ form is depicted in Figure 5.17.[12]

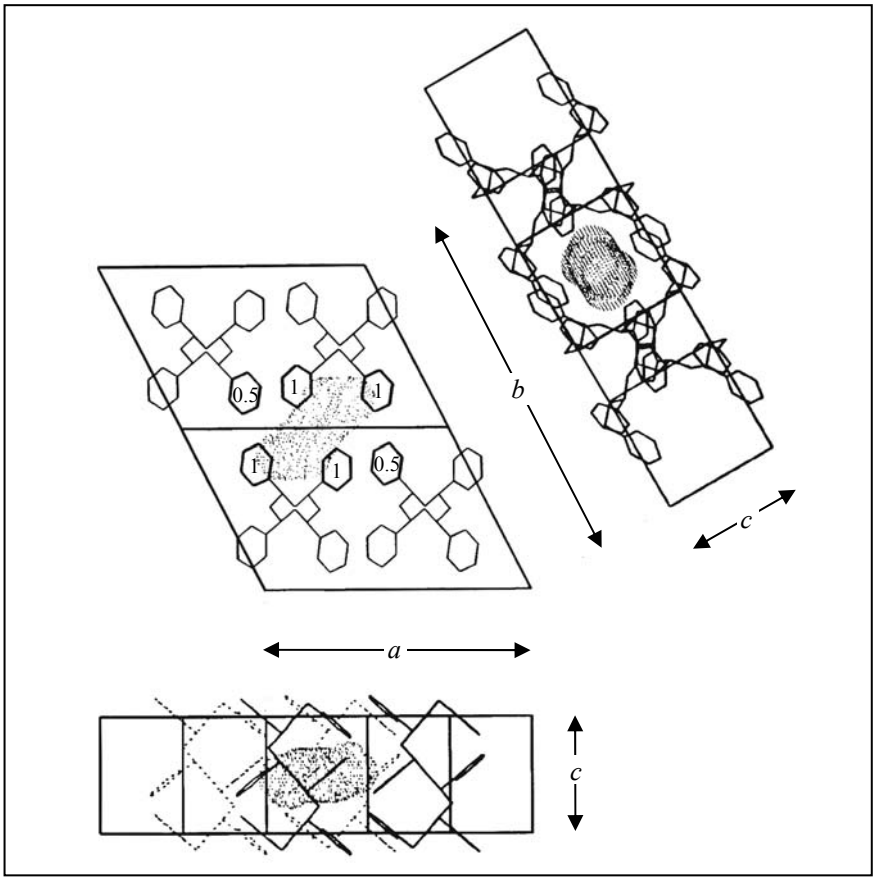

Figure 5. 17: Region of empty space (dotted) calculated for the δ form by mapping the free volume with a sphere of radius r = 1.8 Å (that is the typical van der Waals radius of chlorine atoms or methyl groups) shown for three different views of two unit cells: along c and perpendicular to ac and bc planes. Along the c view the phenyl rings that define the boundary of the cavity are in bold print and labeled by heights (expressed as fraction of c). (Ref.12)

A numerical procedure was performed to determine the empty space in the crystalline cavities of s-PS.[12] For this purpose a sphere of radius r = 1.8 Å, the Van der Waals radius of a chlorine atom, was put inside the cavity and used to map the free space. The free volume obtained by this procedure is shown in Figure 5.17 as a dotted region.

Ten phenyl rings delimit a cavity, six of which can be visualized in the view along the c axis shown in Figure 5.17. The four phenyl rings above the cavity are labeled as 1 indicating the height expressed as a fraction of c = 7.7 Å. The two phenyl rings whose average height is c/2 (labelled as 0.5) are located at the average height of the cavity. The other four phenyl rings are below the cavity at zero height. The free volume, calculated with the probe sphere, results to be 115 Å^3. Furthermore the maximum and the minimum dimension are given: the former is nearly 8.1 Å along the diagonal in the ab plane and the smallest dimension is 3.4 Å along the c axis of the crystalline unit cell.[12]

According to this information the shape of the crystalline cavity, strongly simplified, can be regarded as a parallelepiped presenting the two largest facets perpendicular to the *c* axis of the crystalline cell (Figure 5.18).

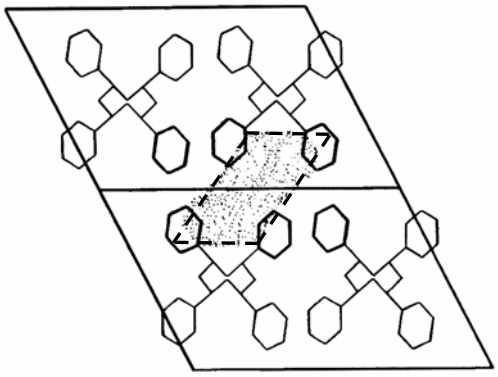

Figure 5.18: Representation of the crystalline cell seen along the *c* axis as in Figure 5.16. The dashed line delimits the surface of the parallelepiped approximately representing the shape of the cavity.

5.2.8 The Polymeric Crystalline Cavity in the Clathrate Form

The ^{2}H NMR investigation of the δ_{CF} sample showed the absence of large amplitude reorientations of the C-^{2}H bond of clathrated CF molecules. As discussed in section 5.2.1 ^{2}H NMR investigation can not detect a rotation about the C-^{2}H bond, therefore an eventual free rotation or a three-site jump of the C-Cl_3 group about the C-^{2}H bond can not be observed. However the small dimension of the crystalline cavities as well as the interaction of the chlorine with the phenyl rings of the polymer represent an obstacle for a free rotation about the C_3 symmetry axis of CF. The exclusion of the possibility of a free uniaxial rotation is supported by the absence of this motion for the other halogenated molecule investigated. The possibility to obtain s-PS clathrate form with chloroform demonstrates that the dimension of the cavity, as well as the electrostatic interactions allow the location of three chlorine in the crystalline void. A model of the cavity should show at least three "pockets" to host three chlorine atoms as very schematically represented in Figure 5.19.

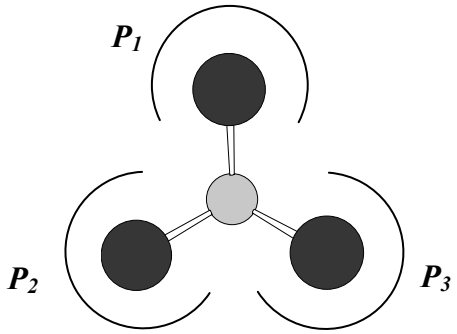

Figure 5.19: Schematic representation of the three "pockets", labelled as P_1, P_2 and P_3, where the three chlorine atoms can be hosted inside the cavity.

The most obvious location of the chloroform molecule inside the cavity is with the plane of the three bulky chlorine atoms lying approximately parallel to the *ab* plane. Furthermore, the small angle reorientation observed for the deuterium atoms of chloroform resulting from the NMR investigation (section 5.2.1) implies that the chlorines must be able to move somewhat out of the plane parallel to the *ab* plane of the cell in order to allow the motion. Therefore the smallest dimension of the parallelepiped, along the *c* axis, must be larger than the smallest dimension calculated using the probe sphere (3.4 Å).

5.2.9 Two-Sites Jump Model Proposed for the Dynamics of DCM.

If we compare the NMR spectra of DCM and CF molecules we notice that the replacement of one chlorine atom with a deuteron enables the DCM molecule to experience a large amplitude fast anisotropic motion which is absent for CF. Before we analyze another dynamical model for DCM molecules it is necessary to precise that in good approximation the guest molecules inside the cavity assume an orientation that minimize the interaction of the halogens with the phenyl rings of the polymer. The possibility to locate three chlorine atoms inside one polymer cavity as shown in the "three pockets" representation leads us to propose a motional model for DCM molecules according to which the chlorine atoms flip between these three allowed positions. Referring to the representation of the "pockets" of Figure 5.19 the two chlorines can alternately occupy two of the sites P_1, P_2 and P_3. We consider the possibility of a 120° jump about an axis containing one of the C-^{2}H bonds (Figure 5.20)

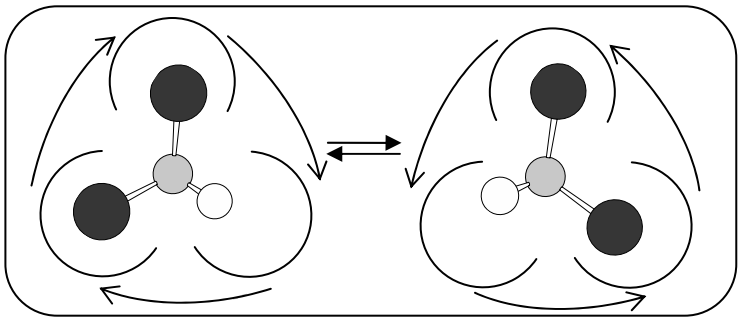

Figure 5.20: Example of exchange between two sites differing for a 120° rotation about a C-^{2}H bond.

This reorientation would yield the superposition of two patterns: a static line shape from the deuteron located on the rotation axis, and a second pattern computed in section 2.5.4 for an analogous 120° jump and shown in Figure 5.12b. The two-site jump motion shown in Figure 5.20 is then excluded because the simulated pattern does not fit the experimental data.

Another possibility to move the chlorines of DCM molecule in the three pockets is to consider only one atom jumping between the other two "pockets". For example the molecule could jump between two orientations in which the chlorines occupy the pockets (P_1, P_2) and (P_1, P_3). This motion is equivalent to a rotation of the Cl-Cl axis (a_{Cl}), about an axis containing one chlorine and perpendicular to a_{Cl}, by an angle $\varphi_{DCM} = 60°$ (Figure 5.21). In free space the -C^{2}H$_2$ group could occupy an infinite number of possible sites by rotating the molecule about a_{Cl}. Several of these orientations are indicated in Figures 5.21a and b as the result from rotations about the Cl-Cl axis by the angle σ' for the chlorines in P_1 and P_2 (Figure 5.21a) and σ'' for the chlorines in P_1 and P_3 (Figure 5.21b). We consider 360 values of each of the angles σ' and σ'' and calculate the spectra which result from a jump from one of the 360 possibilities in Figure 5.21a to each of the 360 possibilities in Figure 5.21b. We obtain in this way 129600 spectra.

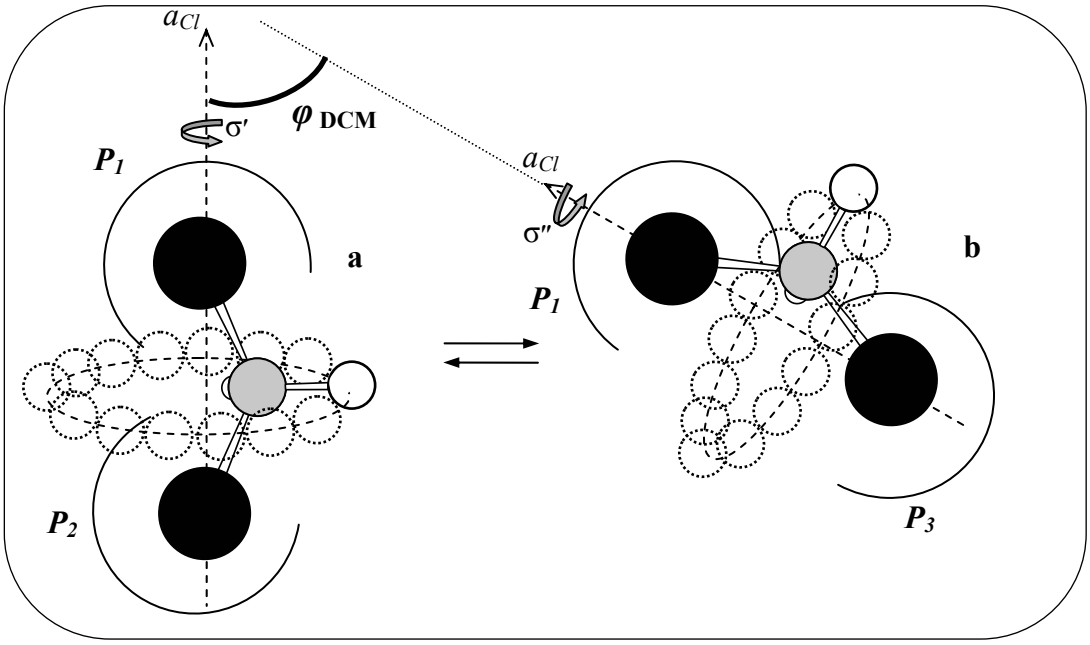

Figure 5.21: Schematic representation of the possible orientation of the deuterium atoms in the two sites differing for a molecular rotation by $\varphi_{DCM} = 60°$.

From these 129600 spectra those are selected which match the experimental δ_{DCM} NMR pattern corrected for the effect of the fast small amplitude librational motion mentioned before. For 1474 pairs of tensors the agreement is good.

The histogram in Figure 5.20 presents the successful combinations plotted as a function of the difference $\sigma_{DCM} = |\sigma' - \sigma''|$, where σ' and σ'' are the angles of rotation shown in Figure 5.21. Unfortunately the results are distributed over two ranges, i.e. $62° \leq \sigma_{DCM} \leq 118°$ and $257° \leq \sigma_{DCM} \leq 298°$ that differ for a 180° rotation therefore it is not possible to univocally define the relative amplitude of the rotations of the deuterons coupled to the reorientation of the chlorines. Actually the results shown in Figure 5.22 are computed by considering an equal probability for all the orientations in Figure 5.21. This assumption can not be true for the molecules in the cavities. Nevertheless the probability that the rotation involves an angle $62° \leq \sigma_{DCM} \leq 118°$ is 75% and $\sigma_{DCM} = 100°$ resulted to be the most probable rotation angle.

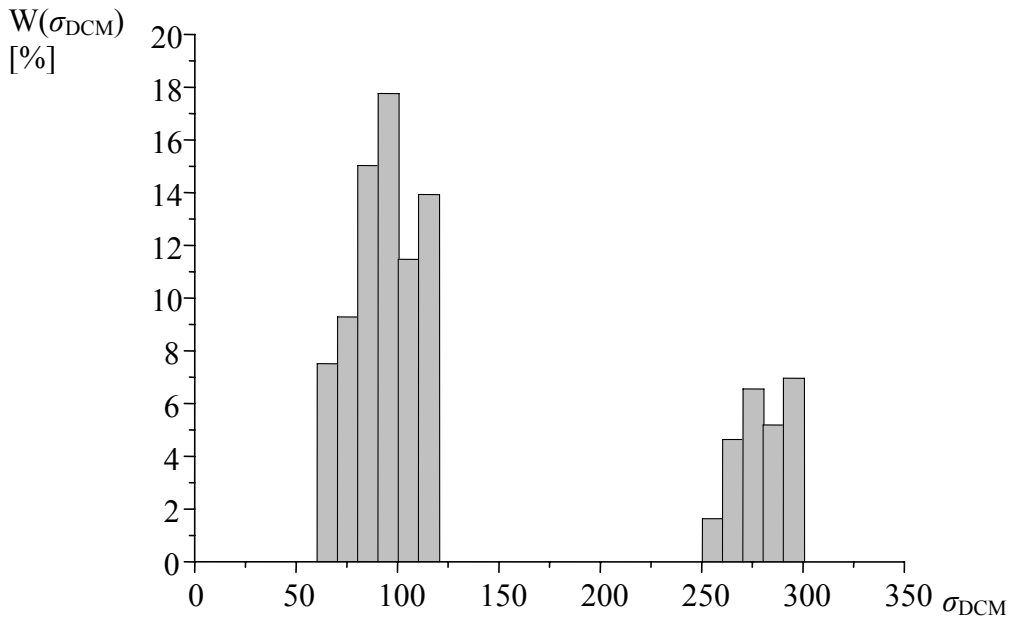

Figure 5.22: Histogram relative to the percentage of successful combinations plotted as a function of the difference σ_{DCM}.

5.2.10 Two-Site Jump Model Proposed for the Dynamics of DCE.

By comparing the dynamical features of the experimental spectra at 298 K of DCM and DCE reported in Table 5.1, the motion of the deuterium atoms of dichloromethane clathrated in the s-PS must be very similar to the dynamics of 1,2-dichloroethane. Therefore also for DCE a two-site jump model is proposed and a procedure analogous to that presented for the analysis of DCM is now used to characterize the reorientation of the DCE in the δ_{DCE} sample. We refer again to the model of the three "pockets" described before and consider the chlorines occupying alternatively the voids (P_1, P_2) and (P_1, P_3). It is worth noting that the longer distance of the two halogens in the DCE with respect to the DCM molecule, as quantitatively evidenced in Figure 5.13, reduces the rotation angle necessary to move one chlorine atom for example from P_2 to P_3. In fact the Cl-Cl axis is now rotated by φ_{DCE} = 40° about an axis containing one chlorine atom, as displayed in Figure 5.23 for an arbitrary orientation of the carbon atoms.

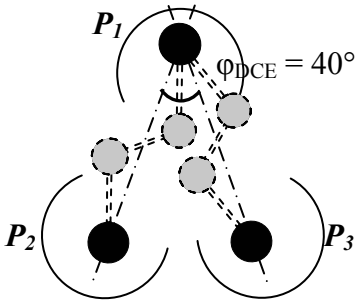

Figure 5.23: Schematic representation of the DCE molecule in the two sites related by a rotation by φ_{DCE} = 40° about a generic axis containing one chlorine atom, i.e. the one in the pocket P_1.

Actually a rotation of the Cl-Cl axis by 40° to reach another energetically stable position was already reported in the literature. In fact by calculations of the minimum interaction energy between host polymer and DCE molecules De Rosa *et al.*[13] found four possible orientations of DCE molecules in the trans conformation, denoted: *a*, *b*, *c* and *d*. The *a* and *b* packing models as well as *c* and *d* show the chlorine atoms approximately in the same position along the diagonal of the parallelepiped but the molecules are rotated approximately 180° about the Cl-Cl axis. A rotation of nearly 40° about the center of symmetry of the molecule in the a-b plane of the crystalline cell transforms the *a* and *b* into the *c* and *d* packing models (Figure 5.24).

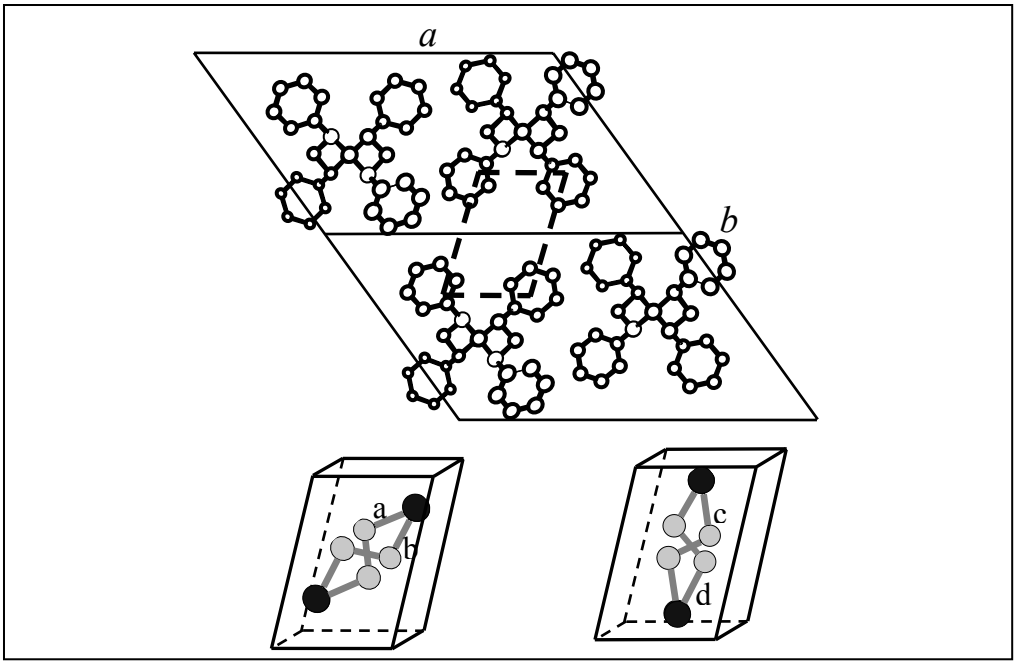

Figure 5.24: Model of packing and unit cell for the crystal structure of the empty δ-form of s-PS and positions of the DCE molecule inside the cavity, schematized as a parallelepiped, according to the models of packing proposed in Ref. 13.

The possibility of a two-site jump of the molecule between these four positions as well as a motion that averages all the four orientations was also considered, but none of the simulated spectra fit the experimental pattern of DCE.

We now simulate a two-site jump reorientation involving the rotation of the Cl-Cl axis as presented in Figure 5.23 following the same procedure as described for the DCM molecules.

The histogram of Figure 5.25 shows the rotations that fit the experimental parameters as a function of $\sigma_{DCE} = \left| \sigma'_n - \sigma''_n \right|$, the angle of rotation about the Cl-Cl axis. Also for the DCE molecule the values of σ_{DCE} for the successful combinations are distributed over two ranges: $74° \leq \sigma_{DCE} \leq 117°$ and $250° \leq \sigma_{DCE} \leq 286°$.

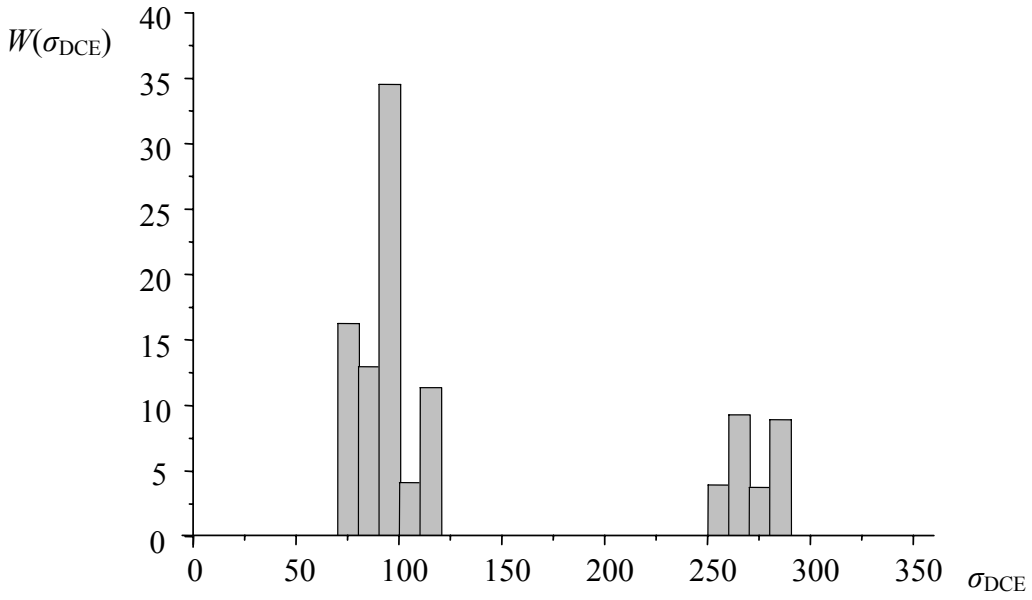

Figure 5.25: Histogram relative to the percentage of successful combinations plotted as a function of the difference σ_{DCE}.

From the histogram it is evident that the most probable value of σ_{DCE} lies between 74° and 117° (75 % probability). In particular the most probable range is between 90° and 100°, but it includes only 33 % of the total results. Two molecular orientations differing for the most probable value of σ_{DCE} (i.e. 97°), are represented in Figure 5.26.

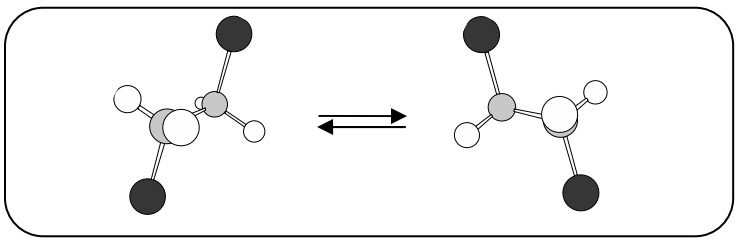

Figure 5.26: Proposed location of the DCE molecule inside the cavity occupying two sites related by a rotation by $\varphi_{DCE} = 40°$ about the y axis and $\sigma_{DCE} = 97°$.

The results of the NMR investigation presented in this work do not supply enough information to elucidate the location of the molecules inside the polymeric cavity. Electrostatic interactions between the phenyl rings of the polymer and the halogens play an important role but the nature of this interaction is still unclear. Therefore further investigation as for example molecular dynamics calculations are necessary to completely define the molecular motion in the investigated systems.

Bibliography

1) Musto, P; Mensitieri, G.; Cotugno S.; Guerra, G.; Venditto, V. Macromolecul, 35, 2296.
2) Xiong, J.; Maciel, G. E. *J. Phys. Chem. B.,* **1999**, *103,* 5543.
3) Fyfe, C. A. In Solid State NMR for Chemists; C.F.C. Press: Guelph, **1983**.
4) Eckman, R. R.; Vega, A. J. J. Phys. Chem. **1986**, *90*, 4679.
5) De Rosa, C.; Guerra, G.; Petraccone, V.; Pirozzi, B. *Macromolecules* **1997**, *30*, 4147.
6) Nishikiori, S.; Kitazawa, T.; Kim, C.-H.; Iwamoto, T. *J. Phys. Chem. A* **2000**, *104*, 2591.
7) Musto, P.; Manzari, M.; Guerra G. *Macromolecules* **1999**, *32*, 2770.
8) Taylor, M.G.; Kelusky, E. C.; Smith, I. C. P.; Casal, H. L.; Cameron, D. G. *J. Phys. Chem.* **1983**, *78*, 5108.
9) Guerra, G.; Manfredi, C.; Musto, P.; Tavone, S.; . *Macromolecules* **1998**, *31*, 1329.
10) Musto, P.; Manzari, M.; Guerra G. *Macromolecules* **2000**, *33*, 143.
11) Chatani, Y.; Inagaki, T.; Shimane, Y.; Shikuma, H. *Polymer* **1993**, *34*, 4841.

12) Milano, G.; Venditto, V.; Guerra, G.; Cavallo, L.; Ciambelli, P.; Sannino, D. *Chem. Mater.* **2001**, *13*, 1506.
13) De Rosa, C.; Rizzo, P.; Ruiz de Ballesteros O.; Petraccone, V.; Guerra, G. *Polymer* **1999**, *40*, 2103.

Appendix A

Active rotation:

A vector performs an active rotation if the vector rotates in a fixed coordinate axis system (Figure A.1).

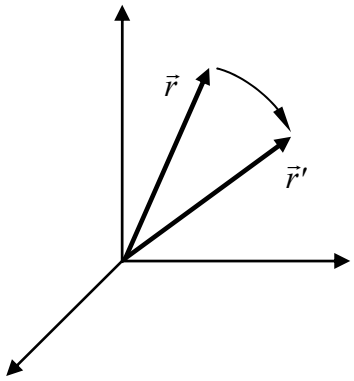

Figure A.1: Representation of an active rotation of the vector $\vec{r}$ to reach a new position labeled as $\vec{r}'$.

The new vector $\vec{r}'$ can be calculated by multiplying the vector $\vec{r}$ with the transformation matrix R:

$$\vec{r}' = \vec{r}\,\mathrm{R} \qquad [A.1]$$

or $r_i' = \sum_{j=1}^{3} \mathrm{R}_{ij}\, r_j$.

A matrix T is transformed into the matrix T' by the equation:

$$\mathrm{T}' = \mathrm{RTR}^{-1} \qquad [A.2]$$

Passive rotation:

A passive rotation consists in a rotation of the coordinate axis system (Figure A.2). The vector $\vec{r}$ in the coordinate axis system (x′, y′, z′) is calculated by the equation:

$$\vec{r}' = \vec{r}\, \mathrm{R}^{-1} \qquad [A.3]$$

A matrix T in the coordinate axis system (x′, y′, z′) is:

$$\mathrm{T}' = \mathrm{R}^{-1}\mathrm{TR} \qquad [A.4]$$

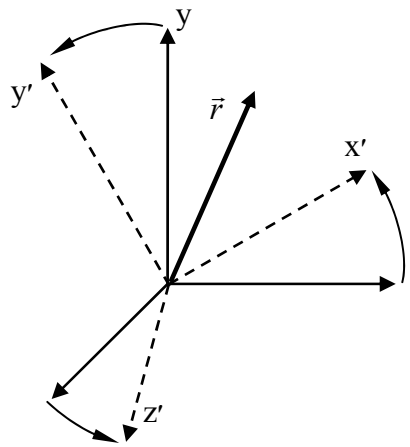

Figure A.2: Representation of a passive rotation of the vector $\vec{r}$. The coordinate axis system rotates from (x, y, z) to become (x′, y′, z′).

The matrix R for a mathematically positive rotation of the coordinate axis system (Figure A.2) by an angle φ is defined as:

$$\mathrm{R}(\varphi) = \begin{pmatrix} \cos\varphi & -\sin\varphi & 0 \\ \sin\varphi & \cos\varphi & 0 \\ 0 & 0 & 1 \end{pmatrix} \qquad [A.5]$$

A rotation is defined mathematically positive according to the right-handed rule: the thumb of the hand pointing along the rotation axis vector and the fingers indicate the direction of the rotation.

It is worth noting that a positive rotation of the coordinate axis system (i.e for a passive rotation) corresponds to a negative rotation of the vector (i.e. for an active rotation).

Summary

The crystalline regions of the δ form of syndiotactic polystyrene (s-PS) contain cavities in which certain small molecules can be absorbed. The mobility of six perdeuterated molecules: benzene, toluene, chloroform dichloromethane, 1,2-dichloroethane and 1,2-dibromoethane, present as a guest in these cavities, has been investigated via ^2H NMR spectroscopy. The NMR spectra show that most molecules included in the cavities, have a certain freedom to rotate.

For all samples the motional behavior of the molecules absorbed in the amorphous phase of the polymer differs from that shown by the molecules clathrated in the crystalline phase. The motion of all six molecules in the amorphous phase is approximately isotropic at a temperature T = 298 K or higher, but severely anisotropic when the molecules are included in the crystalline phase.

The dynamical behavior of each solvent hosted in the crystalline phase of s-PS is investigated by comparing spectra obtained by simulation of the effect of a certain molecular rotation on the ^2H spectra with the experimental spectra.

Benzene molecules show fast diffusional reorientations about the C_6 symmetry axis.

This reorientation of the phenyl ring is hindered for toluene molecules where the only motion observed is a rotation of the C-$^2H_3$ group about the C_3 symmetry axis.

The C-^2H bonds of chloroform molecules included in the cavities reorient only over small angles. The deuteron NMR spectra do not allow the detection of an eventual rotation of the C-Cl_3 group about the C_3 symmetry axis. Nevertheless, by comparing the results obtained for the other halogenated aliphatic molecules, a free uniaxial diffusional rotation of chloroform around the symmetry axis can be excluded.

The formation of s-PS clathrates with chloroform proves, however, that the cavities in crystalline s-PS are large enough to accommodate a molecule with three chlorine atoms. A model of the cavity with at least three "pockets" to locate the bulky halogens is proposed.

The experimental spectra of dichloroethane (DCE) in the δ form of s-PS show that a complicated rotational motion takes place. Several possible motions are considered like a rotation around the C-C axis and a fast *trans-gauche* interconversion. From comparing the experimental spectra to the simulated spectra for these motions it could be concluded that such motions do not take place. According to the FTIR studies reported in literature, we assume that DCE clathrated in s-PS is exclusively in the *trans* conformation.

From the (temperature dependent) spectra it is clear that DCE and dichloromethane (DCM) in s-PS clathrates exhibit the same dynamical behavior but that the motion of DCM is activated at a lower temperature. A dynamical model is proposed according to which the molecules jump between two sites that differ for the location of the chlorine in two of the three allowed "pockets" in the crystalline cavities. For DCM these two sites differ by a rotation around two axes: a 60° rotation around an axis perpendicular to the Cl-Cl axis, accompanied by a rotation of the C-^{2}H bond about the Cl-Cl axis.

The same two-site jump model was also applied to simulate the spectra of DCE. In this case the axis containing the two halogens is assumed to rotate by 40°.

1,2-Dibromoethane (DBE) clathrated in s-PS shows no motion, not even at the highest temperature (T = 333 K). Apparently, the distance between the two bromine atoms in the DBE molecule is too large to allow even a wobbling motion of the Br-Br axis, although the size of the DBE molecule, perpendicular to the Br-Br axis, is not larger than the corresponding size of DCE or DCM.

As a conclusion we want to emphasize that although the two-site jump motions we considered for DCM and DCE reproduced the experimental spectra, other more complex motions may exist which also give the correct spectra. To be honest, the spectra for DCE and DCM are so complex that they do not give enough information to derive from the spectra alone the model of the motion. What is needed is more information about the interactions between the enclosed molecule and the cavities in s-PS by a molecular dynamics calculation.

Zusammenfassung

Syndiotaktisches Polystyrol (s-PS) in der δ-Form besitzt in den kristallinen Bereichen Hohlräume, in denen insbesondere kleine Moleküle absorbiert werden können. Zu diesen Molekülen gehören Benzol, Toluol, Dichlormethan, 1,2-Dichlorethan und 1,2-Dibromethan, die in ihrer perdeuterierten Form bzgl. ihrer Beweglichkeit innerhalb der Hohlräume mit Hilfe der Deuterium-NMR-Spektroskopie untersucht wurden. Die NMR-Spektren zeigen, dass die meisten Moleküle innerhalb der Hohlräume nur eine bestimmte Rotationsfreiheit besitzen.

Das Bewegungsverhalten der in der amorphen Phase des s-PS absorbierten Moleküle unterscheidet sich stark von denen in der kristallinen Phase. Alle sechs Moleküle zeigen hier bei Temperaturen von 298 K und darüber eine nahezu isotrope Bewegung, wohingegen sie in der kristallinen Phase durch einer stark anisotrope Bewegung gekennzeichnet sind.

Das dynamische Verhalten der Lösemittelmoleküle in der kristallinen Phase des s-PS wurde untersucht, indem unter Berücksichtigung bestimmter Bewegungen ^{2}H-NMR-Spektren simuliert und mit den jeweils experimentell erhaltenen Spektren verglichen wurden. So zeigt das Benzol-Molekül eine schnelle Rotation und Reorientierung um seine C_6-Symmetrieachse. Diese Reorientierung des Phenylringes ist im Toluol gehindert, womit als einzige zu beobachtende Bewegung eine Drehung der Methylgruppe um die C_3-Symmetrieachse zu erwähnen ist.

Die C-^{2}H-Bindung im absorbierten Chloroform zeigt nur eine, auf kleine Winkel beschränkte Auslenkung. Im entsprechenden Deuterium-Spektrum ist es zudem nicht möglich, eine Drehung der CCl_3-Gruppe um die C_3-Symmetrieachse zu detektieren. Vergleicht man jedoch die Ergebnisse mit anderen halogenierten, aliphatischen Kohlenwasserstoffen, kommt man zu der Überzeugung, dass eine freie, uniaxiale Rotation um diese Rotationsachse ausgeschlossen werden kann.

Die Bildung einer Einschlussverbindung von s-PS mit Chloroform beweist, dass die Hohlräume im kristallinen s-PS groß genug sind, um Moleküle mit drei Chloratomen aufzunehmen. Somit kann ein Modell des Hohlraumes aufgestellt werden, dass mindestens drei „Taschen“ enthält, in denen die voluminösen Chloratome jeweils lokalisiert sind.

Das experimentell erhaltene Spektrum von Dichlorethan (DCE), absorbiert in der kristallinen Phase der δ-Form des s-PS, weist darauf hin, das dass DCE-Molekül einer komplizierten Rotation unterliegt. Hierzu wurden zahlreiche mögliche Bewegungen angenommen, wie z. B. die Rotation um die C-C-Achse und ein schneller *trans-gauche*-Übergang Bei dem Vergleich des experimentellen mit dem simulierten Spektrum geht jedoch hervor, dass diese Bewegungen nicht stattfinden. In Bezug auf die in der Literatur zu findenden FT-IR-Untersuchungen kann angenommen werden, dass das DCM-Molekül innerhalb der Hohlräume des s-PS ausschließlich in der *trans*-Formation vorliegt.

Bei der Betrachtung der temperaturabhängigen Spektren wird deutlich, dass DCE und Dichlormethan (DCM) in s-PS das gleiche Bewegungsverhalten zeigen, allerdings ist die Aktivierungstemperatur bei DCM niedriger. In dem dazugehörigen Bewegungsmodell wird angenommen, dass die Chloratome zwei der drei „Taschen" innerhalb des Hohlraumes besetzten und nur durch Sprünge in die jeweils freie Tasche gelangen („two-site jump"). Bei DCM kann dieser Sprung zwischen zwei Taschen durch die Rotation um zwei Achsen beschrieben werden: eine 60°-Drehung um die Achse senkrecht zur Cl-Cl-Achse, die von einer Rotation der C-^{2}H-Bindung um die Cl-Cl-Achse begleitet wird.

Das gleiche Modell des Sprunges zwischen zwei Positionen wird auch bei der Simulierung des ^{2}H-NMR-Spektrums von DCE angewendet. In diesem Fall zeigt sich eine gute Übereinstimmung mit den experimentellen Daten, wenn eine 40°-Drehung um die Cl-Cl-Achse angenommen wird.

Bei der Einschlussverbindung von s-PS mit 1,2-Dibromethan (DBE) ist auch bei Temperaturen von bis zu 333 K keine Bewegung zu beobachten. Hier ist anzunehmen, dass die Entfernung der zwei Bromatome voneinander sehr groß ist, so dass nicht einmal eine schwingende Bewegung der Br-Br-Achse erfolgen kann, obwohl die Größe des DBE-Moleküls, hinsichtlich der Ausdehnung senkrecht zur Br-Br-Achse, nicht größer ist als die des DCE- oder des DCM-Moleküls.

Zusammenfassend kann betont werden, dass, obwohl bei der Simulation der experimentell erhaltenen ^{2}H-NMR-Spektren von DCM und DCE nur ein Sprung zwischen zwei Positionen angenommen wurde, es nicht auszuschließen ist, dass andere, komplexere Bewegungen existieren, die ebenfalls ein übereinstimmendes Spektrum liefern können. Um hinsichtlich des Bewegungsmodells genauere Aussagen treffen zu können, sind mehr Informationen über die Wechselwirkungen der in den Hohlräumen eingeschlossenen Gastmoleküle nötig, die über Berechnung der Molekularbewegung erhalten werden können.

Lebenslauf

Name	Elena Trezza
Geboren am, in	18.08.1973 in Salerno (Italien)
Staatsangehörigkeit	Italienisch
Familienstand	Ledig

Schulausbildung

1978-1983	Grundschule in Salerno.
1983-1986	Scuola Media Statale „De Filippis“ Salerno.
1986-1991	Liceo Scientifico Statale „L. Da Vinci“ Salerno und Erlangung der allgemeinen Hochschulreife.

Studium

1991-1998	Chemiestudium an der Università degli Studi di Salerno mit Schwerpunkt in Anorganischer und Physikalischer Chemie. Diplomarbeit Chemie bei Prof. A. Grassi mit dem Thema: *Charakterisierung von Syndiotaktischem Polystyrol und seiner Einschlussverbindungen mit Hilfe der Deuterium-NMR-Spektroskopie.*
1998 – 1999	Durchführung wissenschaftlicher Arbeiten in der Arbeitsgruppe von Prof. A. Grassi an der Universität Salerno.
Seit 1999	Promotion im Fachgebiet Physikalische Chemie in der Arbeitsgruppe von Prof. Dr. W. S. Veeman an der Universität Duisburg-Essen (Standort Duisburg)